Modelling noxious laser stimulation for both Neodymium: Yttrium-Aluminium-Perovskite and Carbon Dioxide lasers

Experimental validation

Alan Tahhan
02-10-2017
MASTER THESIS IN BIOMEDICAL ENGINEERING AND INFORMATICS
Pages: 97, words: 25931 and characters: 140264

Table of content

Title of master thesis:
Modelling noxious laser stimulation for both Neodymium: Yttrium-Aluminium-Perovskite and Carbon Dioxide lasers

Theme:
Mathematical modelling

Project period:
February – October 2017

Project group number:
17gr10410

Group members:
Alan Tahhan

Supervisor:
Steffen Frahm

Copies:
0

Page numbers:
97

Date of completion:
2. October 2017

Abstract

Pain is one of the most important physiological mechanism to ensure survival from external stimuli. In pain research, the use of lasers has been a popular tool in causing pure heat stimulation and selectively activation of A-δ and C-fibres. Different lasers have different levels of penetration throughout the skin. The higher the level of penetration the harder it is to understand how the laser-light is distributed and the heat is propagating in the skin. Through mathematical modelling it is possible to predict and describe the phenomenon. Such a model may simplify the use of lasers in research related or clinical problems where laser stimulation is being used or may be used.

The thesis is based on a previous semester project, where the goal was to build a mathematical model describing laser light absorption and heat transfer in the skin. It was constructed as 2D-axial (r,z) model and implemented via a Monte Carlo method for describing light absorption for λ=250-10600 [nm] and a Finite Element method for describing the heat transfer. The model was verified but not validated. Without a validation, it is uncertain whether the model could produce meaningful results to real problems. The motivation of this thesis is therefore to conduct an experimental validation of the model. The validation was conducted for both Carbon Dioxide (CO_2) and Neodymium: Yttrium-Aluminum-Perovskite (Nd: YAP) lasers on 5 healthy subjects. Experimental data was based on thermographic recordings of the stimulation site and on subject feedback. The laser stimulations were optimized in relation nociceptive activation of A-δ pain fibers. To increase the probability of a successful validation, the model was optimized in relation to the specific stimulation site on the volar forearm and in relation to critical observations derived from the previous semester project. After the optimizations, the experimental data was compared to model data to get a basis for model adjustment as part of the validation. The modelled data and experimental data was compared through temporal heat spot profiles at (0,0) (5,0) and (10,0) [mm] over a period of 7.5 [s] from stimulation onset.

The model was successfully validated for the CO_2 laser. Validation of the Nd: YAP laser was not successful, and needs therefore more adjustments to be able to be validated. Additionally, the stimulation intensities used in the experiment for activations of A-δ pain threshold, must be compared to relevant literature to ensure their reliability.

Summary (Danish)

Smerte er en af de vigtigste fysiologiske mekanismer der findes, for at sikre overlevelse fra eksterne stimuli. Smerte fungerer ved at advare os mod potentielt skadende stimuli der kræver afvigelse eller skader der kræver akut opmærksomhed/behandling. I smerteforskning har brug af lasere været et populært redskab til at forårsage ren termisk stimulering, samt selektiv aktivering af A-δ og C-fibre. Forskellige lasere har forskellige penetrationsdybder i huden. Jo højere penetrationsdybden er, desto sværere er det at forstå, hvordan laserlyset er fordelt og hvordan varmen spreder sig i huden. Gennem matematisk modellering er det muligt at forudsige og beskrive fænomenet. Sådan en model kan forenkle anvendelsen af lasere i forskningsrelaterede eller kliniske problemer hvor laserstimulering anvendes, eller kan anvendes.

Specialet er baseret på en tidligere udviklet 4-lags (Stratum Corneum, Epidermis, Dermis og Hypodermis) 2D-aksial (r, z) model, der beskriver absorption af laserlys for bølgelængder mellem 250-10600 [nm] i huden og hvordan den efterfølgende varmegenerering spreder sig i vævet (Cid Royo et al. 2016). Modellen var konstrueret af en verificeret Monte Carlo model implementering i MATLAB, der beskriver lys-absorption, og en Finite Element-model implementeret i COMSOL, der beskriver varmeoverførslen. I specialet blev modellen optimeret i forbindelse med en eksperimentel validering på 5 raske forsøgspersoner i forhold til smerte fremkaldende activering af A-δ fibre på den volar side af underarmen med både en Carbon Dioxide (CO_2) laser og en Neodymium: Yttrium -Aluminium-Perovskite (Nd: YAP) laser. Hver lasertype har relativt forskellige penetrationsdybder. Eksperimentelle data var baseret på termografiske optagelser af stimuleringsstedet og subjektfeedback relateret til A-δ smertetærsklen.

Som en del af valideringen blev modellen justeret i forhold til at kunne reproducere samme temperaturer i midten af laserstråle punktet som vist i de eksperimentelle data efter mindre end 50 [ms] fra afgivet stimuli. CO_2-laseren blev justeret i forhold til stimuleringsintensiteten, og Nd: YAP-laseren blev justeret i forhold til absorptionskoefficienten af epidermis. Resultater fra CO_2-laser validering viste at det modellerede data lå inden for standardafvigelsen af gennemsnittet fra eksperimentel data af den gennemsnitlige temperatur ved (0,0), (5,0) og (10,0) [mm] over en nedkølingsperiode på 7.5 [s] efter afgivet stimuli. Resultater fra Nd: YAP-laservalidering viste at den modellerede maksimale temperatur var lig med den eksperimentelle gennemsnitlige maksimale temperatur i (0,0) [mm], men de modellerede data lå ikke inden for standardafvigelsen af gennemsnittet fra eksperimentel data over nedkølingsperioden på 7.5 [s] efter afgivet stimuli. Næste trin for modellen ville være at sammenligne de modellerede og eksperimentelle laserstimuleringsintensiteter med andre relaterede laserstimuleringsreferencer i forhold til estimering af nociceptiv aktivering af A-δ fibre.

Den justerede model kan give indsigt i laserlys-absorption og sammenhængende varmeoverførsel ved brug af forskellige typer lasere og indsigt i yderligere planlægning of udførelse af validering. Yderligere justering af koefficienter er nødvendig ved modellering af Nd: YAP laseren, for at kunne opnå en vellykket validering. Gennem en vellykket validering vil det være muligt at evaluere modelfunktionaliteten i forhold til at producere meningsfulde resultater i relation til smerteforskningsrelaterede problemer.

Project context

This project continues the work from the authors 2nd semester project from Spring 2016. The project from 2016 was a fully theoretical modelling project, within the field of nociceptive activation in relation to laser-skin stimulation. This presented continuation of the project attempts to validate and optimize the model in both a theoretical, practical, and experimental way.

The previous project from 2016 was done in collaboration with: Kim Munck Jeppesen, Petr Šipka, and Albert Cid Royo, all master students from Biomedical Engineering and Informatics @ Aalborg University. Supervisor for the project was Steffen Frahm, Adjunkt @ Institut for Medicin og Sundhedsteknologi, Aalborg University. The project is available as a dropbox link through following reference (Cid Royo et al. 2016).

Reading guide

This project audience is directed towards fellow students or professionals within the field of biomedical engineering. All theory needed to understand the previous project from 2016 and the present project is included in the master thesis.

References

The reference method in the project is as following: When a reference is used AFTER punctuation in a paragraph, the reference belongs to the whole content of the paragraph. Following example shows how (Kandel 2013) belongs to both sentences in the paragraph:

A-delta is a nociceptor responsible of first pain nociception. C-fibres are nociceptors responsible for second pain nociception. (Kandel 2013)

When a reference is used BEFORE a punctuation, the reference belongs to the whole sentence before the punctuation. Following example shows how (Kandel 2013) belongs to the first sentence and (Martini et al. 2012) belongs to the second sentence:

A-delta is a nociceptor responsible of first pain (Kandel 2013). The anatomy of the skin is divided into three major structures: Epidermis, Dermis, and Hypodermis (Martini et al. 2012).

This reference method is often used in projects made at Aalborg University. When writing scientific articles, the reference methods of either Harvard or Vancouver would be used.

Unit notation

Units in the project will always be noted in square brackets. E.g. [W] for the unit of watts, [s] for the unit of seconds, and °C for degrees in Celsius. Only SI units will be used along with relevant prefix.

Abbreviations

μ_a – Absorption coefficient

μ'_s – Reduced scattering coefficient

μ_s – Scattering coefficient

A_d – Fraction of energy absorbed in the model

BDF – Backward Differential Formula

Cp – Heat Capacity

FE – Finite Element

FEM – Finite Element Method

g – Anisotropy factor

h – Heat transfer coefficient

k – Thermal Conductivity

Laser – Light Amplification by Stimulated Emission Radiation

LE – Living epidermis

LEP – Laser Evoked Potentials

MC – Monte Carlo

MCM – Monte Carlo Method

ND: YAP – Neodymium: Yttrium-Aluminium-Perovskite laser

OCT – Optical Coherence Tomography

PDF – Probability Density Function

PW – Photon walk

Q – Energy Source

R_d – Fraction of energy of diffused reflectance in the model

ROI – Region of Interest

SC – Stratum Corneum

SD – Standard Deviation

t – Time

T_d – Fraction of transmittance in the model

T_{max} – Maximum temperature

t_{pulse} – Laser pulse duration

w – Photon weight

ρ – Density

ω – Perfusion rate

1   Introduction

Pain perception is one of the most important physiological mechanisms of the human body. Pain serves as a protective system which functions by alerting us from injuries which require evasion or acute treatment. Painful sensations distinguish from hearing, smell, and sight senses because it has both an affective and emotional component. Pure painful stimuli are therefore non-existent in the human organism. The quality of the perceived pain is highly subjective, and may be influenced by several factors. Therefore, pain may be challenging to quantify objectively. (Kandel 2013)

Nociceptors reacts to noxious stimuli which is potential or actual tissue damaging. The related quality of the stimuli is carried out by higher order integration of the afferent volley. Nociceptors covers the entire skin in different concentration all over the body and in parts of the visceral organs, e.g. in ventriculus and intestines, or muscle system, e.g. joints, muscles, also defined as internal nociceptors. In the visceral organs, the modality is primarily seen as stretch responsive receptors, where painful sensations may occur when the organs are overstretched. In the skin, cutaneous nociceptors are responsive to thermal, chemical, and mechanical modalities. Sensations which may cause activation of these nociceptors are related to extremes of temperatures, dissolved chemicals in the tissue (results from a chemical release from a damaged cell), and mechanical damage in the tissue. Powerful stimuli may trigger all three nociceptor types. Pain and pain research has always been a very important field within medicine, primarily because pain often is the reason why people seek medical help. (Martini et al. 2012)

In pain research, it is vital to assesses the perceived stimuli to gain a better understanding of how the pain system functions and the related responses. Assessing pain responses are more complicated than assessing e.g. the sense of hearing, or sight, since they have single modalities where pain is polymodal. (R.-D. Treede et al. 2003) The polymodality of nociceptors increases the complexity of pain perception and distribution (Martini et al. 2012).

Present, following quantitative testing methods are being used to assess neuropathic pain: Von Frey filaments, wind-up ratio – temporal pain summation, pinprick stimulation with weighted needles, vibrational stimulation, pressure pain stimulation, and thermal stimulation (Rolke et al. 2006). Thermal stimulation in the form of laser stimulation has been confirmed to selectively activate thermal responsive free nerve endings, making it a monomodal painful stimulation (Cruccu & Truini 2009).

Light Amplification by Stimulation Emission Radiation, laser, are characterized by having a narrow spectrum of emitted light. Theory of principles behind laser technology derives from Albert Einstein's theory in *Quantum Theory of Radiation*. The theory describes excitation energy levels of atoms, and how they may emit light when the energy level changes from one to another. Here the theory describes both spontaneous and stimulated emission, where lasers are based on stimulated emission. (Hecht 2005)

In a medical context, lasers are being used in a variety of fields, e.g. Dentistry, ophthalmology, surgery, dermatology and neurology. See examples of laser applications in

Table 1.

Table 1 – Table lists a variety of scientific fields where laser technology is being applied, and examples of practical research related uses.

Scientific fields	Use
Dentistry	Laser stimulation may be used to function as a facilitator of chemical processes (Udart et al. 2011)
Ophthalmology	In ophthalmology lasers may be used in the imaging technique optical coherence tomography (OCT) (Welzel 2016; Kirillin et al. 2015) or as a treatment tool (Seifert et al. 2013)
Surgery	In surgery laser stimulation may be used to cause ablation in cardiovascular tissue (Rohde et al. 2013; Lanvin et al. 2015)
Dermatology	In dermatology lasers has been used in tattoo removal (Cenčič et al. 2013), 2-photon imaging technology (Göppner et al. 2011), laser-skin modeling (Karsten & Singh 2013), investigating skin melanoma (Jakovels et al. 2013), and investigate how different laser stimulation causes subsurface lesions in skin (Chang et al. 2015)
Neurology	In neurology lasers may be used to make laser evoked potentials (LEP) for research in a number of neurological disorders, such as Diabetic neuropathy, Wallenberg's syndrome, Multiple sclerosis, Tension-type headache, Central neuropathic pain, and Fibromyalgia (R.-D. Treede et al. 2003)

Based on this short review of lasers in different medical contexts, it is seen that laser technology is applied within the medical field. Especially in pain related diseases, lasers has become an important technology (R.-D. Treede et al. 2003).

Different laser types with different emitted wavelengths does not have similar penetration depths and light propagation profiles in the skin. The longer the wavelength, the more the skin will act as a black body and thereby have high amounts of energy absorbed from laser stimulation at the skin surface. When a laser has a low penetration, the nociceptors will be activated by passive heat transfer in the tissue. For lasers within the visible wavelengths, reflectance may cause high amount of light to not be absorbed in the skin. High penetration lasers, e.g. neodymium-YAG (1064 [nm]) and thulium-YAG (2000 [nm]), are harder to use and it is therefore more likely they will cause tissue damage, but may directly cause nociceptive activation. Some lasers, e.g. Argon and copper vapour, may cause coagulations with the superficial plexus in the skin, and other chemical reactions). (Arendt-Nielsen & Chen 2003)

The ability of withdrawal from stimuli which may cause damage is one of the most important protective systems in the human organism. Pain has both an emotional and affective component and multiple modalities, thus, making it hard to describe and quantify objectively. Laser stimulation has proven to provide one of the purest nociceptive stimulations, because it selectively activates only thermal responsive nociceptors. Lasers are used in many different medical fields, where pain research is one of them. Different laser types appear to have different properties when used on skin tissue. High penetration laser may cause directly activation of the nociceptors in the skin, while low penetration lasers may cause indirect activation of the nociceptors by passive heat transfer. It is unclear how the heat from laser stimulation is distributed in the skin using different laser types and how it may be effectively applied to cause painful sensations without

causing any tissue damage in a practical use. These observations lead to following initiating problem statement:

How can stimulation from different types of lasers be analysed in relation to causing pain without causing tissue damage and how can it be more accessible for future practical use?

2   Problem analysis

The solution of the initiating problem statement is based on a laser-skin stimulation model (Cid Royo et al. 2016), which dealt with a similar problem and will be referenced to as the previous model. In the previous model the solution to make laser stimulation easier to analyse and easier to use for future practical use, was to create a mathematical model. The mathematical model described how light propagates through the skin and consequently transfers into heat energy in the skin over time, and how the heating of the skin may be equal to nociceptive activation of A-delta fibres. The previous model was only assessed mathematically, thus, missing the experimental validation. Without the validation, it is hard to estimate practical application of the model. The experimental validation is therefore the motivation of this master thesis.

To analyse how such a model may be validated it is important to have get an overview of all the context related theory and how the model is constructed. It will be done by describing following items:

1. What mathematical modelling is and what it may be used to solve for
2. The anatomy of the skin
3. The underlying related physiological mechanisms of which highlights the efficiency of laser stimulation to induce pain on the skin surface
4. The previously mode, through an adequate description of model elements, physics, and important algorithms.
5. Critical elements of the previous model

This information will allow a narrow and precise problem formulation to be formulated to effectively validate the previous model.

2.1   Mathematical modelling

Mathematical modelling may be used to predict the behaviour of a physical or theoretical phenomenon. A model may be constructed of several systems or sub-models to describe the complexity of the phenomenon. The methods of the model may include; logical deductions from mathematical assumptions, solving equations, numerical or analytic methods, simulations and parameter estimations. Through a model, it is possible to gain insights into the complex system the model describes. The model itself is always a simplification of the real system, mechanism, or phenomenon. The process of building a model require insights into relevant objects, data, relations, conditions and assumptions related to the real-world problem. (Blum et al. 2007)

Mathematical modelling may be used to predict the outcome of laser stimulation applied to the skin. (Nasouri et al. 2014; Marchandise et al. 2014; Lu et al. 2012; Frahm et al. 2010) To ensure that a constructed mathematical model describing laser to skin stimulation is relevant, it is important to perform a mode validation. Through a validation process, the model will be checked whether the output of the model is related and comparable in relation to information given from the original problem. Without the validation, it will remain unknown whether a model is accurate in relation to the original problem or not.

2.2   Anatomical composition and structures of the skin

The skin organ covers around 1.5-2 m^2 of the surface of the body, and accounts for around 16 % of the total body weight. The skin functions as a defensive barrier towards the external environment, and protects against bacterial attacks, microorganisms, chemical exposure, sunlight screening, fluid loss, friction, and changes in temperature. The skin consists of two major components: The cutaneous membrane and accessory structures, see Figure 1. The cutaneous membrane contains the epidermis consisting epithelium cells and the dermis, primarily consisting of connective tissue. The accessory structures include: Multicellular glands, sensory organs, nerve fibres, hair and hair glands, and blood vessels. (Martini et al. 2012)
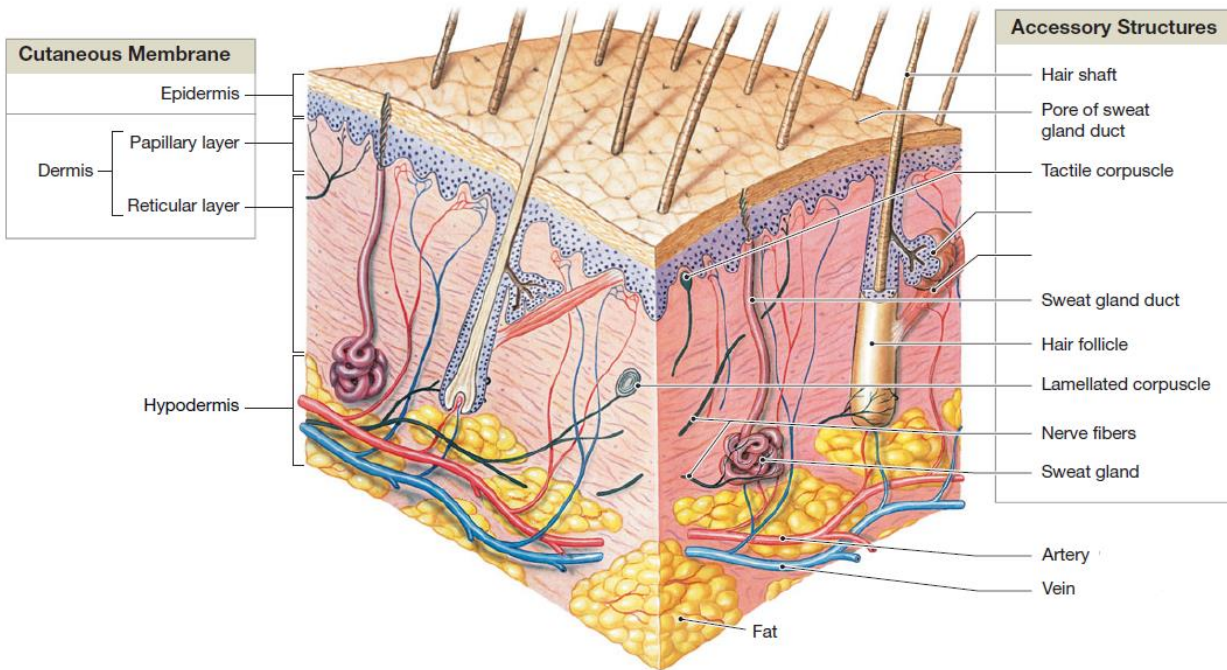
Figure 1 – Figure illustrates a cubic segment of skin tissue, including following layers from the outermost layer to the innermost layer: Epidermis, Dermis, and Hypodermis. The figure also shows examples of accessory structures in the skin tissue. Modified from (Martini et al. 2012)*.*

The epidermis is subdivided into following sublayers from outermost layer towards external environment to the dermis: Stratum Corneum, stratum lucidum, stratum granulosum, stratum spinosum, and stratum basale. (Martini et al. 2012) In this context, all epidermal layers, except stratum Corneum is defined as living epidermis.

The stratum corneum is a cornified layer, consisting of 15-30 layers of keratinized cells. The keratinization is a hardening, drying and flattening of the cells, enabling them to stack together in protective sheets or layers, forming relative waterproof membrane to the skin. The layer is not offered nutrition, and is expendable towards frictional damages and other damages. The skin thickness may variate dependent on location. (Martini et al. 2012)

The living epidermal tissue is contributing to pigmentation of the skin, contains sensory organs – such as tactile receptors, free nerve endings, and immune response organs. Absorption of light in the skin, is highly dependent on the amount of pigmentation in the skin. The living epidermis receives nutrition by diffusion from blood vessels in the dermis. (Martini et al. 2012)

Underneath the epidermis, the dermis is located. Blood vessels in dermis serves to provide nutrition to the tissue. The tissue has a higher concentration of water compared to epidermal tissue, because of local blood vessels in dermis. Furthermore, the dermis contains: Hair follicles, sweat glands, and sensory organs. (Martini et al. 2012)

Below the dermal tissue, lies the hypodermis. The hypodermis contains adipose and areolar tissue. The layer functions to stabilize the position of the dermis in relation to underlying structures such as bone, muscle, or organs. It also functions as a blood reserve for the general circulatory system and as insulation. (Martini et al. 2012)

2.3   Nociception

Nociception is the event of a noxious stimulation which may lead to a painful sensation/perception. Pain perception is subjective and may therefore be affected by several known and unknown factors, making pain a product of many different sensory inputs evaluated by the brain. Noxious stimulation may be perceived in a number of different ways e.g. pricking, burning, cold, aching, stinging, and soreness, which are some of the most common and distinctive pain modalities. (Kandel 2013)

The nociceptors nociception, the sensory response to noxious stimuli. There are three main classes of nociceptors: Thermal, mechanical and polymodal. Thermal nociceptors are generally responsive to temperatures under 5 °C and over 45 °C (Kandel 2013). The nociceptors are terminals, free nerve endings, of myelinated axons called A-δ, with action potential conduction velocities between 9.9±4.4 [m/s] (Kakigi et al. 1991). Mechanical nociceptors are also free nerve endings of A-δ fibres, are optimally most responsive to pressure. Polymodal nociceptors are responsive to mechanical, chemical, and thermal stimuli (Kandel 2013). They are free nerve endings of C-fibres, which are unmyelinated fibres and has an action potential conduction velocity of 0.87±0.21 [m/s] (Treede et al. 1995).

Stimulating the skin with noxious heat stimulation above 45 °C may activate both A-δ and C-fibres. Since both fibres have very different action potential conduction velocities, the quality and intensity of the perceived pain is different dependent on which fibre is activated. Activating A-δ fibres result in a phenomenon called first pain and activating C-fibres result in a phenomenon called second pain. First pain, A-δ activation, is perceived as an intense stinging or prickling feeling, while the second pain, C-fibre activation, is perceived less intense, compared to first pain, as a burning sensation. (Kandel 2013)

An important mechanism related to pain and pain perception is the gate-control theory. It is important when understanding the effectiveness of laser stimulation in relation to pain research. (R.-D. Treede et al. 2003)

2.3.1   Gate-control theory

Many interneurons are responsive directly to painful input while other receives convergent input both from nociceptive and non-nociceptive input. Where, the convergent input from non-nociceptive afferents inhibits the pain perception from a painful stimulus. This theory was first propose in 1965 by (Melzack & Wall 1967), and was described as the *Gate-control theory*. The theory describes the interaction between A-β fibre, C-fibres, projection neurons and inhibitory neurons. Non-nociceptive stimuli (C-fibre activation) acts as 'gate'-closer for central transmission of nociceptive input. (Melzack & Wall 1967) See mechanism construction in Figure 2.
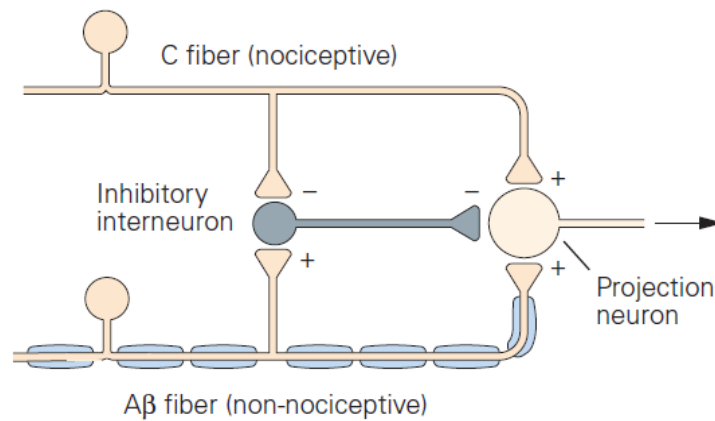
Figure 2 – The figure describes the theory of the gate-control mechanism. Activation of C fibre excites the projection neuron which oversees central transmission of noxious stimuli, and inhibits the inhibitory interneuron which remains inactive. Activation of Aβ fibre excites the inhibitory interneuron to actively inhibit the projection neuron, and excites the projection neuron. (Kandel 2013)

The level of non-nociceptive stimulation has a direct effect on how much of the noxious stimuli is being perceived as painful sensations. The mechanism is located at the dorsal horns of the spinal cord and may also occur at a supraspinal level. (Kandel 2013)

Noxious laser stimulation may therefore bypass the gate-control mechanism, as it only activates thermal receptors or/and thermal responsive nociceptors. In pain research, related brain activity cause by noxious laser stimulation is also referred to as laser evoked potentials (LEP). (R. Treede et al. 2003)

2.4   Nociceptive activation estimation laser-skin model

This section will describe the previous model, (Cid Royo et al. 2016), in relation to gaining a basic understanding of the model elements, physics, and functionality. To understand such a model, it is important to understand the flow of energy from the laser to heating of the skin and the consequently nociceptive activation:

When laser stimulate skin, wavelength specific photons interact with the surface of the skin by either, reflection, refraction, or diffusion within the tissue. Photons which are propagating inside the tissue may transfers into: Heat energy, chemical reactions, or be reemitted as light. Most of the photon energy will consequently be transferred into heat. The heat propagates over time throughout the tissue and may cause nociceptive activation, depended on the laser intensity and stimulation time. (Welch & Gemert 2011)

The model consists of two major parts: A Monte Carlo Model (MCM) and a Finite Element Model (FEM), see Figure 3. General for both model parts, is the specific geometry related to the anatomy of the skin.
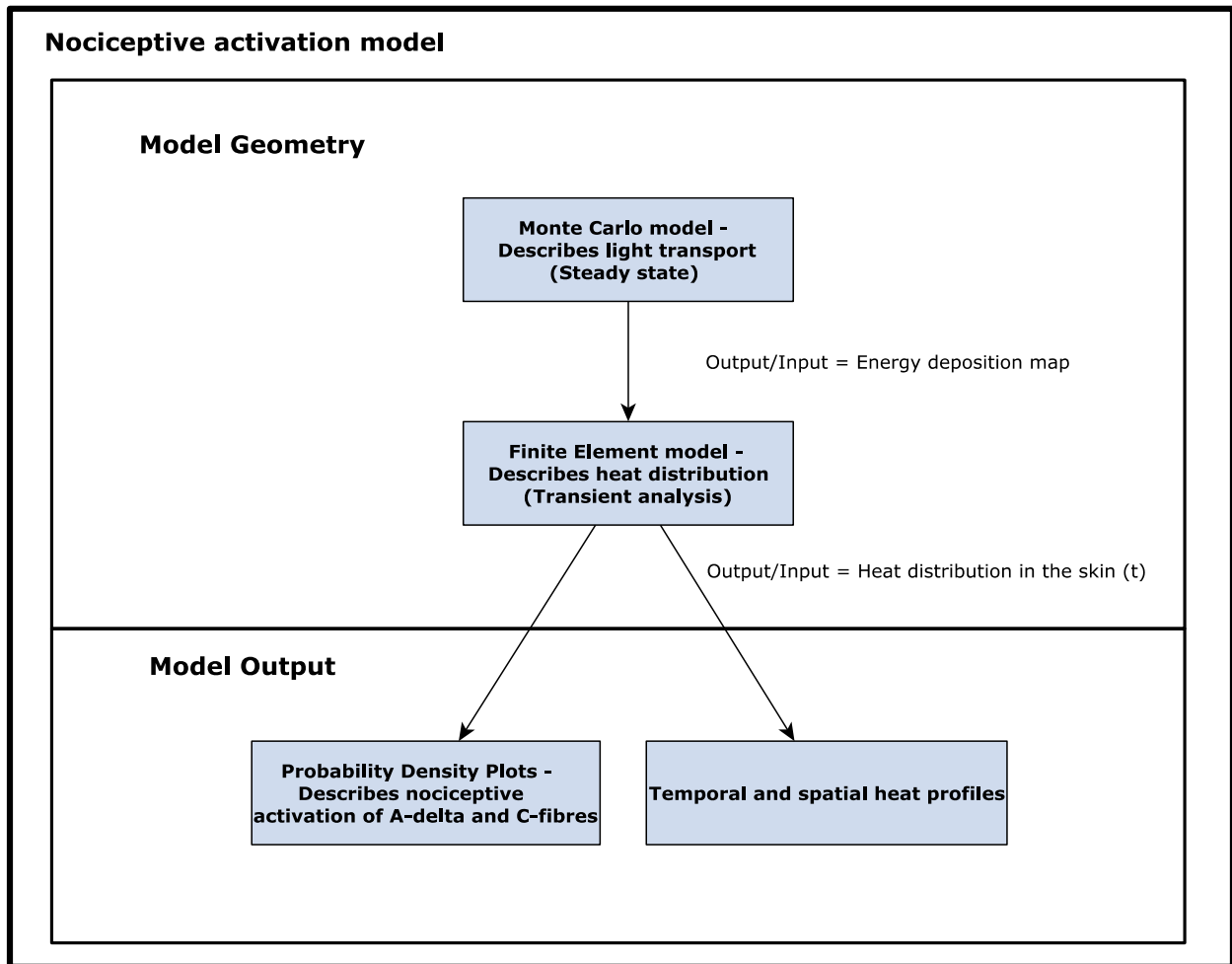
Figure 3 – The figures illustrates a simple overview of the model and the underlying elements. The model consists two mayor elements. The MCM and the FEM. Both elements share same geometry, which is a representation of the anatomy of the skin. The MCM describes how light in transported in the geometry, and output a steady state energy deposition map equivalent to 1 [W/m³]. The FEM takes the energy deposition map as input to described how the energy translates into heat and how the heat distribution in the geometry over time. Based on the FEM output, the model may generate approximated temporal and spatial heat profiles. The output may also be used to estimate the probability of nociceptive activation.

The MCM describes how the light is distributed in the skin, by simulating packages of photon equivalent to laser stimulation. It is an iterative process, which goal it is to replicate the natural distribution of photons in the skin. Specific material coefficients are input to the model to ensure a meaningful approximation of the phenomenon. The output of the MCM is a steady state analysis equivalent to how 1 [W] is distributed in the skin. This output will function as the input to the FEM.

The FEM describes how the resulting energy from the MCM over time translates into heat and how the heat propagates in the model over time. Specific material coefficients are used to ensure a meaningful estimation of the heat distribution.

The model is a simplification of the natural phenomenon and the deviations will be described in the implementation.

2.4.1   Methods of the model

The MCM implementation of the light absorption in the skin is derived from (Welch & Gemert 2011). The MCM is a statistical method which computes repeated random samples to create a numerical result. The more iterations included in the analysis, the more the result points towards a deterministic result. (Kroese et al. 2014) The implementation of the MCM is derived from (Welch & Gemert 2011), and will be described below.

After the light propagation is described, the relative consequential heat generation and distribution over time in the tissue is described. This is implemented through a FEM implementation in COMSOL (COMSOL Multiphysics, version 5.2, Sweden). The heat transfer throughout the geometry is described as a transient problem.

FEM generate an approximation of the solution. The method describes how energy transfers between a finite number of elements in a specified geometry. A higher number of elements might result in longer computational time and a more precise solution, compared to creating results using lesser number of elements which would require less computational time. It is possible to achieve convergence between number of elements and the precision of the solution. The accuracy of the model depends on the quality of the implementation. (Cook et al. 2001)

2.4.2   Light propagation physics of the model

To understand the physics behind light and skin interaction, the following sub-section will describe a photons path when directed towards skin. A photon traveling interacting with the skin may either be; absorbed or not absorbed in the medium at incident. If the photon is not absorbed, it may either be reflected on the surface of the medium or be transmitted through the medium in another direction (referred to as scattering), this is also referred to as scattering. If the photon is absorbed in the tissue, follow three processes may occur: Generation of heat, energy is used to drive a chemical reaction, or re-emitted as light.

To understand how the light propagates in the tissue, the different concepts of tissue-light interaction will be described:

2.4.2.1   Anisotropy factor

The anisotropy factor describes the directional dependence of a photon, following a scattering event in a specific medium. The coefficient ranges from 0 to 1, where 0 displays an equal probability to all possible scattering angle regardless of incident angle and 1 displays a scattering angle equal to the incident angle.

The factor may be described by the Henyey-Greenstein scattering function in a two-dimensional space. See the function in Figure 4. Generally, the anisotropy factor is dimensionless. (Jacques & Prahl 1998)
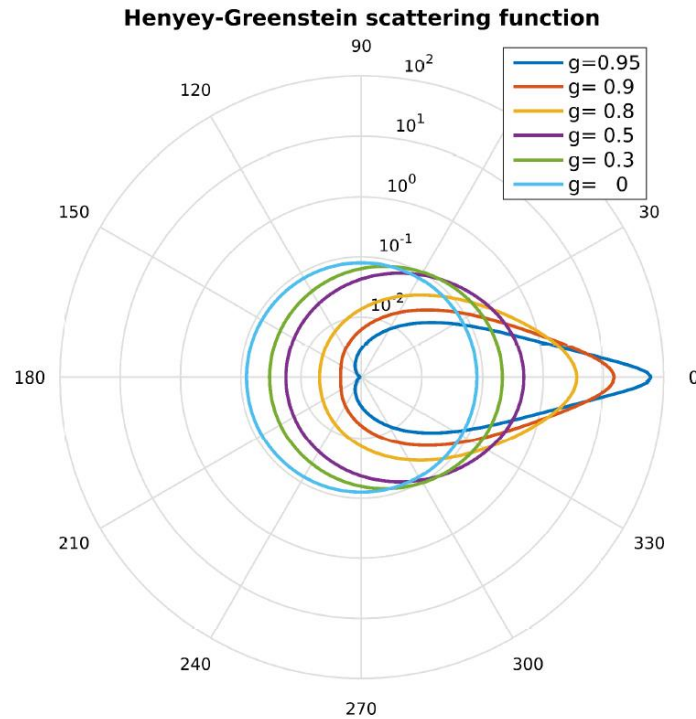
Figure 4 – Illustrates the Henyey-Greenstein scattering function, describing scattering at different anisotropy values ranging from 0 to 0.95. 0 degrees indicates same direction as incident angle before scattering event. 180 degrees indicates the opposite direction of incident light. The radial direction relates to the probability of a specific angle. The anisotropy factor is dimensionless and may be generalized to all spatial dimensions. Illustration from (Cid Royo et al. 2016)*, data from* (Jacques & Prahl 1998)

Scattering angle is sampled by following equation:

$$\cos\theta = (\frac{1 + g^2 - (\dfrac{1 - g^2}{1 - g + 2g \cdot RND})^2}{2g})$$

Where, θ is the scattering azimuth angle of the new trajectory, *RND* is a random number between zero and one and *g* is the anisotropy factor of the specific material.

2.4.2.2   Scattering and reduced scattering coefficient

The scattering coefficient describes the probability of light being scattered in a medium. The probability, T_r, is dependent on photon travel path length and scattering coefficient, μ_s. T_r is described by following equation:

$$T_r = e^{-\mu_s * L}$$

Equation 2

Where *L* is the specific photons path length in [cm] up until the specific scattering event. Along with the anisotropy factor they describe the diffusion of light in a medium. This relationship may be described in the reduced scattering coefficient, μ_s':

$$\mu_s' = \mu_s(1 - g)\ [cm^{-1}]$$

Equation 3

Where μ_s is the scattering coefficient and *g* is the anisotropy factor. The reduced scattering is in some cases used to calculate *g,* since *g* may be hard to measure experimentally. (Jacques & Prahl 1998)

2.4.2.3   Reflection and Refraction index

When a photon interacts with a medium surface, two things may occur, reflection or refraction. Reflection is defined as when the photon does not propagate from the one medium (incident medium) to another (transmission medium), but is instead reflected from the surface between the two mediums. Refraction is defined as when a photon is propagating from incident medium to transmission medium, along with a change in direction. The refraction angle is depended on the refraction index of both incident and transmission mediums, and may be described by following equation:

$$n_i \sin(\theta_i) = n_t \sin(\theta_t)$$

Equation 4

Where n_i is refraction index of incident medium, θ_i is the angle of the incident light on boundary between the two mediums, n_t is refraction index of transmission medium, and θ_t is the exit angle of the transmitted light in the transmission medium. (Wells et al. 2011)

2.4.2.4   Absorption coefficient

Refraction of light include absorption of energy in the tissue. The absorbing molecules change energy state at the event of the absorption where three different outcomes will happen: Heat generation (increase of

vibrational or rotational energy) or an increase of electric state of the molecule. A change of electric state of a molecule may result in either re-emission as light (fluorescence or phosphorescence) or may function to drive a chemical reaction. (Wells et al. 2011)

The probability of which event may occur at absorption is dependent on the wavelength of the photon and specific material elements/properties. Some material elements in skin tissue are large light absorbing molecules known as chromophores. Chromophores are the largest contributor to absorption of infrared light. (Jacques & Prahl 1998)

The absorption coefficient, μ_a, is defined as the probability of photons being absorbed in a material at a specific wavelength. It can be found by measuring amount of light surviving propagation through a material.

2.4.3   Implemented Monte Carlo algorithm

Following general assumptions are made of the implemented Monte Carlo algorithm:

- An isotropic distribution of R- and P-polarized photons from the light source, and does not change over time.
- Each layer in the model is modelled as a uniform mass, excluding possible structures in the tissue.
- Photon packages are modelled instead of individual photons. This is assumed to produce similar results.
- Energy deposited outside of the model geometry is excluded from the model - this includes energies outside of the radial and horizontal boundaries of the model towards internal environment of the body.

Following section describes the implemented MC algorithm:

Implementation is based on the MC implementation from (Welch & Gemert 2011). All incident light in the model may be summed in following three definitions:

- R_d, Remission – fraction of energy which is not absorbed in the medium, e.g. reflection, radiating light from the surface of the model to external environment
- A_d, Absorption – fraction of energy which is absorbed in the medium
- T_d, Transmission – fraction of energy which is transmitted through the medium

A_d, will be distributed along a 3-D grid where the size of each bin in the grid define the resolution of the simulation. The 3-D simulation will then be translated into a 2-D axial model to fit with the FE implementation. The smaller the bins of the grid, the more iterations are needed to give a satisfying approximation. The recommended amount of iterations is equal to the number of bins in the r direction times the number of bins in the z direction. (Prahl et al. 1989)

The implemented algorithm is divided into following nine steps:

2.4.3.1   *Step 1 – Initiate photon packages*

The photons are directed and fired towards the surface of the model. The incident position on the surface is defined by a random location derived from the beam PDF. At initiation, the photon is assigned a photon weight, *w*, of 1. Every iteration of a simulation begins at *Step 1*.

2.4.3.2 Step 2 – Surface reflection or refraction

When the initiated photon directed towards the surface of the model, it is determined if the photon is either reflected from the surface or refracted within the surface. If the photon is reflected from the surface, the energy is added to R_d

2.4.3.3 Step 3 – Step

If the photon is refracted the path of the photons must be determined. Refraction only occurs if a boundary has been crossed. Here individual discrete steps of the photon path are calculated using following equation:

$$s = \frac{-\ln(RND)}{\mu_a + \mu_s}$$

Equation 5

Where *s* is the step length and RND is a random number between zero and one. As part of the step calculation, the algorithm checks if a boundary has been crossed with the calculated step length, *s*. See *Step 4*.

2.4.3.4 Step 4 – Boundary check

As part of *Step 3* the algorithm checks if a boundary between two mediums has been crossed. If a boundary has been crossed, a new *Step 3* is calculated with the material properties of both interacting mediums at the crossed boundary. Energy reflected from the tissue surface to the air is added to R_d and energy propagating through the model, model to internal environment, is added to T_d.

2.4.3.5 Step 5 – Energy absorption

Now the photon deposits a fraction of energy in the tissue. The amount of energy deposited is dependent on μ_a, μ_s and the photon weight, *w*. The amount of energy absorbed is calculated with following equation:

$$w_{absorbed} = w_{old} \cdot \frac{\mu_a}{\mu_a + \mu_s}$$

Equation 6

Where $w_{absorbed}$ is the fraction of weight absorbed at the energy absorption event and w_{old} is the weight of the photon from before the absorption event. The new photon weight is then derived by subtracting $w_{absorbed}$ from w_{old}. (Prahl et al. 1989) All absorbed energy is added to, A_d, the fraction of absorbed energy.

2.4.3.6   Step 6 – Scattering

The photon is now scattered into a different angle relative to incident angle at scattering event. The new angle is defined by a deflection angle and an azimuth angle. The deflection angle is a dependent on a number between zero and 2π. The azimuth angle is dependent on the anisotropy factor, g, and is calculated via the Henyey-Green Scattering Function. (Prahl et al. 1989) See the Henyey-Green Scattering function sampled in subsubsection Anisotropy factor 2.4.2.1.

2.4.3.7   Step 7 – Terminate photon package?

As the photon propagates through the tissue the equivalent photon weight become smaller and smaller as it is partly absorbed at each step. When the photon weight reaches a chosen low threshold, it is decided whether to terminate the photon or not. The decision of termination is made if the photon weight is below 10^{-4}. (Prahl et al. 1989)

If the photon weight is below the low threshold a random number between 0-1 is generated. If the number is below a certain CHANCE threshold (implemented as 0.1) the weight is divided by the CHANCE threshold, increasing the weight by a 10-fold, and propagation may continue. Consequently, every ninth photon out of ten will continue propagation after the chance roll. Energy conservation is statistically still preserved as the simulation is run with millions of iterations. This method is known as the *"Roulette method".* (Prahl et al. 1989)

2.4.3.8   Step 8 – Terminate simulation?

This step evaluates how many iterations have gone in the simulation. If the simulation count has not reached the desired amount of iterations another iteration is made (back to step 1). When the iteration count has reached the number of wanted iterations, the simulation is stopped and may proceed to the final step. (Prahl et al. 1989)

2.4.3.9   Step 9 – Generate energy absorption profile

Here at the final step, the Cartesian coordinates from the 3D MC implementation needs to be transformed into polar coordinates which fit the 2D-axial geometry. The generated result is normalized relative to total amount of iterations run in the specific simulation.

See a flowchart of the implemented MC algorithm in Figure 5.
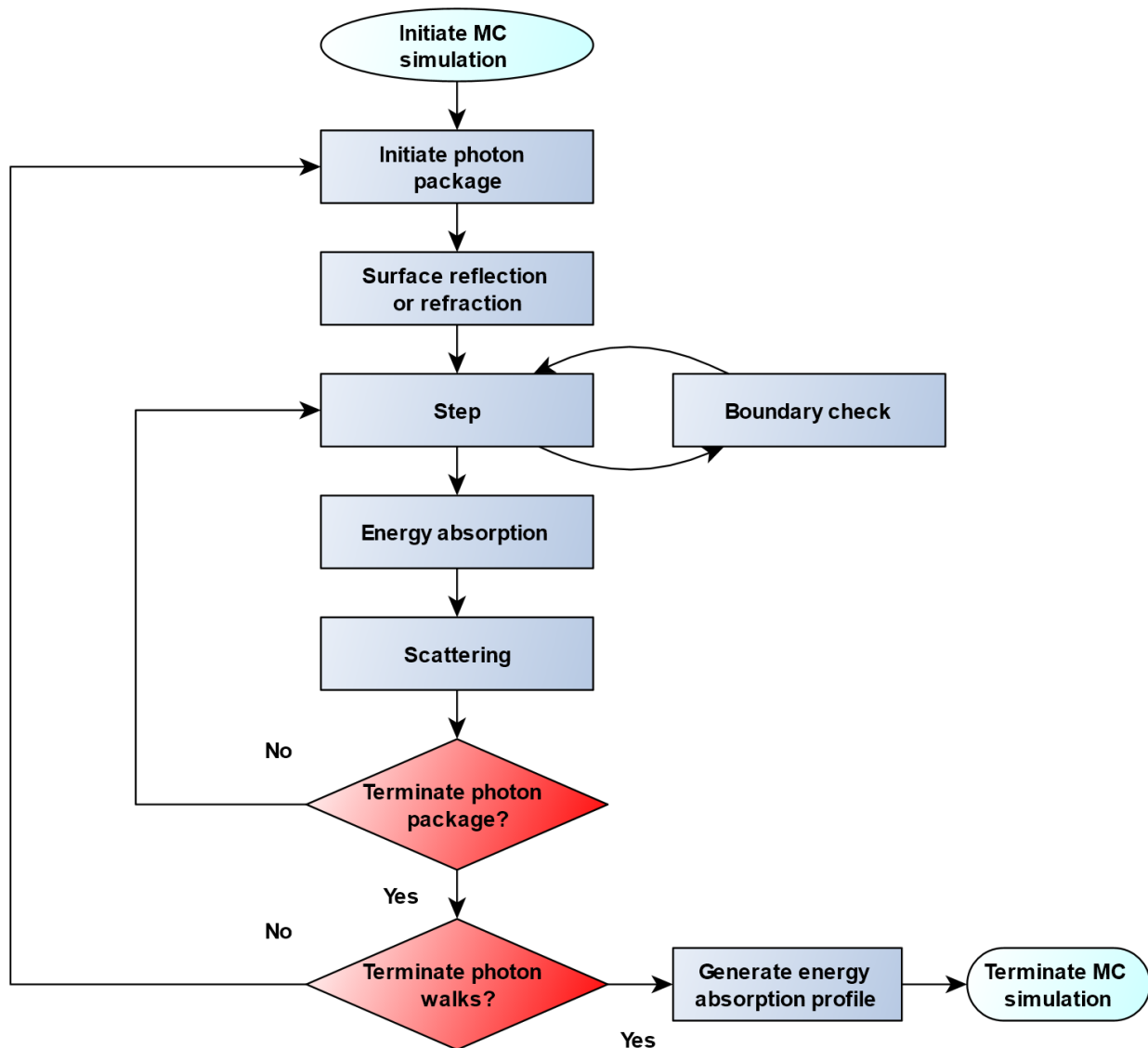
Figure 5 -The figure illustrates a flowchart describing the implemented MC algorithm.

2.4.4 Coefficients of the MC implementation

In this section, the calculations and references of the coefficients in the MC implementation will be described and displayed. Absorption coefficient, scattering coefficient, and refraction index will be modelled as being dependent on wavelength and the anisotropy factor will be modelled as being independent on wavelength

2.4.4.1 Absorption coefficient

To describe the absorption coefficient for the skin, major elements and their absorption must be considered. The absorption coefficient of the skin includes elements of water, oxy-hemoglobin, deoxy-hemoglobin, melanosome, and lipid, and may be described by following equation:

$$\mu_{a.layer} = f_{v.blood}SO_2\mu_{a.oxy}(\lambda) + f_{v.blood}(1 - SO_2)\mu_{a.deoxy}(\lambda) + f_{v.water}\mu_{a.water}(\lambda) + f_{v.lipid}\mu_{a.lipid}(\lambda)$$
$$+ f_{v.mel}\mu_{a.mel}(\lambda)$$

Equation 7

Where, $\mu_{a.water}$ is the absorption coefficient of water (Hale & Querry 1973), $\mu_{a.oxy}$ is the absorption coefficient of oxy-hemoglobin (Prahl 1999), $\mu_{a.deoxy}$ is the absorption coefficient of deoxy-hemoglobin (Prahl 1999), $\mu_{a.mel}$ is the absorption coefficient of melanosomes (Jacques 2013), $\mu_{a.lipid}$ is the absorption coefficient of lipids (Veen & Sterenborg 2004; ElMasry & Nakauchi 2015), f_v is the volume fraction of each specific element in a specific layer, and SO_2 is the saturation of haemoglobin.

The volume faction of each skin element, f_v, is also defined by the literature. See references and values in Table 2.

Table 2 – Table shows volume fractions of each skin element in each layer. Values are derived from following references (Meglinski & Matcher 2002)[a], (Karsten & Smit 2012)[b] , (Zamora-Rojas et al. 2013)[c]. Dash-symbol means that the value has not been identified through the listed references, or that the volume faction is assumed to be neglectable small.

Layer	SO_2	$f_{v.blood}$	$f_{v.mel}$	$f_{v.water}$	$f_{v.lipid}$
Stratum Corneum	-	-	-	0.05[a]	-
Epidermis	-	-	0.0255[b]	0.20[a]	-
Dermis	0.60[a]	0.12[a]	-	0.65[a]	-
Hypodermis	0.60[a]	0.05[a]	-	0.81[c]	0.10[c]

Inserting given functions, from Equation 7, with given values, from Table 2, in Equation 7 yields values for the absorption coefficient, μ_a, for each skin layer. See Figure 6.
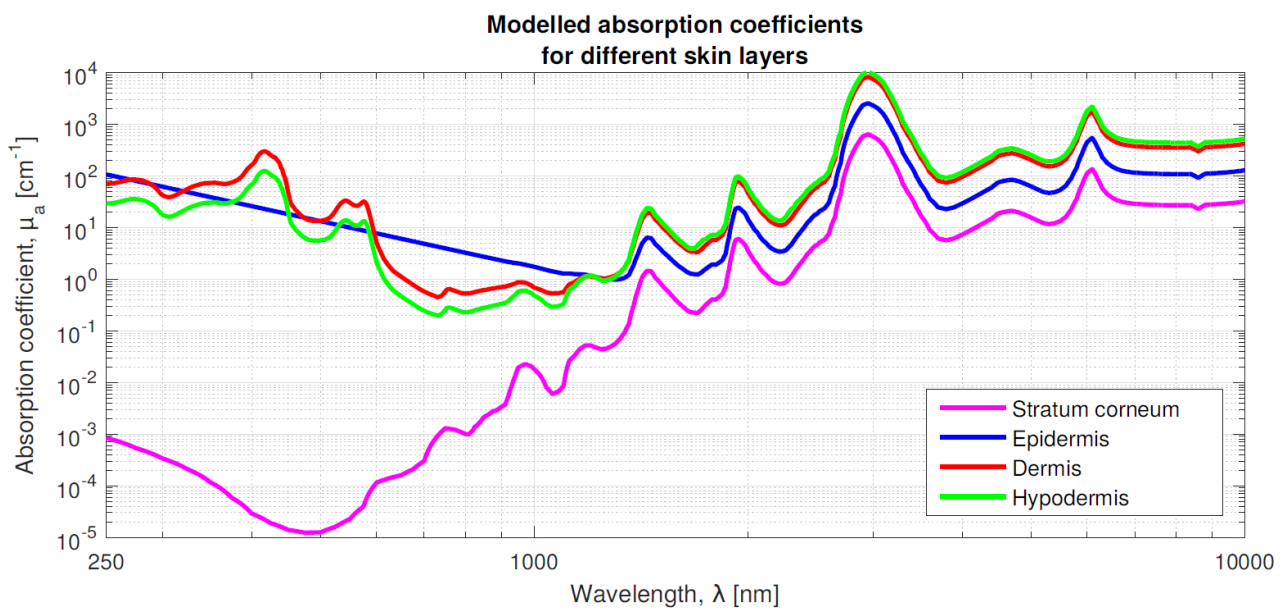
Figure 6 – Figure illustrates a graph describing modelled absorption coefficients, μ_a, using Equation 7, for the different skin layers in the model, for wavelengths, λ, between 250 and 10,000 [nm]. Stratum Corneum is marked in pink, Epidermis is marked in blue, Dermis is marked in red, and Hypodermis is marked in green. Figure is borrowed from (Cid Royo et al. 2016).

2.4.4.2   Anisotropy factor and scattering coefficient

Anisotropy factor for SC is defined as 0.9 and is a derived mean from (Meglinski & Matcher 2002; Zeng et al. 1997; Bashkatov et al. 2011; Van Gemert et al. 1989). For living epidermis, anisotropy is defined as 0.75 and derived from mean of values from (Bashkatov et al. 2011; Van Gemert et al. 1989). Values for dermis is defined as 0.8 and is a derived mean from (Bashkatov et al. 2011; Zeng et al. 1997). Anisotropy for hypodermis is defined as 0.85 and derived from mean of values from (Meglinski & Matcher 2002; Hartmann et al. 2015; Bashkatov et al. 2005). See quality of used studies in Table 3.

Table 3 – Table shows the references of the anisotropy factor, their corresponding study type and the related tissue used in determination of the anisotropy factor. The table has the purpose of getting an overview of the quality of the references.

Reference	Type of study	Tissue
(Meglinski & Matcher 2002)	Mathematical modelling	SC
(Zeng et al. 1997)	Mathematical modelling	SC, dermis
(Bashkatov et al. 2011)	Review study	SC, living epidermis, dermis, hypodermis
(Van Gemert et al. 1989)	Review study	SC, living epidermis
(Hartmann et al. 2015)	Mathematical modelling	Hypodermis
(Bashkatov et al. 2005)	Tissue study (Porcine)	Hypodermis

To obtain values for the scattering coefficient in the different layers in skin tissue, the reduced scattering coefficient is being used to calculate it. The scattering coefficient is dependent on the reduced scattering coefficient and the anisotropy factor, thus it may be calculated by following equation:

$$\mu_s = \frac{\mu'_s}{1 - g}$$

<div align="right">Equation 8</div>

Where, μ'_s is the reduced scattering coefficient, g is the anisotropy factor, and μ_s is the scattering coefficient. The reduced scattering coefficient is modelled according to (Chaoying & Wang 2015), which is a model combining theory including Rayleigh and Mie scattering. Rayleigh scattering includes modelling of scattering caused by small structures such as cellular structures and small collagen fibres. Mie scattering includes modelling of larger structures such as large collagen fibres. The model does not consider sublayers in epidermal tissue, thus, Stratum Corneum will be modelled equally as the epidermis.

Following equations are used to calculate reduced scattering coefficient for epidermis:

$$\mu'_s(Epidermis) = 2 \cdot 10^5 \cdot \lambda^{-1.5} + 2 \cdot 10^{12} \cdot \lambda^{-4} \ [cm^{-1}]$$

<div align="right">Equation 9</div>

Where, the red part of the equation is related to Mie scattering and the blue part of the equation is related to Rayleigh scattering (Chaoying & Wang 2015). The μ'_s for dermis is calculated by:

$$\mu'_s(Dermis) = 0.5 \cdot \mu'_s(Epidermis)$$

<div align="right">Equation 10</div>

Where, λ is the wavelength (Chaoying & Wang 2015). Reduced scattering coefficients for hypodermis is derived from (Petrov et al. 2012) and is calculated with following equation:

$$\mu'_s(Hypodermis) = 177.7 \cdot e^{-0.007978 \cdot \lambda} + 8.047 \cdot e^{-0.001208 \cdot \lambda} \ [mm^{-1}]$$

<div align="right">Equation 11</div>

See graph for the scattering coefficient each layer for wavelengths between 400 and 10,000 [nm] in Figure 7.
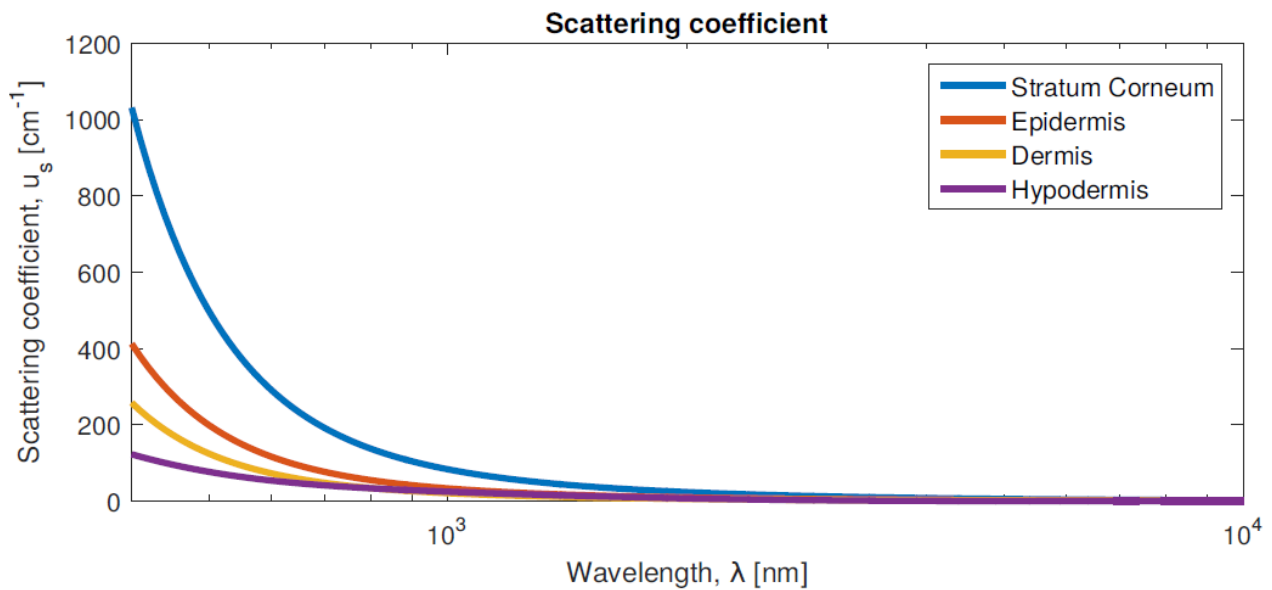
Figure 7 – Figure illustrates the values for the scattering coefficient for Stratum Corneum, Epidermis, Dermis, and Hypodermis. Values are included for wavelengths between 400 and 10,000 [nm], calculated using Equation 9, Equation 10, Equation 11, and Equation 8. Figure is borrowed from (Cid Royo et al. 2016).

2.4.4.3   Refraction index

Refraction index dependent on wavelength for epidermis, dermis and hypodermis is being modelled with Cauchy dispersion. Cauchy dispersion is described with following equation (Ding et al. 2006):

$$n = A + \frac{B}{\lambda^2} + \frac{C}{\lambda^4}$$

Where, n is the refraction index, A, B and C is the specific coefficients for the specific skin layer, and λ is the wavelength. Coefficients A, B and C are based on experimental data and were for epidermis and dermis borrowed from (Ding et al. 2006) and coefficients for hypodermis were borrowed from (Zamora-Rojas et al. 2013). See specific coefficients in Table 4.

Table 4 – Table shows specific coefficients for calculating refraction index for all skin layers, dependent on wavelength using Cauchy dispersion, see Equation 12. †(Ding et al. 2006) , ‡(Zamora-Rojas et al. 2013).

Layer	A	B	C
Epidermis†	1.4134	7907.9596	-3899784
Dermis†	1.3696	3916.8026	-2558.7704
Hypodermis‡	1.4753	4392.2	$0.952385 \cdot 10^{-8}$

Refraction index for Stratum Corneum is modelled as having the same value for all wavelengths. See values for refraction index for all skin layers in Figure 8.
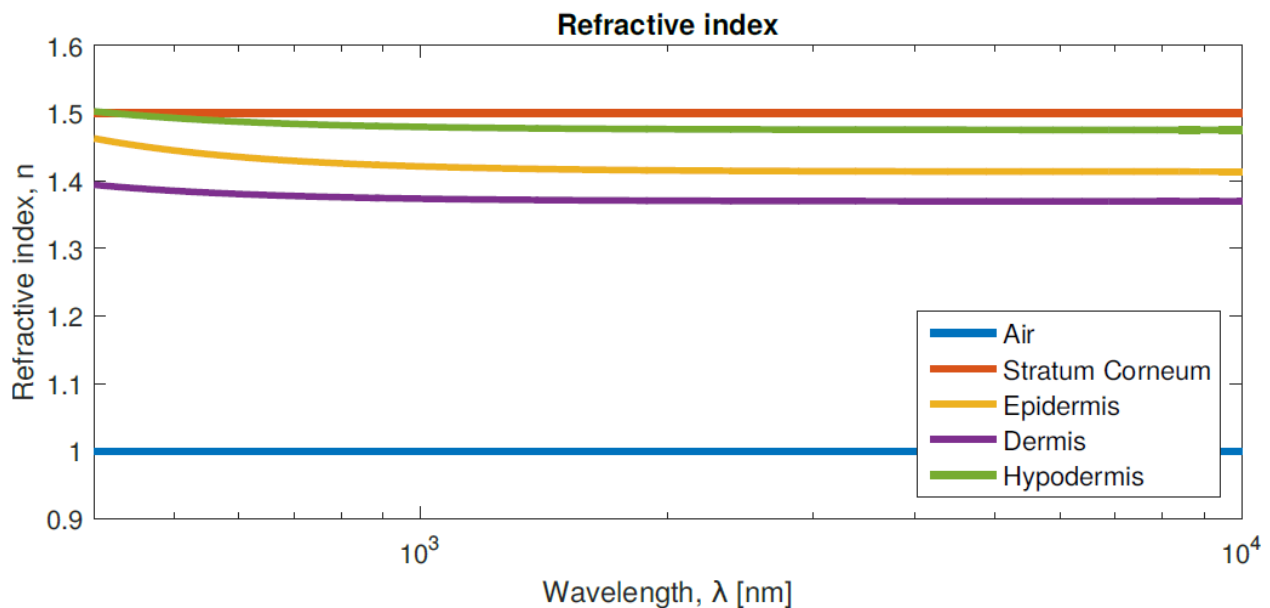
Figure 8 – Figure illustrates functions of refraction index values for each skin layer and air, for wavelengths between 400 and 10,000 [nm]. Functions for epidermis, dermis, and hypodermis are based on Cauchy dispersion, see Equation 12. Refraction index for Air does not change in relation to wavelength. Figure is borrowed from (Cid Royo et al. 2016).

2.4.5 Physics of the heat transfer in the model and implementation in COMSOL

The resulting distribution of energy in the 2D-axial model, is now transferred into heat, as vibrational or rotational energy in the molecules of the tissue. As soon as the energy starts to stimulate the skin, heat is

transferred and heat propagation initiates in the skin. The different layers in the skin has several material properties which is important to describe how the heat may propagate. To describe how the heat propagates, the Bioheat equation, (Pennes 1948), is used in the study:

$$\rho_t Cp_t \frac{\partial T}{\partial t} = \nabla \cdot (k_t \nabla T) + Q_{bloodPerfusion} + Q_{metabolism}$$

<div align="right">Equation 13</div>

Where, ρ_t [kg/m³] describes tissue density, Cp_t [J/kg·K] describes heat capacity at constant pressure in the tissue, k_t [W/m·K] describes the thermal conductivity in the tissue, T °C is the temperature in the tissue, $Q_{bloodPerfusion}$ describes the rate of heat generated from blood flow in the tissue, and $Q_{metabolism}$ [1/s] describes the energy generated in the tissue due metabolic heat generation. The equation is solved for $\partial T/\partial t$ to describe changes in temperature over time. The bioheat equation is a further development of the Fourier equation, which is often used in heat transfer in solids. The Fourier equation is equal to the Bioheat equation minus $Q_{bloodPerfusion}$ and $Q_{metabolism}$. (Welch & Gemert 2011)

$Q_{bloodPerfusion}$ is further defined by following equation:

$$Q_{blood} = \rho_b Cp_b \omega_b (T_b - T)$$

<div align="right">Equation 14</div>

Where ω_b [1/s] is equal to the blood perfusion rate in the tissue and T_b °C is the body core temperature at stimulation site.

Implementation in COMSOL is made by applying the, Pennes 1948, bioheat equation plus applied energy from the laser multiplied by the step function, see following equation:

$$\rho_t Cp_t \frac{\partial T}{\partial t} = \nabla \cdot (k_t \nabla T) + Q_{bloodPerfusion} + Q_{metabolism} + (Q_{laser} * LaserPower * StepFunction)$$

<div align="right">Equation 15</div>

Where Q_{laser} is the output of the MC model and is defined as a linear interpolation of the beam profile across the geometry. The Q_{laser} is therefore not dependent on the mesh of the model. The *LaserPower* is a value corresponding to the Wattage of the laser output. $Q_{metabolism}$ is only added to epidermis and hypodermis (Xu et al. 2008).

*Table 5 – Boundary conditions and heat sources are shown in the table, along with the mathematical expression. Description includes both stationary and transient boundary conditions. **q** is the total energy applied at the boundary, **n** is the rate at which the total energy is applied, **u** is change of temperature over time, **T**$_{stationary}$ is defined as the boundary temperatures of the external environment to the model derived from the stationary study, **T** is the temperature at the boundary, **h** is the heat transfer coefficient between the air and skin surface (value of 4.7 [W m^{-2} K^{-1}] from (de Dear et al. 1997)), **Q**$_{laser}$ is the applied laser energy, **Q**$_{metabolism}$ is the applied energy from tissue metabolism, and **Q**$_{bloodPerfusion}$ is the energy applied from blood perfusion in the tissue. Changed boundary conditions is marked with †.*

Boundary	Expression
All layers	Rotated around z-axis, model cornered (geometry to external environment) at r=0
Boundaries between the model and internal environment	Stationary: $\quad -q \cdot n = 0$ Transient: $\qquad T = T_{stationary}$
Boundary between the model and external environment	Stationary: $\quad -q \cdot n = 0$ Transient: $\quad -q \cdot n = h \cdot (T_{ext} - T)$
Heat sources	
Laser energy (All layers)	$Q_{laser} \cdot 1$ [W]
Metabolic (All except SC) and blood perfusion energy (Dermis and hypodermis)	$Q_{metabolism} + Q_{bloodPerfusion}$

2.4.6 Implementation of heat transfer in COMSOL

This section describes the implementation of heat transfer in COMSOL, and the disposition of the section is following the specific workflow of COMSOL, where constructing a model has following six steps: *Definitions, Geometry, Materials, Physics, Mesh, and Studies*.

2.4.6.1 Definitions

The laser stimulation is defined as a heat source (Q_{laser}) of 1 [W] layered over the entire geometry. The specific form and distribution of the heat source is computed in the MC simulation and is dependent on the wavelength of the laser and thicknesses of each layer in the model. The geometry from the MC implementation follows the geometry of the FEM implementation in COMSOL. The heat source is implemented as an interpolation of the computed results from the MC simulation, which makes the heat source resolution independent from the resolution of the FEM implementation.

To control the ON/OFF output of the laser in the FEM implementation, the Q_{laser} is multiplied by a rectangular step function (ranging from 0-1), with the width of the specific pulse length.

2.4.6.2 Geometry and Mesh

The model creates solutions for a r-z plane which is defined as a skin slice perpendicular to the skin surface. The slice is then rotated around the z-axis to create a 3-D visualization, see Figure 9. This is also defined as a 2-D axis symmetrical model, which has the advantage of having fast computational times compared to the equivalent of a real 3-D model (Comsol 2012).
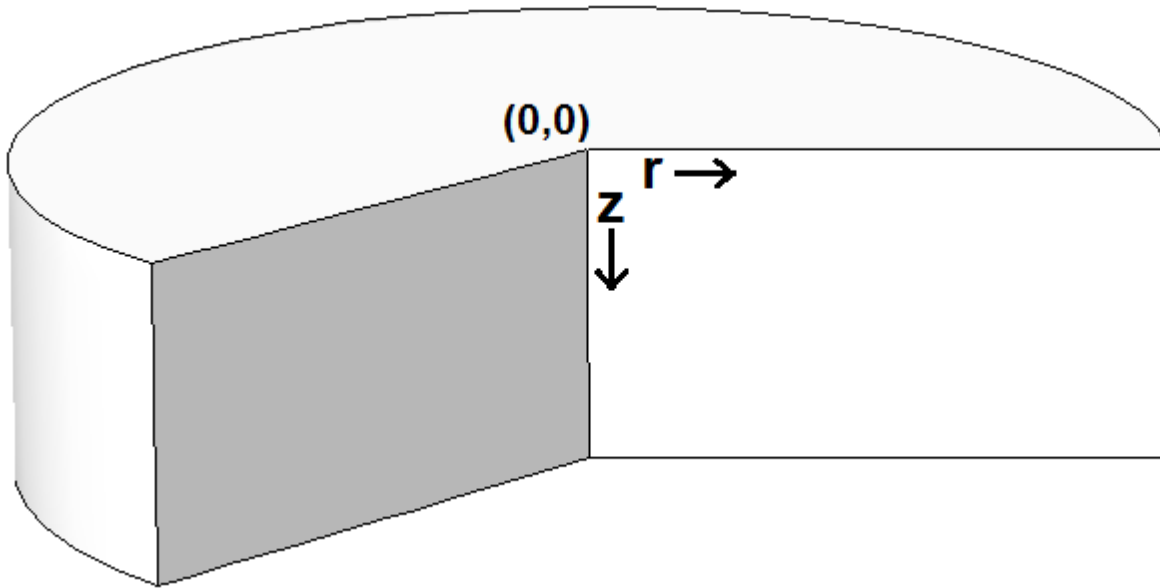
Figure 9 – Shows an example of a 2-D axial geometry. The difference between a simple 2-D geometry and the 2-D axial is the visual representation where the geometry is rotated around the z-axis. The geometry is cornered at (0,0) in the centre of the image.

Following four layers are included in the model: SC, living epidermis, dermis, and hypodermis. Each layer thickness is derived from experimental studies, where a mean of the values was used. This created a model provides a general solution of the problem. The specific layer thickness was for: SC = 18 [μm], epidermis = 82 [μm], dermis = 1.55 [mm], and hypodermis = 4 [mm]. The width of the model was defined as 30 [mm].

Table 6 – Table gives an overview of each layer and their specific thickness and coefficient values. Cp is defined as heat capacity, k is defined as thermal conductivity and ρ is the density of the material. Q_{met} is related to the heat generation in the tissue related to metabolism from (Xu et al. 2008)*s.*

Layer	Thickness	Coefficient values
Stratum Corneum	18 [μm]	k = 0.2375 [W m^{-1}K^{-1}], ρ = 1330 [kg m^{-3}], Cp = 3616 [J kg^{-1}K^{-1}]
Living epidermis	82 [μm]	k = 0.2375 [W m^{-1}K^{-1}], ρ = 1300 [kg m^{-3}], Cp = 3616 [J kg^{-1}K^{-1}], Q_{met} = 368.1 [W m^{-3}]
Dermis	1.55 [mm]	k = 0.48 [W m^{-1}K^{-1}], ρ = 1150 [kg m^{-3}], Cp = 3363.4 [J kg^{-1}K^{-1}], Q_{met} = 368.1 [W m^{-3}]
Hypodermis	4 [mm]	k = 0.173 [W m^{-1}K^{-1}], ρ = 950 [kg m^{-3}], Cp = 2443.75 [J kg^{-1}K^{-1}], Q_{met} = 368.3 [W m^{-3}]

See Table 6 for specific coefficient values and thicknesses for the different layers and see Figure 10 for complete geometry.
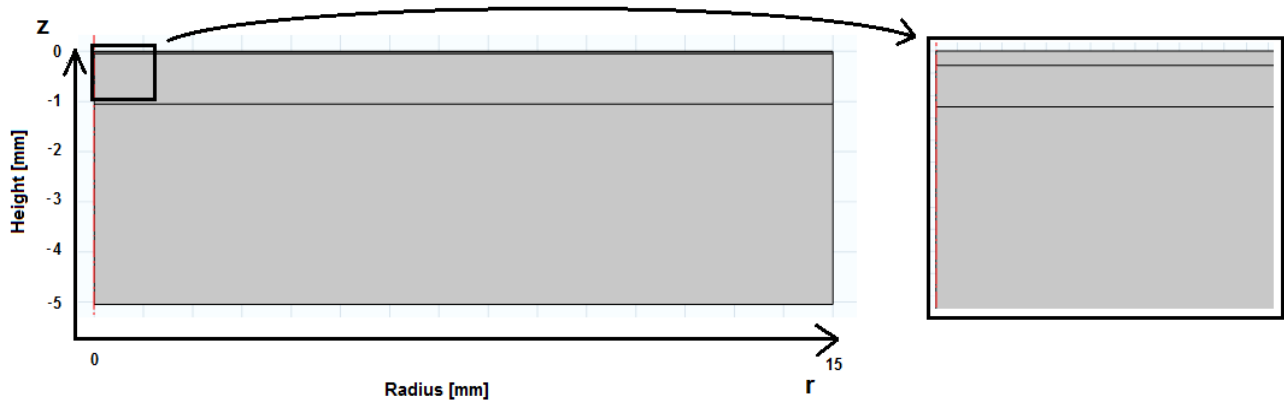
Figure 10 – The left figure illustrates the implemented geometry of the model. The right figure is a zoomed part of the geometry, cornered at (0,0), which shows top layers of the model.

The mesh of the model was set to a default autogenerated triangular mesh with a setting of *Extremely Fine,* see mesh in Figure 11. Choosing this setting ensures a high-resolution mesh and was assumed to produce an accurate solution.
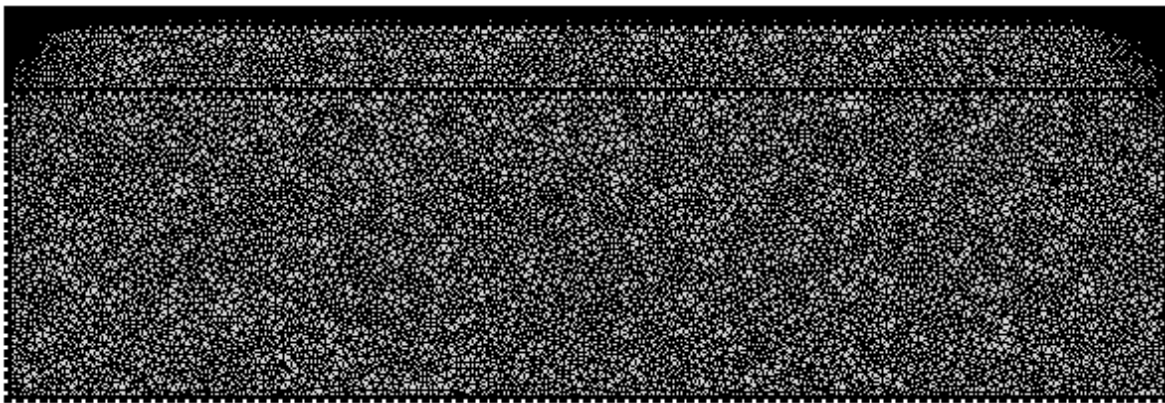
Figure 11 – Illustrates the default autogenerated triangular mesh set to Extremely Fine, implemented in the model from Cid Royo et al. 2016*.*

2.4.6.3   Materials

Each layer has specific material property values for: *Cp*, *k*, and *ρ*. The values were derived from previous literature. See Table 7, Table 8, and Table 9, for the specific values, ranges, and references. Furthermore, specific tissue related and other relevant values are listed in Table 10.

Table 7 –Material density, ρ, expressed in [kg/m³]. See the used values in the model in the bottom row. The used values are mean values of available values from included references.

Literature/Material	Blood	Stratum Corneum	Epidermis	Dermis	Hypodermis
(Jiang et al. 2002)	1060	-	1200	1200	1000
(Wilson & Spence 1988)	-	-	1200	1200	850

(Gowrishankar et al. 2004)	-	-	1200	1200	1000
(Museux et al. 2012)	1080	-	-	-	-
(Blank et al. 1984)	-	1330	-	-	-
(Seteikin & Krasnikov 2006)	1000	-	1600	1000	-
Used Values	*1047*	*1330*	*1300*	*1150*	*950*

Table 8 – Material thermal conductivity of the skin, k, expressed in [W/m·K]. See the used values in the model in the bottom row. The used values are mean values of available values from included references.

Literature/Material	Stratum Corneum	Epidermis	Dermis	Hypodermis
(Jiang et al. 2002)	-	0.24	0.45	0.19
(Wilson & Spence 1988)	-	0.21	0.53	0.16
(Gowrishankar et al. 2004)	-	0.23	0.45	0.19
(Seteikin & Krasnikov 2006)	-	0.27	0.49	-
Used Values	*0.2375*	*0.2375*	*0.48*	*0.173*

Table 9 – Heat capacity at constant pressure, Cp, expressed in [J/kg·K]. See the used values in the model in the bottom row. The used values are mean values of available values from included references.

Literature/Material	Blood	Stratum Corneum	Epidermis	Dermis	Hypodermis
(Jiang et al. 2002)	3770	-	3590	3300	2500
(Wilson & Spence 1988)	3800	-	3600	3800	2300
(Gowrishankar et al. 2004)	-	-	3590	3300	2675
(Seteikin & Krasnikov 2006)	-	-	3700	3200	-
(Museux et al. 2012)	3300	-	3600	3222	2300
Used Values	*3617.5*	*3616*	*3616*	*3363.4*	*2443.75*

Table 10 – Tissue related coefficients, $Q_{metabolism}$, $Q_{bloodPerfusion}$, $h_{air2hand}$, and T_a. †Only epidermis and dermis, ‡only hypodermis.

Reference/Coefficient	$Q_{metabolism}$	$Q_{bloodPerfusion}$	$h_{air2hand}$	T_a
(Xu et al. 2008)	368.1 [W m^{-3}] † 368.3 [W m^{-3}] ‡			
(Jiang et al. 2002)		0.00125 [s^{-1}] ‡		
(de Dear et al. 1997)			4.7 [W m^{-2} K^{-1}]	
(Pennes 1948)				34.8 °C

2.4.6.4   *Studies*

Before running a transient analysis describing heat propagation over time, it is important to stabilize the initial temperatures across the geometry. The heat generated from blood perfusion, body core temperature, and metabolism locally in the tissue, are all contributing to the initial temperatures. Initial temperatures of the model are found when the model is in equilibrium. This problem may be solved by running a stationary analysis, and then using the output temperatures across the model from the stationary analysis as input of the initial temperature values of the model in the transient analysis.

2.4.7   Verification and validation of the model

The implementation of the MCM must be verified to ensure it is done correctly. The validation is only related the mathematics of the implementation. Without a verification, the implementation would possibly not be able to produce correct MC simulations. Validation of the model provides insights into how and if the model can be related into solving the real-life problem it tries to answer (Blum et al. 2007). If the model performs reasonable and are compatible with the information given from the real-life problem it may be evaluated to see if the model may be useful for its purpose (Blum et al. 2007).

A three-step verification of the MCM implementation (Wang & Jacques 1992) was conducted and was consequently successful (Cid Royo et al. 2016). Implementation in COMSOL is assumed to be verified since COMSOL is a professional recognized tool for modelling heat transfer problems. The modelled refraction index for all skin layers were validated with experimental studies. The modelled absorption coefficient was not validated since data was not available for all wavelengths. The model in general was not validated.

2.5   Critical observations of the previous model

Contents on this subsection is derived from the discussion chapter in the previous study, (Cid Royo et al. 2016).

The previous model was not validated. Without a validation of the model, it is hard to conclude whether the model is an accurate representation of how laser light heats up the skin and related estimation of nociceptive activation. Additionally, the absorption coefficient, μ_a, was not validated.

The convergence analysis was not performed with a laser wavelength with a high penetration depth. Using a low penetrating laser wavelength provided an inadequate convergence analysis, because of the higher uncertainties linked to high penetration lasers. The deeper the penetration depth of the laser, the more spread out the energy is in the energy distributions and the more iterations is needed for a natural distributed solution of the light propagation. If the analysis converges for high penetration lasers, it is certain that analysis for low penetration lasers also converge. Therefore, high penetrations lasers are better candidates for conducting convergence analysis. The convergence analysis from previous model included: Amount of iteration for each simulation and bin size in the MC implementation. Bin size of the model is equivalent to the resolution of the model. Choosing a high resolution would result in high amount of iterations needed for precise and reliable solutions, while a lower resolution would require less iterations but also less precise solutions. Other important convergence analysis excluded in the previous study, consists of: Solver step size and solver stepping type, geometry size, and MESH size.

The boundary condition between the model and internal environment would enable energy to bounce of the sides of the model. This might cause unrealistic heat transfer within the model.

The nociceptive activation estimation from the previous study (Cid Royo et al. 2016), was described as inadequate since it only included a temperature threshold as a key feature. E.g. the method could only produce a Boolean output for nociceptive activation.

Solving the problems related to the critical observations are important in terms of conducting a successful validation of the model.

2.6 Summary of the problem analysis and aim of the thesis

The different layers and elements of the skin has been described. Laser stimulations has been identified as an efficient pain stimulation method because of their mono-modality stimulation nature in relation to the port-control mechanism.

Theory and implementation of the previous model, (Cid Royo et al. 2016), has been described to gain a basic understanding of development and construction of such a model. All implementations of the MCM and FEM in the model has been verified, but the model has not been validated. Without the validation, it is uncertain whether the model generates meaningful results. The conducted convergence analysis was found to be inadequate along with the boolean estimation of nociceptive activation.

In pain research, only a few lasers are used based on the commercial availability and previous experience/research. In the previous model following laser wavelengths were analysed: Ar$^+$ 488 [nm], Nd: YAP 1340 [nm], Tm-YAG 2010 [nm], Er-YAG 2940 [nm], and CO_2 10600 [nm] lasers.

It has been chosen to focus on Nd: YAP and CO_2 lasers because they have been found to be frequently used in pain research, based on the amount of laser-pain research related references identified, see listed studies in Table 11. All identified studies are related to laser stimulation with intensities strong enough to cause LEP.

Table 11 – Tables gives an overview of the identified studies related to use of Nd: YAP 1340 [nm] or CO_2 10,600 [nm] lasers. Nd: YAP laser studies range from 2008-2017 and CO_2 laser studies range from 1997-2010. All listed studies are related to LEP, and laser stimulation intensities around the pain threshold.

Type of laser used in study	Nd: YAP 1340 [nm]	CO_2 10,600 [nm]
Studies	(Perchet et al. 2008; Kamping et al. 2013; Krahé et al. 2015; Isak et al. 2016; González-Roldán et al. 2016; Paloyelis et al. 2016; Madden, Catley, et al. 2016; Madden, Bellan, et al. 2016; Stancak et al. 2016; Hüllemann et al. 2017)	(Svensson et al. 1997; Iannetti et al. 2001; Truini et al. 2003; Perchet et al. 2008; Ragé et al. 2010)
N	10	5

Based on these information, the aim of this master thesis is:

To validate the model in an experimental setting using both Neodymium: Yttrium-Aluminium-Perovskite laser and Carbon Dioxide lasers by measuring temporal thermal surface profiles and estimating nociceptive activation.

3   Methods

To solve aim of the thesis, the first step in the validation is to optimize the model in relation to the critical observations of the model stated in the problem analysis and by specifying stimulation site of the model. The previous model provided general solutions (Cid Royo et al. 2016), but in a validation of the model, it is important to be more specific about stimulation area and related layer thicknesses to ensure higher probability of success in the validation.

The elements of the optimization are as following:

1. Specifying stimulation area and setting up the model accordingly
2. Grid size in the MC implementation
3. Convergence analysis of simulation iteration count in the MC implementation
4. Boundary conditions for model in COMSOL
5. Convergence analysis of solver type, solver step sizes and MESH in COMSOL
6. Estimation of nociceptor activation (add nuances to the estimation)

To increase the quality of the implementation in COMSOL, following element are also being optimized:

7. Laser ON/OFF function (remove discontinuities)

Predictions from the model will be compared to experimental data, describing thermal changes in the skin surface temperatures dependent on laser stimulation. Additional model adjustment and validation, in relation to results from the experiment will finalize the chapter.

Experiment will be performed with a Carbon Dioxide laser (CO_2) 10,600 nm laser and a Neodymium: Yttrium-Aluminium-Perovskite (Nd: YAP) 1340 nm laser. Each laser has very different light absorption profile and are both used in pain research, and they are both available at the laser laboratory at SMI, AAU.

This chapter will describe the methods of the model where focus will be set on first optimization of the MC implementation and secondly the FE implementation. Then the methods of the experiment and validation will be described.

3.1   Model optimization

This section will describe the deliberate changes made to optimize the model. These changes are both derived from the discussion of Royo et al. 2016 and by the setup used for validation of the model. First the MC model will be optimized, then the FE model, and lastly the nociceptive estimation model.

3.1.1   MC - Modelling beam profiles

In the previous study both ND: YAP and CO_2 lasers were modelled as having a Gaussian beam profile, where radius was defined as $1/_{e^2}$ (Cid Royo et al. 2016).

In the present experimental validation, the CO_2 laser (Synrad Firestar, TI-100, USA) have a Gaussian fit. Equally the laser beam of the model is modelled to have a Gaussian fit. See section 6.2.1 in (Cid Royo et al. 2016), for Gaussian beam profiles. Modelling the CO_2 laser as having a perfect Gaussian spot profile, is assumed in the validation of the model.

To validate the ND: YAP laser in the model, there will be used a ND: YAP laser (STIMUL 1340, El.En. S.p.A., 50041 Firenze, Italy). The laser is defined to have a flat-top profile when using the smallest laser spot diameter at 4 [mm]. As diameter becomes larger, the flat-top profile becomes more Gaussian (El.En. S.p.A. 2005). In the present study, the 1340 nm laser will be modelled as a Gaussian spot profile for all chosen beam diameters.

The smoothness in the natural distribution of the Gaussian fit or flat-top beam profiles in the model are depended on the amount of iterations being run in a simulation. A true deterministic result of beam profile is practically not possible through the stationary MC implementation.

3.1.2   MC - Specifying model geometry in relation to specific stimulation site

Stimulation site is set to be at the volar side of the forearm. Local layer thickness data is partly derived from (Frahm et al. 2010), where epidermis (including SC) have a thickness of 49.6 [μm] and dermis 1 [mm] for hairy skin at the volar forearm, estimated from ultrasound data. The thickness of SC is derived from (Holbrook & Odland 1974) measured to be 12.9 [μm] average (n=6) for volar forearm. New living epidermis thickness is derived from both studies as 49.6 [μm] - 12.9 [μm] = 36.7 [μm]. See the optimized geometry in Figure 12.
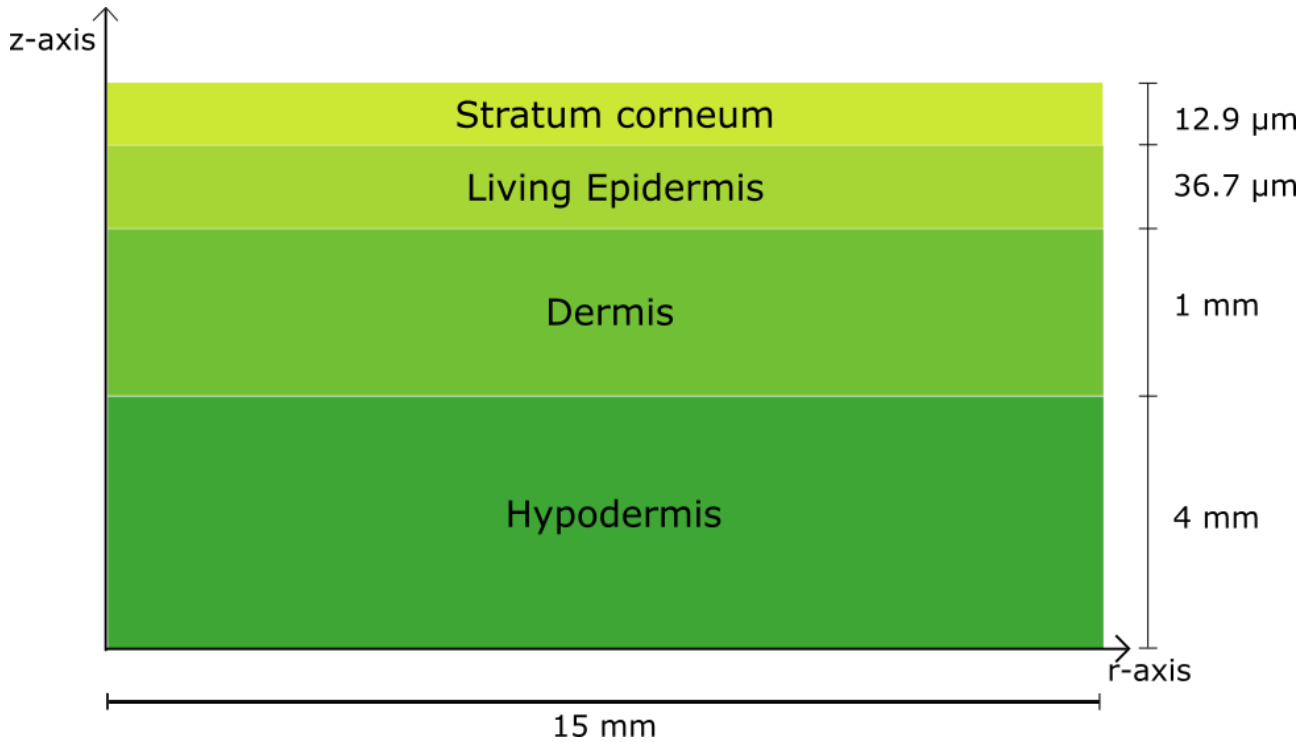
*Figure 12 – Geometry of the present study. The r-axis moves along the radius of the geometry, equal to 15 mm. The z-axis moves perpendicular to the surface of the skin. Here the different layers and their thickness are specified. The outermost layer to external environment is **Stratum Corneum**, and the innermost layer to internal environment is **Hypodermis**.*

3.1.3   MC - Optimizing grid size of the MC implementation

In relation to changes of the geometry, it is important to reiterate the current grid size of the MC simulation. If the simulation is not run with proper amount of iterations, it is possible that larger quantities of energies will form close to the z-axis, which will consequently form unrealistic heating of the tissue in small areas. From previous study the grid size of 18 [um] was chosen, because it was the thickness of the slimmest layer, SC, and because of computational load increase if resolution of grid size would decrease. If the same resolution of grid size is used in the present study, with an even smaller SC than before, SC would be neglected in the analysis. Choosing a higher grid size resolution would solve the problem but dramatically increase computational time. It is unknown whether choosing a grid size of SC is compromising the precision of the model. To overcome the problem of computational time, first the implemented code must be optimized.

In the previous study, energies for individual photon walks (PW) were summed by following equation:

$$A = A + newA$$

Where **A** is the absorption matrix with the size of the geometry divided by the resolution, and **newA** is the same sized matrix with the energies calculated for newest PW. After each iteration count the two matrices would be added. The code was optimized for parallel computing which had limiting code implementation complications such as implementing following solution. In the following solution, only the energies and their actual coordinates are added to the *A* matrix. See following equation:

$$A(\bar{x}(i), \bar{y}(i)) = A(\bar{x}(i), \bar{y}(i)) + E(i)$$

Where $\bar{x}(i)$ and $\bar{y}(i)$ are vectors with the coordinates of where energy is deposited at the actual PW for each simulation iteration, and *E(i)* is the related energy to the specific coordinates. Optimization did not result in any changes to the final output of the MC algorithm, but optimized the code by over 800 % and made run time independent on grid size. See Table 12 for optimized MC simulation timing.

Table 12 – Table shows MC implementation mean run times per iteration in the simulation. Both before optimization of the implementation of the algorithm and after optimization of the algorithm.

	Previous MC algorithm	New MC algorithm	MC simulation, run time optimization
Average mean PW	~2.52 [ms]	~0.30 [ms]	~840 %

In the previous model the grid resolution was the same for each *r* and *z* directions. In the present study, they are redefined to be different, where z resolution is 12 [um] / bin (thickness of SC) and r resolution is 150 [um] / bin to decrease the amount of iterations needed, since the minimum amount of iterations needed is equal to the resolution of the grid (Welch & Gemert 2011), resulting in 42622 iterations/simulation and a factor 10 decrease in resolution of *r*. The code optimization and the new grid size will ensure faster computation while maintaining accuracy in the generated solutions of the model.

The new grid size is more robust to not forming very high and very low energy artefacts close to the z-axis. If the same high-resolution grid size (12 [um] x 12 [um]) is chosen with same amount of iterations e.g. 10000 iterations, it is possible the simulation will form relative high or low energies close to the z-axis of the model, see Figure 13, which may result in unrealistic high temperature rises in small areas. Choosing a smaller resolution for the *r* direction, results in reduction of these artefacts, by still maintaining same iteration count, see Figure 14. Both simulations are run with the same parameters. Increasing amount of iterations for each simulation is assumed to produce similar comparable results.
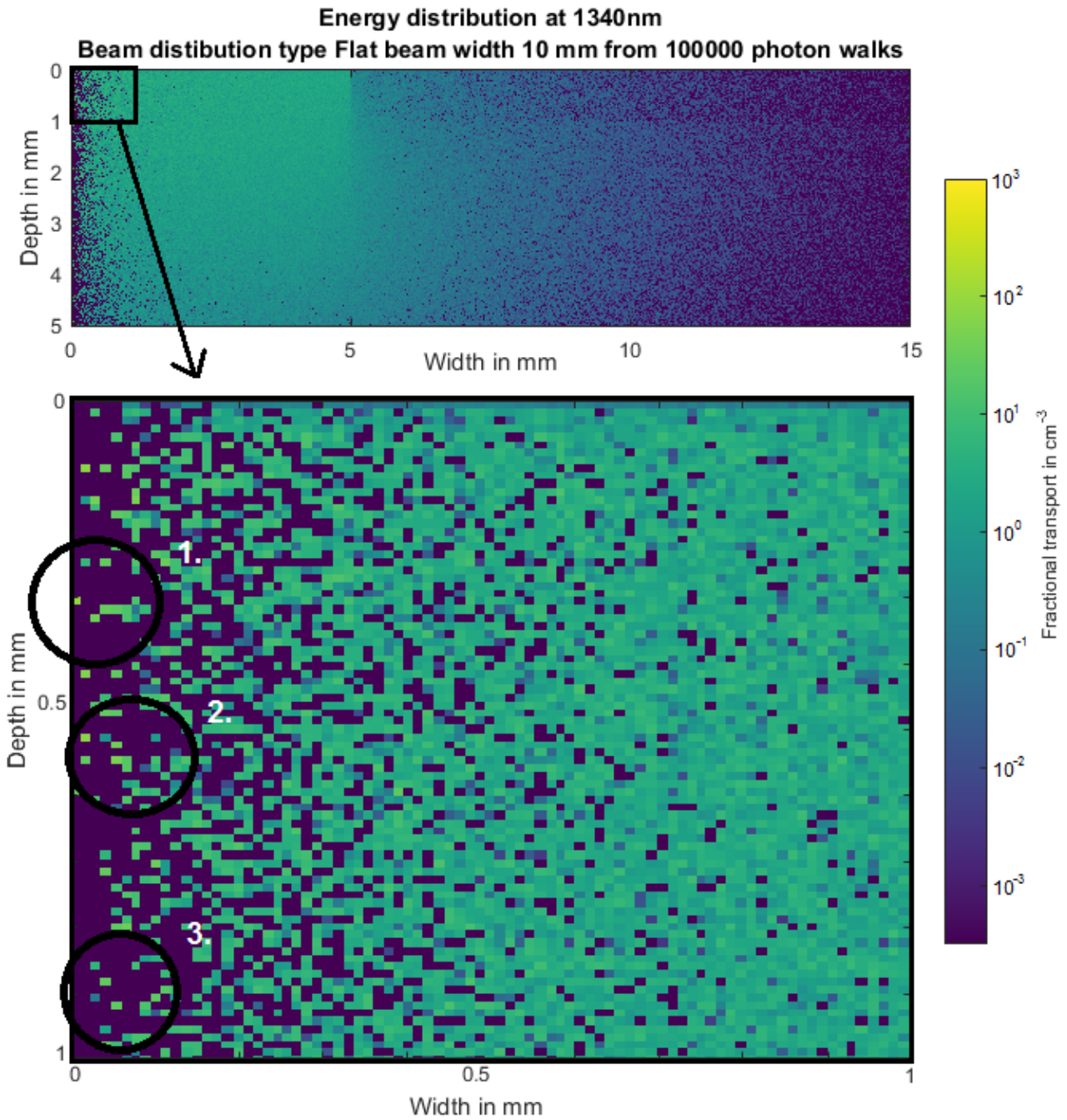
*Figure 13 – MC simulation run at 10000 iterations for ND: YAP at 10 mm spot diameter, grid resolution of 12 [um] / bin in both r and z directions. Top image shows the right half of the beam profile in the geometry. Bottom image shows a 1 x 1 mm zoomed version of top image cornered at (0,0). **1.**, **2.**, and **3.** Illustrates examples of energies being relative high and relative low to the energies in the simulation. Increasing amount of iterations for the simulation would ultimately remove the artefacts, but also heavily increase computation time. The colorbar values are fixed with the colorbar values on Figure 14.*
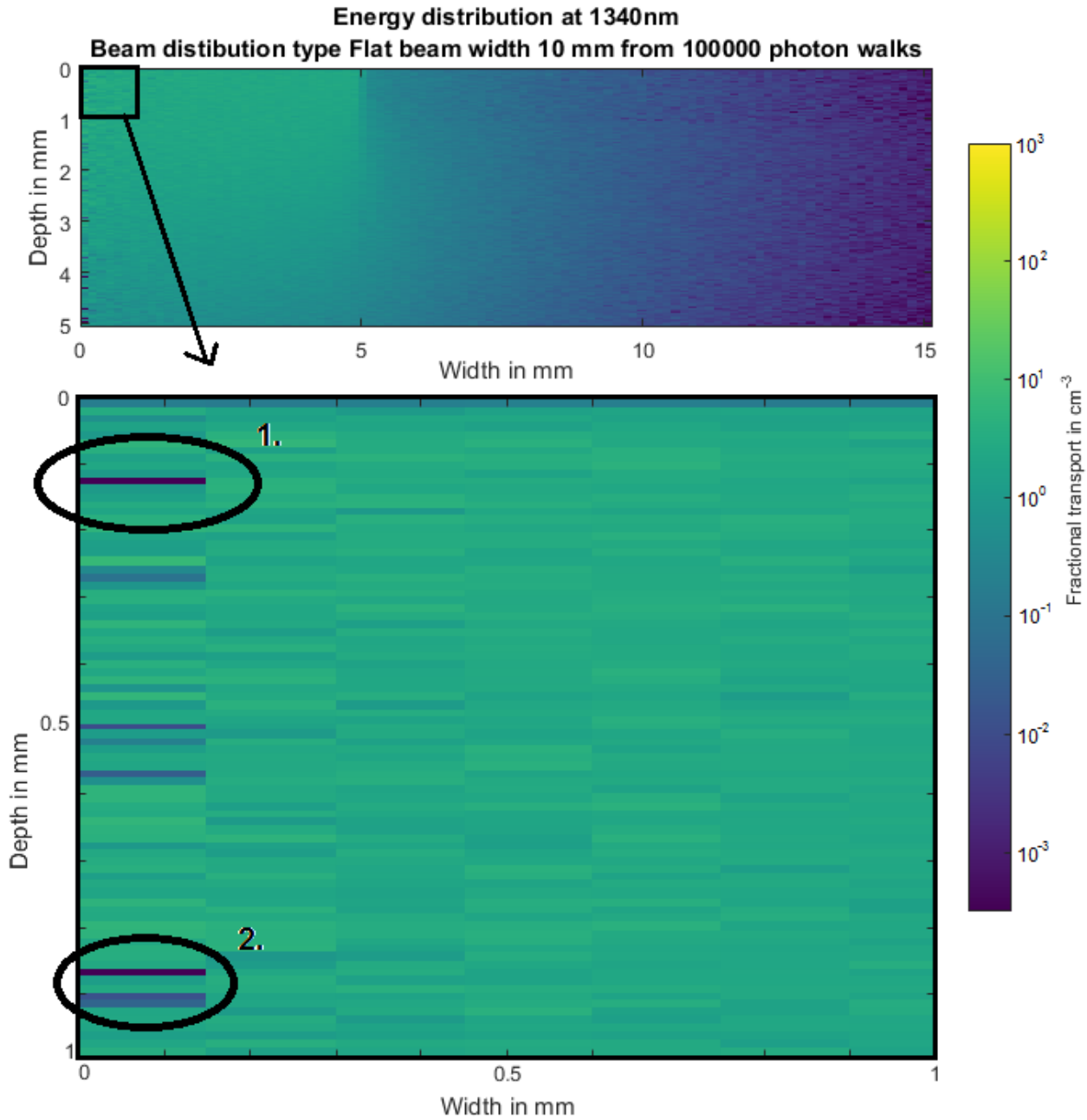
*Figure 14 - MC simulation run at 10000 iterations for ND: YAP at 10 mm spot diameter, grid resolution of (150 [um] x 12 [um]) / bin for r and z directions, respectively. Upper image shows the right half of the beam profile in the geometry. Bottom image shows a 1 x 1 mm zoomed version of top image cornered at (0,0). **1.** and **2.** Illustrates examples of energies being relative low to the energies in the simulation. Notice the relative high energy artefacts are reduced in relation to examples seen in Figure 13. The colorbar values are fixed with the colorbar values on Figure 14.*

3.1.4   MC - Optimization of model in relation to iterations per simulation

Convergence analysis for previous study did not identify the convergence of iterations count and was only done for one laser type. Therefore, a new convergence analysis was conducted by extracting mean and SD of T_{max} for 10 simulations at a specific iteration amount per simulation. Since both laser types have different

penetration depths (Weber 1999), individual convergence analysis is run for each laser type. Convergence is met when SD of mean T_{max} between different iterations/simulation is < 0.1. At this convergence point it is estimated that the mean or SD does not change if iterations/simulation is increased.
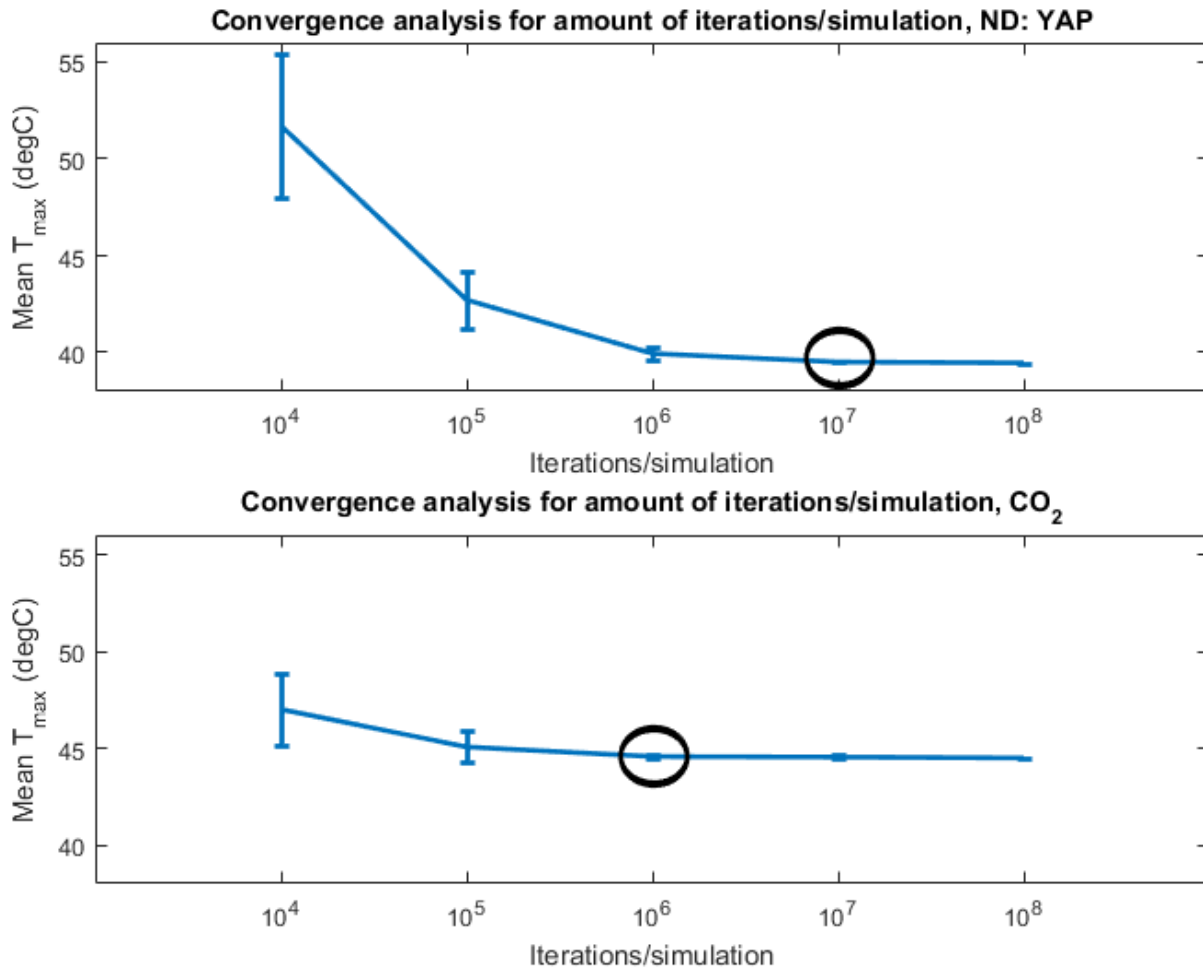
Figure 15 - Figure show convergence analysis of the mean and standard deviations of T_{max} across 10 simulations for different iteration counts per simulation in the MC model, for each 1340 and 10600 nm wavelengths. Increasing amount of iterations/simulation has an impact on both SD and mean of the model. A beam width of 10 [mm] and grid resolution set to 150 x 12 [µm] / bin. Convergence is reached at SD < 0.1, equal to 10^7 and 10^6 iterations/simulation for the ND: YAP and CO_2 lasers, respectively.

The convergence analysis show convergence at SD < 0.1 for both ND: YAP and CO_2 laser types at iterations count between 10^6 - 10^7 and 10^5 - 10^6 iterations/simulation, respectively, see Figure 15 and *Table* 13. All simulations in the convergence analysis were performed with a beam width of 10 [mm].

Table 13 – Table show statistical analysis of the mean and standard deviations of T_{max} across 10 simulations for different iteration counts per simulation in the MC model for each laser type. Increasing amount of iterations/simulation has an impact on both SD and mean of the model. A beam width of 10 [mm] and a grid resolution set to 150 x 12 [µm] / bin for all simulations. The used stimulation intensities are arbitrary, but the same for each laser type. Analysis show convergence at SD < 0.1 for both ND: YAP and CO_2 laser types at iterations count between 10^6 - 10^7 and 10^5 - 10^6 iterations/simulation, respectively

Amount of Iterations/simulation	10^4	10^5	10^6	10^7	10^8
ND: YAP					
Mean-T_{max} °C	51.7	42.7	39.9	39.5	39.5
SD-T_{max} °C	3.8	1.4	0.3	<0.1	<0.1
CO_2					
Mean-T_{max} °C	47.0	45.1	44.6	44.5	44.5
SD-T_{max} °C	1.8	0.8	<0.1	<0.1	<0.1

All ND: YAP simulations in this specific analysis were run with 10^7 iterations and all CO_2 simulations were run with 10^6 iterations.

3.1.5   FE - Updated boundary conditions and heat sources

Changes at model-internal environment from constant temperature to outflow with a temperature at the boundary. This allows the heat to propagate over the boundary, thus, disabling heat from reflecting back and forth in the model. (Comsol 2012)

See update boundary conditions and heat sources in Table 14.

Table 14 – Both updated boundary conditions and heat sources are shown in the table, along with the mathematical expression. Description includes both stationary and transient boundary conditions. q is the total energy applied at the boundary, n is the rate at which the total energy is applied, u is change of temperature over time, T_{ext} is defined as the temperature of the external environment to the model, T is the temperature at the boundary, h is the heat transfer coefficient between the air and skin surface, Q_{laser} is the applied laser energy, $Q_{metabolism}$ is the applied energy from tissue metabolism, and $Q_{perfusion}$ is the energy applied from blood perfusion in the tissue. Changed boundary conditions is marked with †.

Boundary	Expression
All layers	Rotated around z-axis, model cornered (geometry to external environment) at r=0
Boundaries between the model and internal environment	Stationary: $-q \cdot n = 0$ Transient: $\quad T = T_{ext}, \quad if\ n \cdot u < 0^†$ $\quad -q \cdot n = 0, \quad if\ n \cdot u \geq 0^†$
Boundary between the model and external environment	Stationary: $-q \cdot n = 0$ Transient: $-q \cdot n = h \cdot (T_{ext} - T)$
Heat sources	
Laser energy	Q_{laser}
Metabolic and blood perfusion energy	$Q_{metabolism} + Q_{perfusion}$

3.1.6   FE - Optimization of solver in COMSOL

Preliminary studies have shown that the precision of high frequency changes of temperature, such as laser pulses on skin tissue, is very sensitive to the solver configuration. In the previous study, (Cid Royo et al. 2016), the default setting of solver was used with a fixed time step size for each solution. In the present study, following convergence analysis of the solver configuration is were conducted to increase the precision of the model.

First step in solver optimization is choosing a solver method which handles the demands of the model. Since relative short pulses are used, when modelling the ND: YAP laser, the solver method must be able to handle high frequency content in the solutions. Here the Generalized alpha method is used over the default; Backward Differential Formula (BDF), because it may vary dampening of high frequency content, thus being able to be adjusted to produce more accurate solutions (Comsol 2012). Dampening of high frequencies may be controlled via a specific alpha value, ranging from 0-1 where 0 equals low dampening and 1 equals high dampening of frequencies. Preliminary studies have shown that an alpha value of 0.3 is fitting when working with this type of frequency content of the applied laser stimulation. To ensure the solver is handling errors between steps, the absolute and relative tolerance of the errors have been set to $\leq 10^{-5}$ and $\leq 10^{-6}$, respectively.

The smallest time step the solver may take is influencing the convergence of the solution. Following convergence analysis shows the relationship between time step size and the corresponding convergence of the model. The solver in the analysis is set up to either:

1. Force the time-stepping to strictly follow the minimum step size for all time steps (*Strict*)
2. Force the time-stepping solver to take minimum one step of specified minimum step size before increasing step size (*Intermediate*)
3. Let the time-stepping method choose time step size freely (*Free*)

Strict setting may require more computational time steps in the solver than *Intermediate*, and *Free* require less computational time than *Intermediate*. Convergence is identified via following equation, by using T_{max} as estimator.

$$Convergence = \frac{T_{max,L} - T_{max,S}}{T_{max,L}}$$

Equation 16

Where $T_{max,L}$ is T_{max} of a larger stepping size, and $T_{max,S}$ is T_{max} of a smaller stepping size.

Stable convergence is defined as when the previous and next step is under the chosen threshold of 0.5 %. Convergence is found at a time step size of a quarter of the laser pulse duration (t_{pulse}), see Figure 16, while the solver method is set up to *Free*. The *Free* solver stepping method is chosen, because it is the fastest in relation to *Intermediate* and *Free* without losing convergence. Simulations in the analysis were only run with the simulated Nd: YAP laser from the output of the MC simulation.
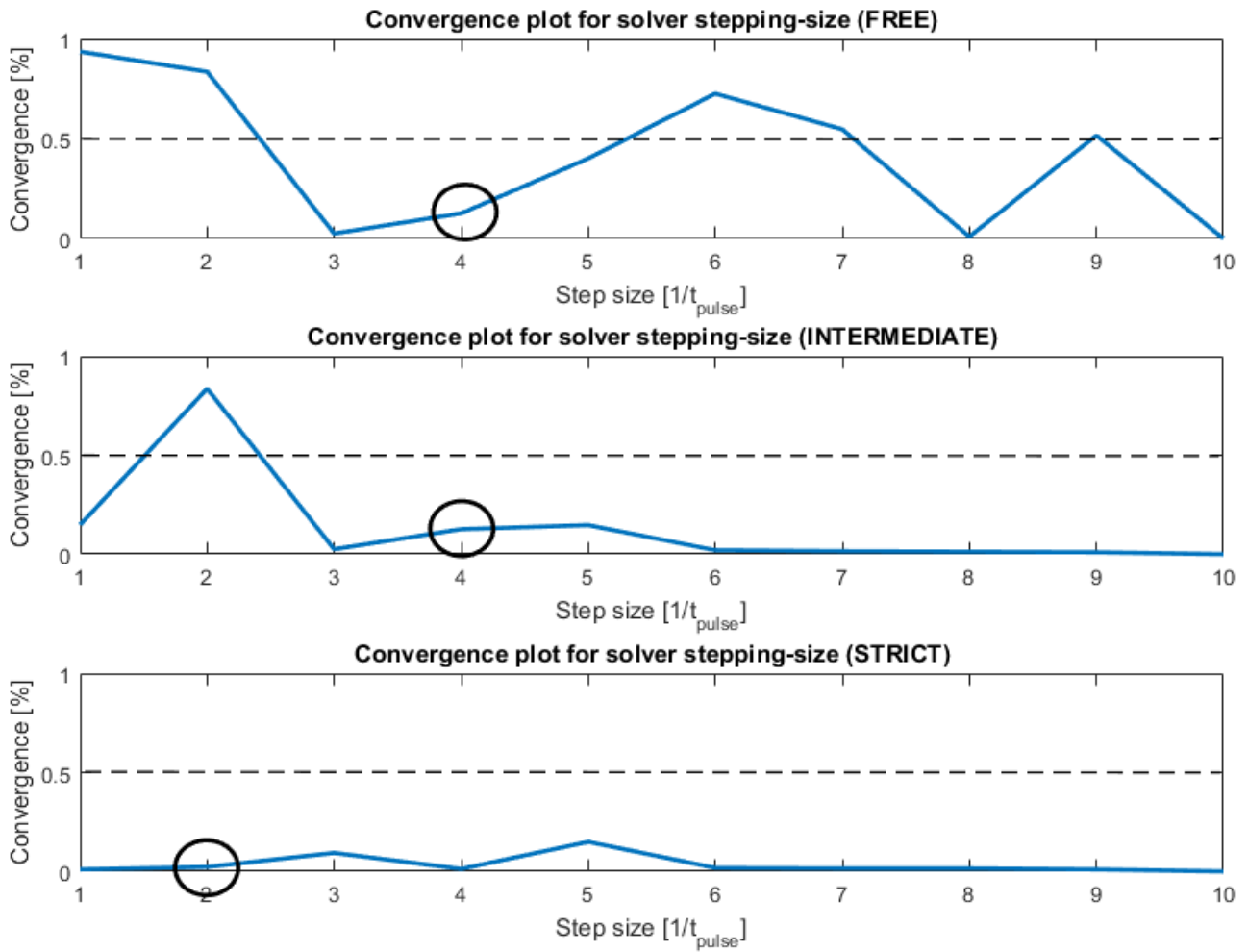
Figure 16 – Figure illustrates convergence analysis for T_{max} at different smallest step size of t_{pulse} for three different solver-stepping settings (**Free, Intermediate,** and **Strict**), in COMSOL. Convergence is established under 0.5 %, where convergence is under threshold for the previous step and next step, and is marked on the figure with a black circle. Strict setting requires most computational time compared to the Intermediate (10 % faster than strict) and Free (40 % faster than strict). The analysis was run with 1340 nm laser, 10 [J] over 10 [ms] equivalent to 1000 [W]. 1 % convergence error is equivalent to ≈ 0.5 °C in this specific example.

3.1.7   FE - Optimization of Mesh in COMSOL

In the previous study, the mesh of the FEM was not optimized, but was set to a default setting of an extremely fine mesh. (Cid Royo et al. 2016) In the present study, follow convergence analysis is presented of the mesh quality and convergence. The analysis is conducted to increase the precision of the model and lowering computational time.

Simulations is run with the ND: YAP laser, due high penetration depth. The higher penetration depth, the more coefficients have an impact on the results, thus increasing the theoretical error of the analysis. Simulating with this specific laser encourage higher gradients in all layers the model. Following equation is used to calculate convergence in the analysis:

$$Convergence = \frac{T_{max}(Finer\ mesh) - T_{max}(Coarser\ mesh)}{T_{max}(Finer\ mesh)}$$

Equation 17

In Equation 17 it is assumed that the finer the mesh equals lower convergence (Cook et al. 2001). Convergence is defined as when it is below 0.75 % both for the next comparison and the previous comparison. The analysis is run with three user-defined meshes and nine autogenerated meshes. User defined meshes are denoted Ui and autogenerated default meshes are denoted Di. The coarsest (U3) to the finest (D9) meshes ranges from: U3-U2-U1-D1-D2-D3-D4-D5-D6-D7-D8-D9.

Convergence is then identified when using the D3 mesh (see D3 mesh in Figure 18), see convergence analysis in Figure 17. See all used mesh's in the analysis in Appendix D – COMSOL Mesh's.
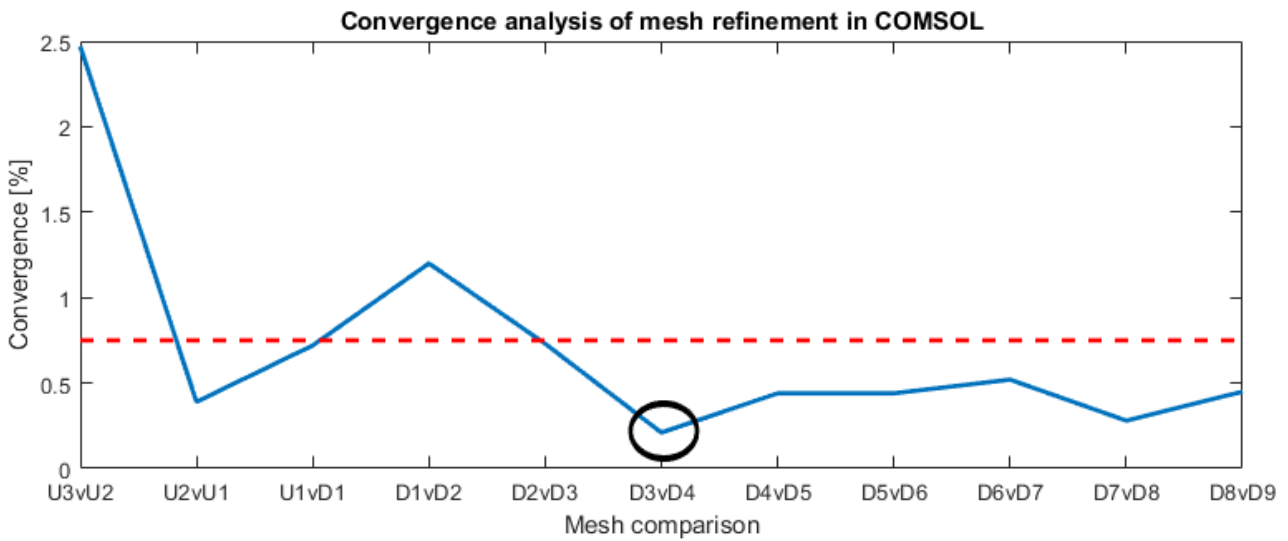
*Figure 17 – The figure represents the convergence analysis of mesh refinement of the model in COMSOL. Each x-tick represents a mesh comparison of **a coarser mesh** vs **a finer mesh**. The coarsest to the finest mesh ranges from: U3-U2-U1-D1-D2-D3-D4-D5-D6-D7-D8-D9. Convergence is found when the previous comparison and the next comparison is under the specific threshold at 0.75 %. Convergence is established when choosing D3 mesh. See Appendix D – COMSOL Mesh's for used mesh's in the convergence analysis and see the chosen mesh in Figure 18.*
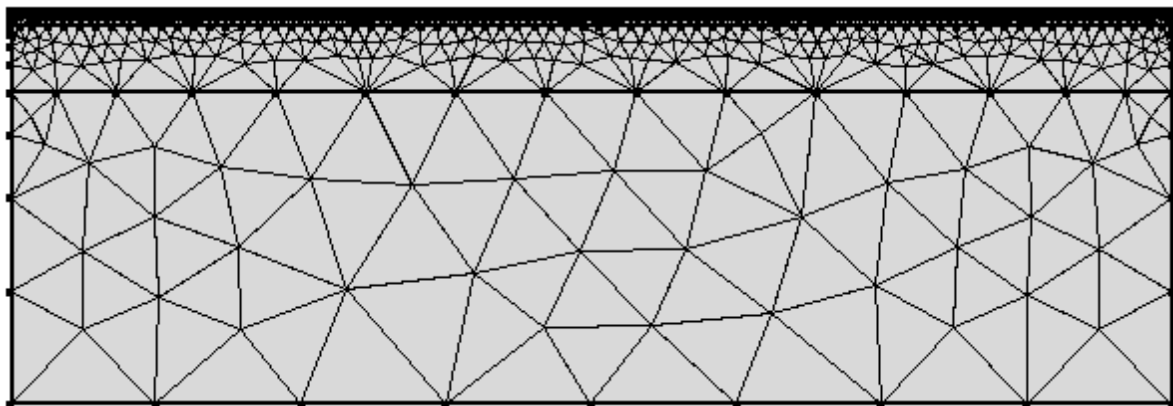
Figure 18 – The figure illustrates the D3 mesh used in the present FE model. The mesh contains 7390 domain elements and 2084 edge elements.

3.1.8 FE - Laser ON/OFF function

To model when the laser energy source, Q_{laser}, is ON, there is defined a rectangular stepping function where the width is equal to t_{pulse}. The function is smoothed at the corners to mimic the physical ramps of powering ON and OFF the laser in a real setting. Thus, eliminating unrealistic discontinuities in the analysis. See function in Figure 19.
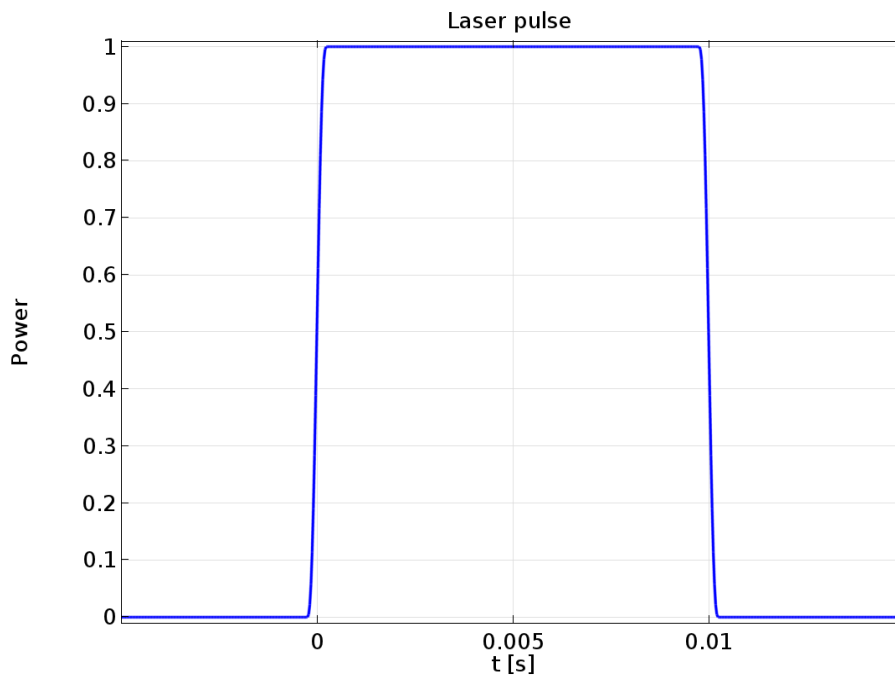
Figure 19 – Illustrates a graph representing the smoothed stepping function used to control laser stimulation ON/OFF in COMSOL. This concrete graph is an example of a stimulation time of 10 [ms]. The corners of the rectangular form are smoothed with a second derivative function with a transition zone of 0.0005 [s].

The function is slightly smoothed at the corners, to mimic the ramps of powering ON and OFF the laser in a real setting. Smoothing the function enhances convergence of the solver (Comsol 2012). The smooth transition from 0 to 1 is equal to 0.5 [ms], for all t_{pulse} durations.

3.1.9 Optimizing estimation of nociceptor activation

In the previous model, a simple threshold was used as method for estimating nociceptor activation. The method allowed a Boolean expression of the activation when an area of the model was over threshold. (Cid Royo et al. 2016)

This simplification is further developed to following method which is based on probability and relates to the experimental mean and standard deviation of the A-δ and C-fibre thresholds, and assumes a normal distribution. Two probability density functions (PDF) are formulated based on the mean and SD of the A-δ and C-fibre threshold from (Churyukanov et al. 2012), which is an expression of how likely a nociceptive activation will occur, equal to the integral of the PDF from zero to the temperature of perceived nociceptive activation. The estimations in following expressions:

$$P_{A-\delta \, activation} \;=\; \int_0^{T_{max}} p_{A-\delta}(x)\,dx$$

And:

$$P_{C-fibre \, activation} \;=\; \int_0^{T_{max}} p_{C-fibre}(x)\,dx$$

Where $p_{fibre}(x)$ is the probability of nociceptive activation at $x = T_{max}$, T_{max} is the maximum temperature at the skin surface and $P_{nociceptive \, activation}$ is the accumulated probability of nociceptive activation. See Figure 20 for PDF of A-δ and C-fibre nociceptive activation.
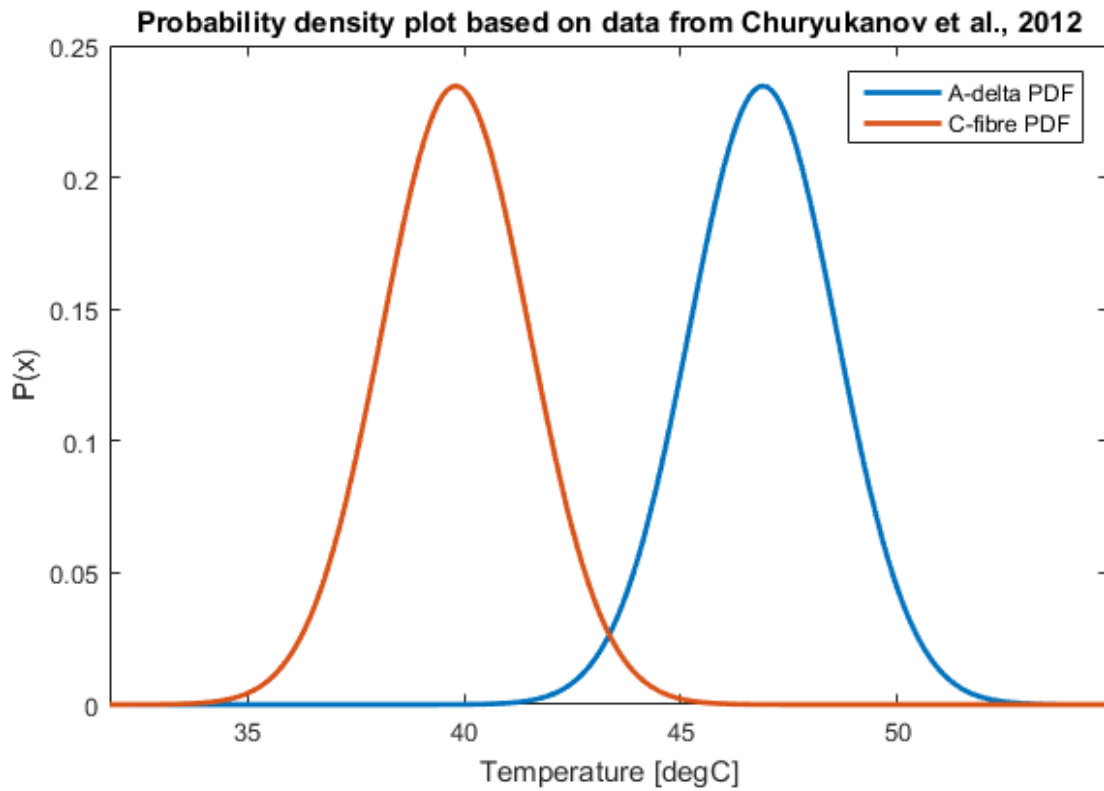
Figure 20 – Figure illustrates the PDF (p(x)) for nociceptive activation for T. Both in relation to C-fibre and A-delta nociceptive activation. SD at 1.7 °C remains the same for both PFD's, while mean values is defined as 39.8 °C and 46.9 °C for C-fibre and A-δ, respectively.

3.2   Experimental methods

The purpose of the experiment is to collect spatial and temporal data of how the skin surface is heated when laser stimulation is applied by both Nd: YAP and CO_2 lasers. The extracted data will be used in validation of the model.

3.2.1   Subjects

Six subjects participated (3 males and 3 females, age ranging from 20-32 years) in the study, one subject was excluded due failed recording of thermal data. Informed written consent was given, see Appendix B – Participant information, and signed from all participants in accordance to the Helsinki Declaration.

3.2.2   Nociceptive stimulation

Laser stimulation is produced by a CO_2 laser at 10,600 nm (Synrad Firestar, TI-100, USA) and a Nd: YAP laser system at 1340 nm (STIMUL 1340, Nd: YAP laser system, El.En. S.p.A., Italy). The CO_2 laser is controlled by a custom made Labview (National Instruments, USA) script. Inter-stimulus-interval were for set to at least 120 [s]. Since the specific lasers are not able to stimulate with the same pulse times without causing tissue damage they are kept different in the experimental stimulation procedures. Used pulse durations is defined as; ND: YAP t_{pulse} = 10 [ms] and CO_2 t_{pulse} = 200 [ms], throughout all stimulation procedures. These stimulation times are comparable to stimulation times from LEP studies found in Table 11.

Beam diameter for the Nd: YAP laser is changed by moving the fibre of the laser back or fourth in the optical fibre guide The Nd: YAP laser is defined to have a flat-top profile when using the smallest laser spot diameter at 4 [mm]. As diameter becomes larger (maximum of 15 [mm]), the flat-top profile becomes more Gaussian (El.En. S.p.A. 2005). It is not possible to change the beam diameter of the CO_2 laser and is always 11.4 [mm]. However, moving the laser spot quickly in small circles may simulate increased beam diameters.

3.2.3   Stimulation procedure

The experiment is divided into two parts. First part has the purpose of identifying A-δ pain threshold in subjects. The A-δ pain threshold will be identified for manually approximated beam diameters at 6 [mm] and 10 [mm] for each laser, resulting in a total amount of four A-δ pain thresholds found for each subject. Stimulation parameters for each A-δ pain thresholds will be used in the second part of the experiment, which has the purpose of collecting thermal imaging from the stimulation sites before, during, and after stimulation (10 [s] pre-stimulation + 60 [s] post-stimulation). The data will describe how the skin surface is heated up and how the heat dissipates radially from the beam spot centre at the stimulation site. See Appendix A – Experimental protocol for the specific experimental procedure.

3.2.4   Identifying A-δ pain threshold

The method of identifying A-δ pain threshold is derived from the staircase method discussed and described by (Gracely et al. 1988; Cornsweet 1962). The method is a validated and widely used method for describing thresholds.

To ensure the detection of A-δ fibre activation, the subject is instructed to report if the noxious stimuli is perceived as a stinging or prickling pain, or as a burning sensation. The stimulation intensity is categorized as A-delta activation if the pain is perceived as a stinging or prickling pain (Kandel 2013).
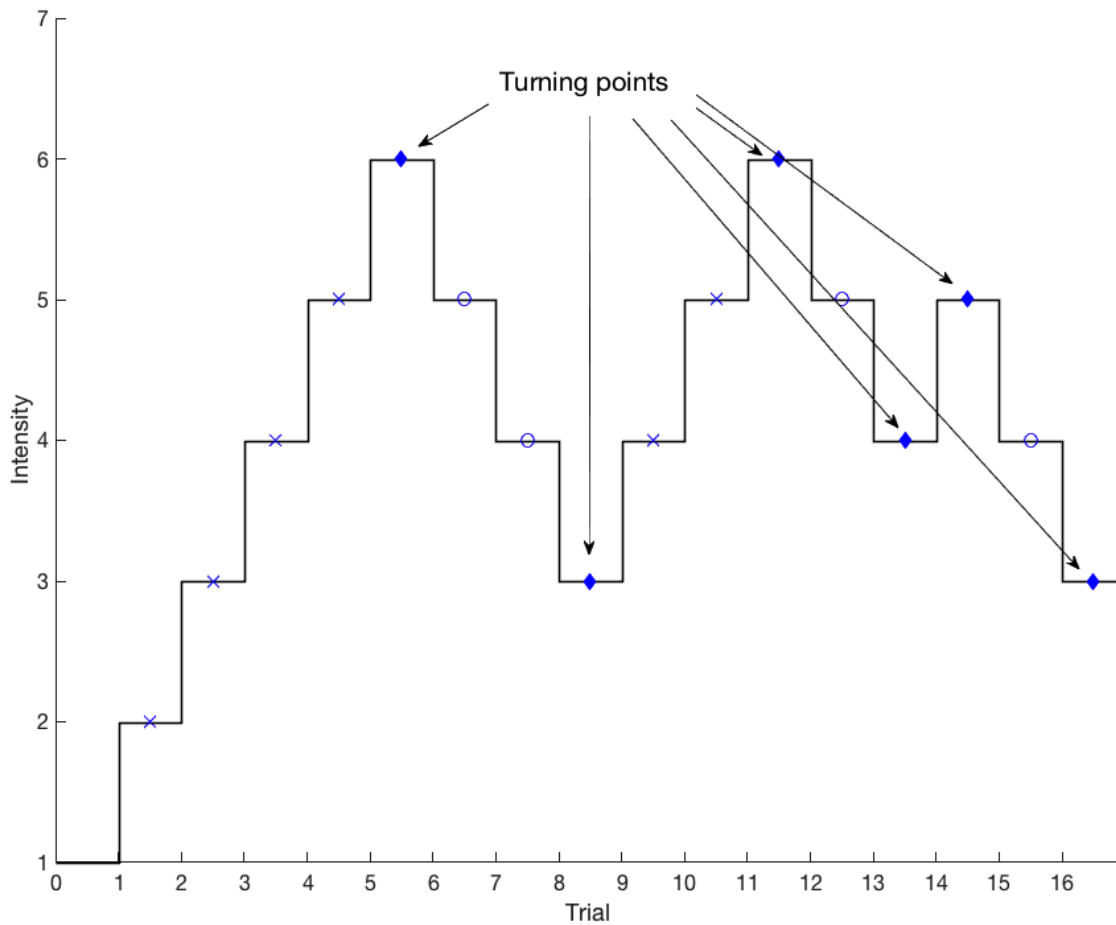
Figure 21 – Figure illustrates an example of the precedence of the staircase method. Stimulation start from a low intensity, incrementing until stimulation is perceived as painful. Here first turning point is found. Then intensity is decreased until stimulation is no longer painful, here the next turning point is identified. This precedence of followed until an acceptable amount of equal turning points is reached. Exact threshold is identified by taking the mean value of all turning points. In the figure, × states that stimulation was not painful, blue filled ◊ states a turning point either on a up flank (stimulation was painful) or down flank (stimulation was not painful), and ○ states that stimulation was painful. (Gracely et al. 1988)

The procedure of the method starts by stimulating at the lowest intensity possible. If the subject does not perceive the stimuli, the intensity for the next stimulation is increased until the subject reports the A-δ detection criteria. When the subject reports detection of A-δ activation, the first turning point is reached, and the intensity for the next stimuli is decreased. If the subject now still feels activation of A-δ, the intensity for the next stimuli is decreased until the subject does report activation of A-δ anymore where a new turning point is found. This is done until three up's and down's of A-δ activation are reached. Taking the mean of an equal number of up's and down's turning point intensities, reveal the quantified threshold. (Gracely et al. 1988) See Figure 21 for an illustration of the staircase method.

3.2.5 Thermal imaging acquisition

Thermal images will be recorded with an infrared camera (Thermovision 900, Agema Infrared Systems, Sweden) responsive at 2 – 5.4 µm, at 20 frames per second (FPS) at directed at stimulation site (Agema Infrared Systems 1992). The camera offers a spatial resolution equivalent ≈ 8x10 pixels/cm^2 on the surface of the skin in the specific experimental setup of the present study. This was measured by placing a 1x1 cm aluminium plate in the field of view of the camera during a recording for each subject as a size reference. ThermalCAM Researcher PRO 2.8 SR-1 is used as data acquisition software.

3.3   Data analysis and statistics

The data analysis of the comparison of the model is divided into two parts. The first part will describe how the thermal temporal and spatial profiles are extracted from the experiment. The second part will describe how well the model's estimation of nociception correlates with A-δ thresholds identified in the experiment.

3.3.1   Data analysis of thermal spatial and temporal profiles

Information about spatial and temporal profiles will be extracted from thermal imaging obtained from the experimental sessions.

For each recording:

1.   Extract Region of Interest (ROI). See 1 and 2 on Figure 22.

This is done by first identifying an initial spot centre by finding the frame which has the highest max value of all frames, whereupon the spot centre coordinates are extracted. ROI is then extracted from the first frame around stimuli onset by using the found coordinates as centre for a new 50x50 cut out image of the original frame. Reducing the number of pixels being worked on, increase computational time and removes low and high intensity artefacts outside of ROI.

2.   Remove final artefacts from corners of ROI by multiplying a Boolean circle to ROI. See 2 and 3 on Figure 22.
3.   Interpolate ROI. See 2 and 3 on Figure 22.

This is done to enable more approximated measuring points between actual measured points. This allows easier comparison between experimental and model data. The interpolations are done by up-sampling the image   x10   and   then   applying   a   Cubic   Spline   Interpolation   function. The Cubic Spline Interpolation function is used to find the smoothest curve which passes through a set of data points. The functionality of the technique is similar to forcing an elastic rod through a set of points. (Sandwell 1987) Using this technique, removes the risk of an overshoot in the interpolation at an arbitrary data point in the set, while still maintaining a non-linear approximation between data points. This is assumed to be more realistic than a linear interpolation.

4.   Extract four profiles for all t for all recordings. See 4 on Figure 22.

This is done by first smoothing ROI to find the highest intensity pixel, which is then defined as the centre of the heat spot. The coordinates from the found centre pixel is then used on ROI whereupon four half profiles are extracted, horizontally, left and right and vertically, up and down. This technique is practically seen as a x4 multiplication of total data, compared to only extracting one sigmoid profile for each recording.
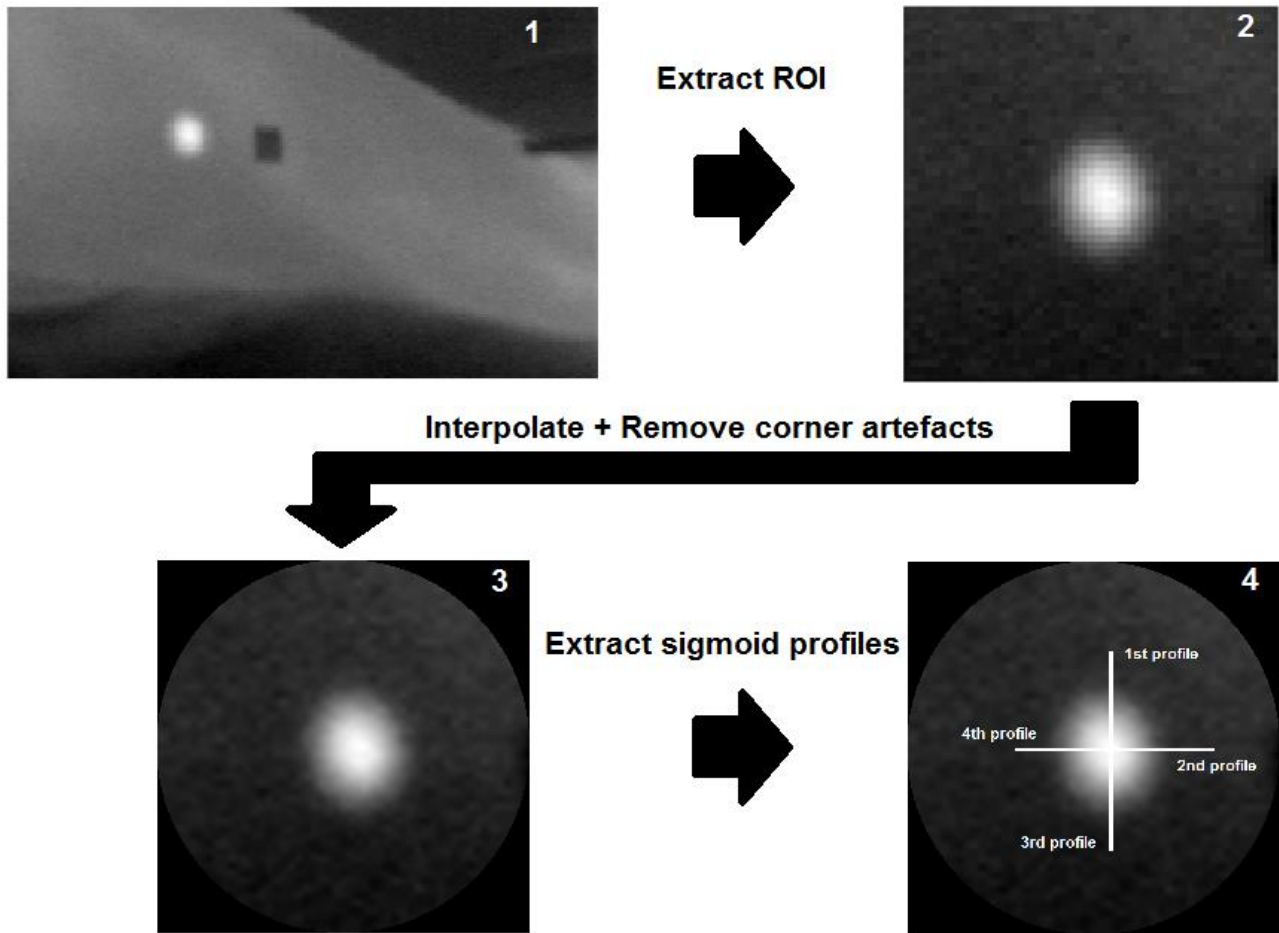
Figure 22 – The figure illustrates the process of extracting sigmoid profiles from experimental data. 1 illustrates a raw thermal image of the volar forearm, where laser stimulation has been applied and is a bright spot on the image. The black square is the reference 1x1 cm² aluminium plate. From 1 ROI is extracted. 2 is the extracted ROI (50x50 pixels, centred at stimulation spot). Corner artefacts are cut with a Boolean circle and ROI is interpolated with a cubic spline function to reach an approximated higher resolution, see 3. From 3, four sigmoid profiles are extracted from data, see 4. The sigmoid profiles are afterwards corrected for vertically skewness.

All extracted profiles are corrected for specific camera angle, where 8 horizontal pixels and 10 vertical pixels are defined as equivalent to 1 cm². This is done by using a physical 1 [cm²] square reference aluminium plate in the recordings, see black square object in picture 1 of Figure 22.

For all recordings:

5. Mean and SD are calculated across all extracted profiles for all subjects
6. Experimental spot diameter is calculated from the definition of radius equal to $1/e^2$

This is done by integrating the experimental sigmoidal curve at 50 [ms] to area under the curve equal to $1-1/e^2$. Since there may not be a data point at the exact definition of the radius, the experimental calculated radius is floored to nearest integer, which adds a theoretical 0-0.99 [mm] error.

3.3.2   Comparing experimental data with modelled data

A-δ pain thresholds in the experiment will be compared with the model using the same specific stimulation parameters as were used in the experiment for each threshold. Here maximum surface temperatures will be derived as a mean T_{max} of subjects and the related SD compared to the mean $T_{threshold}$ from the model, by using Equation 19. This will result in a probability of nociceptive activation for A-δ and C-fibres, see mathematical expressions of each estimation in Equation 18 and Equation 19.

Furthermore, results including temporal surface profiles, mean and SD for delta-T(T_{max}) at stimulation spot locations (0,0), (5,0), (10,0) for experimental data will be plotted along with modelled data. Since the temporal resolution of the experimental data is at 20 FPS, it is not consistent in the recordings, if the absolute surface maximum temperature is captured in the recording.

3.4   Model validation

Validation of the model will be performed with following steps.

1. First the model is compared to experimental data to use as a guideline for model adjustment.
2. Then there is conducted a sensitivity analysis on the implemented coefficients of the model, both in the MC and FE implementation.
3. Based on the results of the sensitivity analysis, the model is once again compared with experimental data. The adjustments of the model will be discussed in the discussion.

3.4.1   Sensitivity analysis on implemented coefficients and model adjustment

There is conducted a sensitivity analysis of the FE implementation coefficients by sweeping individual coefficients at the high and low range values, found in Table 7, Table 8, and Table 9. If there is a coefficient sweep which gives a T_{max}(delta T) > 2 °C the model will be adjusted. Since the coefficients for the MC implementation is modelled, except the anisotropy factor, and the SD of the model is unknown the explicit uncertainties from related experimental studies. Especially μ_a was criticized in the previous study, (Cid Royo et al. 2016), and was not validated for SC and epidermis. Modelling the Nd: YAP laser is more sensitive to changes in coefficient values because if the high penetration, compared to modelling the CO_2 laser. Following the modelling of μ_a, low absorption is occurring in SC mainly because of the low H_2O content (Welch & Gemert 2011). The experimental study (Salomatina et al. 2006) described the μ_a in epidermis and shows uncertainties between 1300 and 1400 [nm], in relation to the model, varying μ_a between 0.71 and 15.53 [cm^{-1}]. The modelled value for the μ_a in epidermis for the Nd: YAP laser in the present study is defined as 1.05 [cm^{-1}]. Following the experimental study (Salomatina et al. 2006), the value might possibly be 1-20 times higher than currently modelled. See experimental and modelled values in Figure 23.

Equally there is high uncertainties linked to the modelled μ_a for hypodermis but is excluded in the sensitivity analysis because of the low amounts of energy being deposited there.
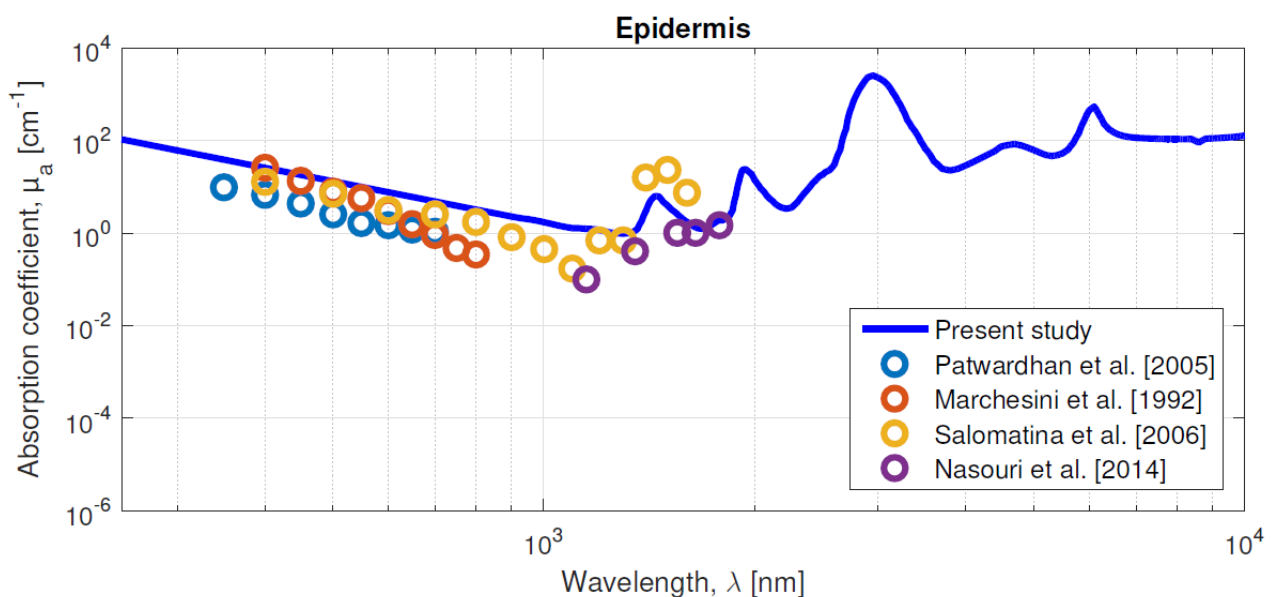
Figure 23 – The figure represents the absorption coefficient (y-axis) [cm^{-1}] in relation wavelength (x-axis) ranging between 250 and 10,000 [nm], in comparison with experimental studies. Blue line represents modelled coefficient from the previous (Cid Royo et al.

2016) *and present study, blue circles represents* (Patwardhan et al. 2005)*, red circles represents* (Marchesini et al. 1992)*, orange circles represents* (Salomatina et al. 2006) *and purple circles represents* (Nasouri et al. 2014)*. Figure borrowed from* (Cid Royo et al. 2016)*.*

The outcome of the analysis will be measured by extracting changes to T_{max}(delta T) when changing the individual coefficient values. There will be done one sweep per parameter, and the highest changes in T_{max}(delta T) will be noted. This approach will contribute to get an overview of how sensitive maximum temperature in the model are in relation to both heat transfer related coefficients. μ_a for epidermis will be adjusted until modelled T_{max}(delta T) reach T_{max}(delta T) of experimental data.

Sensitivity analysis will only be conducted if the form of the cool down curve does not match between the experimental and modelled data. If the form of the curves fit, the model will only be adjusted in terms of stimulation intensity. If the modelled data lies within the SD of the mean of experimental data, the model is deemed to produce meaningful results.

4   Results

This section provides the results of the thesis. First the new generated output from the MC simulations will be presented. Secondly, the experimental data will be presented in relation to stimulation parameters, found A-δ threshold and estimation of nociceptive activation. Thirdly, the model is compared to the experimental data in form of temporal surface profiles at (0,0), (5,0) and (10,0) [mm]. The validation of the model and the corresponding results will be presented after this chapter.

4.1   Output from MC simulations

The section gives an overview of the output of the MC implementation, and includes following four simulations; CO_2 laser with 10 [mm] diameter, CO_2 laser with 16 [mm] diameter, Nd: YAP laser with 6 [mm] diameter, Nd: YAP laser with 12 [mm] diameter, see energy distributions in Figure 24 and Figure 25. The CO2 laser has a far lower penetration (0.1-0.2 [mm]) in the tissue in relation to the Nd: YAP laser, where the energy distribution of > 5 [mm] through the tissue. Fraction of energy absorbed in the tissue, A_d, in CO2 simulation equal to 93-96 %, where only 72-73 % is absorbed with the Nd: YAP laser. See energy distribution of A_d, R_d, and T_d in Table 15.

Table 15 – The table gives an overview of the fractions of energy deposited in the tissue - A_d, fraction of energy reflected from the model surface - R_d, and fraction of energy transmitted through the model - T_d, for all laser setups used in the experiment.

Energy/Laser	CO₂ 10 [mm]	CO₂ 16 [mm]	Nd: YAP 6 [mm]	Nd: YAP 12 [mm]
A_d	95.9 %	93.3 %	73.0 %	72.4 %
R_d and T_d	4.1 %	6.7 %	27.0 %	27.6 %
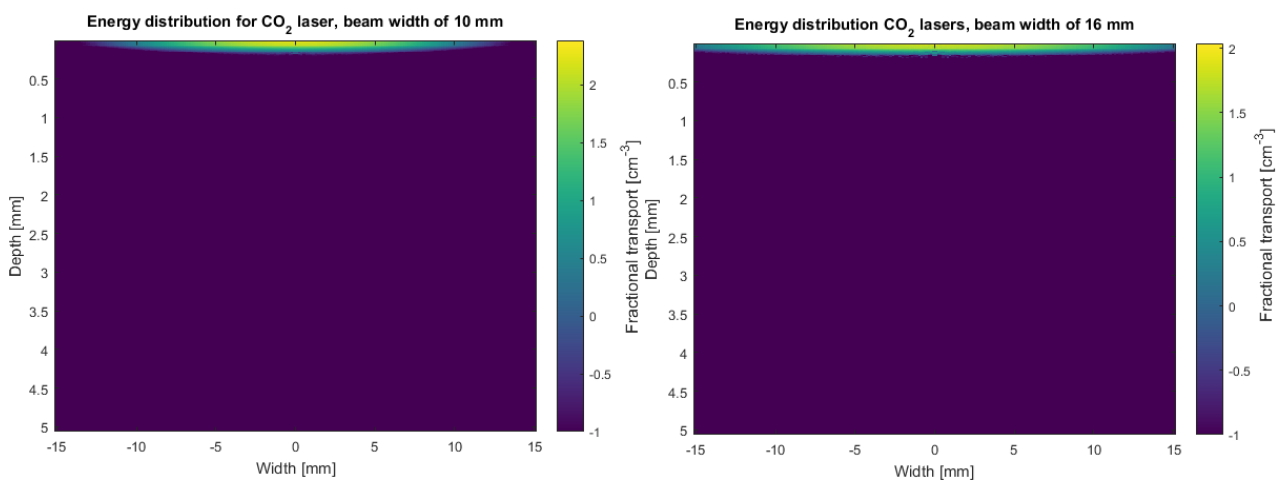
Figure 24 – Figure illustrates the output, beam energy distributions, of the MC simulations for the CO_2 laser with a wavelength of 10600 [nm], for 10 [mm] diameter (left) and 16 [mm] diameter (right). Most of the energy is distributed around a depth of 0.1-0.2 [mm]. The energy is noted in a logarithmic scale. Radius of the beam profile is mirrored at r = 0. Each simulation is run with 1.000.000 iterations.
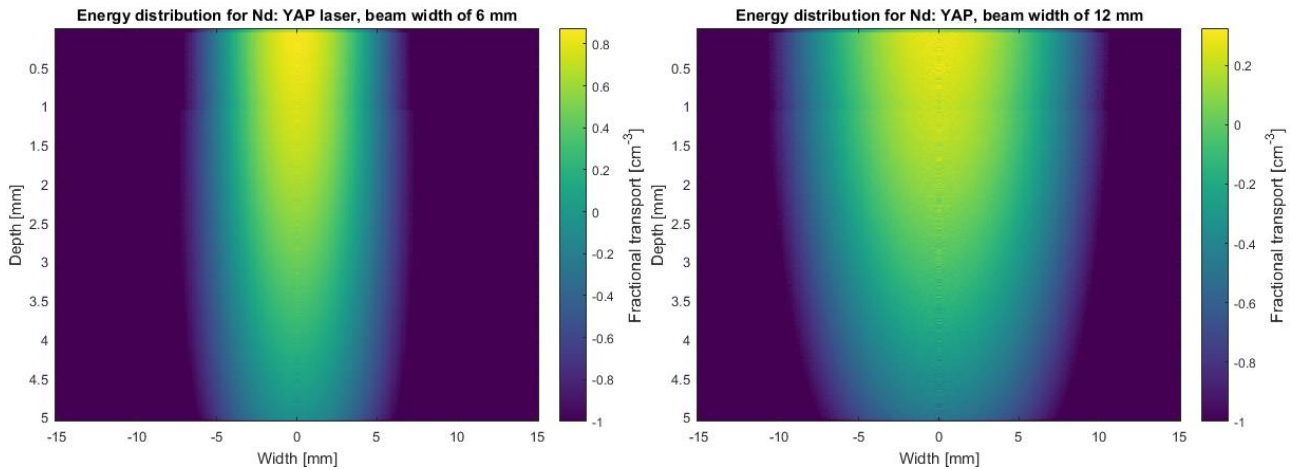
Figure 25 - Figure illustrates the output, beam energy distributions, of the MC simulations for the Nd: YAP laser with a wavelength of 1340 [nm], for 6 [mm] diameter (left) and 12 [mm] diameter (right). Most of the energy is distributed in all depths of the model, with highest intensities closest to the surface. The energy is noted in a logarithmic scale. Radius of the beam profile is mirrored at r = 0. Each simulation is run with 10.000.000 iterations.

4.2   Model comparisons with experimental study

First section presents the parameter setup along with the nociceptive activation estimation both for A-δ and C-fibres. Second section presents temporal profiles at spot centre. Third section presents spatial profiles for specific times. All results are derived from the specific stimulation parameter setup described in the first section. Third section presents experimental pain thresholds in relation to experimental pain thresholds used to estimate nociceptive activation.

4.2.1   Stimulation parameters and nociceptive activation estimation

The nociceptive activation estimation was calculated by setting up the model with same laser stimulation intensities as measured from the experiment. The stimulation intensities which were used, were intensities equal to the identified A-δ thresholds from each laser setting. Highest nociceptive activation estimations for the probability of C-fibres activation were seen for the ND: YAP laser at 0.73 % at a beam diameter of 6 [mm] and 0.15 % at a beam diameter of 12 [mm]. All other probabilities were < 0.1 %.

See all stimulation parameter setup and nociceptive activation estimations in Table 16.

Table 16 – Table shows stimulation parameter setup run in the model equivalent to stimulation parameters run in the experiment, and corresponding results from the nociceptive activation estimation. †Value estimated from experimental data, where laser spot radius is defined as 1/e^2. ‡ Values measured via a dosiometer (Coherent FieldMaxII + Coherent PM150). Measured intensities from the ND: YAP laser, were given directly from the ND: YAP laser system.

Stimulation parameter setup

Laser type	CO2 – 10,600 nm	CO2 – 10,600 nm	ND: YAP – 1340 nm	ND: YAP – 1340 nm
Laser spot diameter	10 [mm] †	16 [mm] †	6 [mm] †	12 [mm] †
t_{pulse}	200 [ms]	200 [ms]	10 [ms]	10 [ms]
Energies to reach A-δ pain threshold	48 [mJ]	200 [mJ]	2250 [mJ]	5750 [mJ]

Energy per area	611.2 [J/m^2]	994.7 [J/m^2]	79577 [J/m^2]	50841 [J/m^2]
Released wattage	0.24 [W] ‡	1.0 [W] ‡	225 [W]	575 [W]
Results from nociceptive activation estimation				
Estimated probability of A-δ activation	< 0.01 [%]	< 0.01 [%]	< 0.01 [%]	< 0.01 [%]
Estimated probability of C-fibre activation	< 0.01 [%]	< 0.01 [%]	0.73 [%]	0.15 [%]
A-delta activation threshold - Mean±	44.13±3.02 °C	44.75±3.35 °C	44.33±2.54 °C	43.93±1.41 °C

The found A-delta and C-fibre activation threshold from the experimental data is plotted in following figures: Figure 26, Figure 27, Figure 28, and Figure 29. Generally, the found A-delta pain threshold has a lower mean and larger SD compared to thresholds found in (Churyukanov et al. 2012) where the A-δ pain threshold are identified as 46.9±1.7 °C.
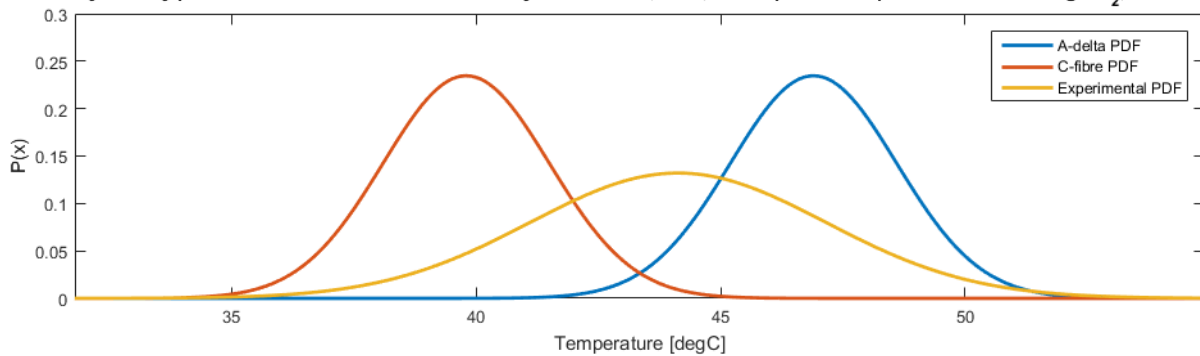
Figure 26 – Figure illustrates the pain activation thresholds when using a CO$_2$ laser with a 10 [mm] laser spot diameter. A-δ and C-fibre activation pain thresholds from (Churyukanov et al. 2012) are plotted along with experimental data from the present study as PDFs. The red line represents the PDF of C-fibre activation, blue line represents the PDF of A-δ activation, and the yellow line represents PDF of experimental data.

Probability density plots of A-delta and C-fibre from Churyukanov et al., 2012, and experimental pain thresholds using CO₂, 16 mm diameter
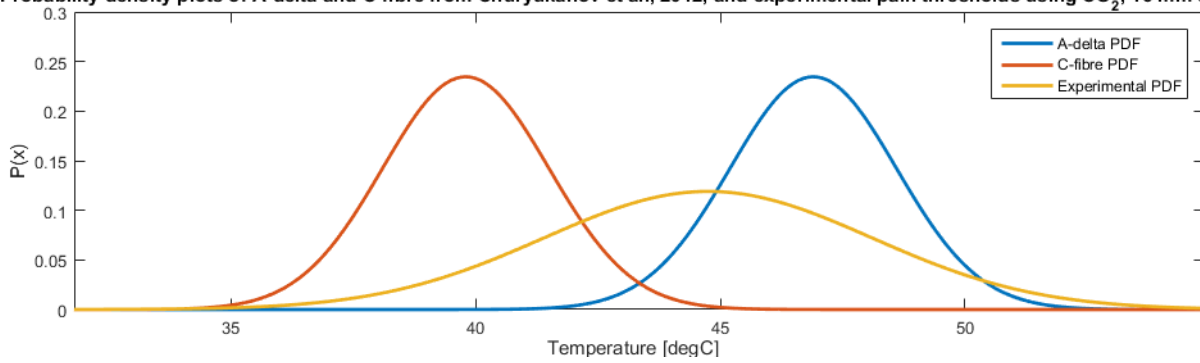
Figure 27 – Figure illustrates the pain activation thresholds when using a CO$_2$ laser with a 16 [mm] laser spot diameter. A-δ and C-fibre activation pain thresholds from (Churyukanov et al. 2012) are plotted along with experimental data from the present study as PDFs. The red line represents the PDF of C-fibre activation, blue line represents the PDF of A-δ activation, and the yellow line represents PDF of experimental data.

Probability density plots of A-delta and C-fibre from Churyukanov et al., 2012, and experimental pain thresholds using ND: YAP, 6 mm diameter
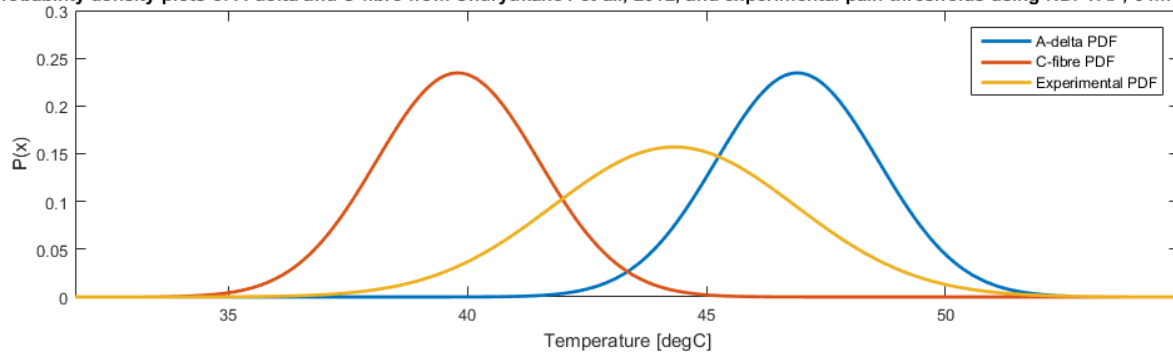
Figure 28 – Figure illustrates the pain activation thresholds when using a Nd: YAP laser with a 6 [mm] laser spot diameter. A-δ and C-fibre activation pain thresholds from (Churyukanov et al. 2012) are plotted along with experimental data from the present study as PDFs. The red line represents the PDF of C-fibre activation, blue line represents the PDF of A-δ activation, and the yellow line represents PDF of experimental data.

Probability density plots of A-delta and C-fibre from Churyukanov et al., 2012, and experimental pain thresholds using ND: YAP, 12 mm diameter
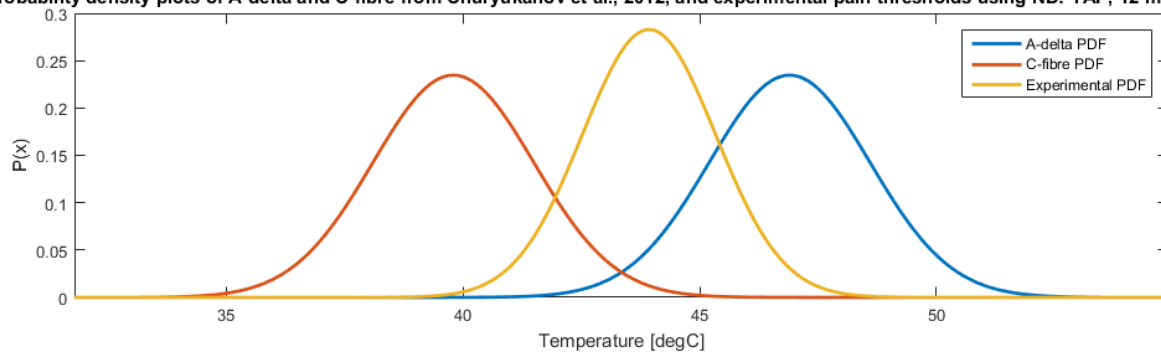
Figure 29 – Figure illustrates the pain activation thresholds when using a Nd: YAP laser with a 12 [mm] laser spot diameter. A-δ and C-fibre activation pain thresholds from (Churyukanov et al. 2012) are plotted along with experimental data from the present study as PDFs. The red line represents the PDF of C-fibre activation, blue line represents the PDF of A-δ activation, and the yellow line represents PDF of experimental data.

4.2.2 Temporal surface profiles

In following sub-section, the temporal surface profiles will be described. The profiles are based on experimental data and modelling data. The laser is shoot and modelled with the same laser parameters to ensure comparability. The surface profiles are described from following three locations: (0,0), (5,0), and (10,0), and is analysed over 7.5 [s] from ≤ 50 [ms] from stimulation onset.

Data from CO_2 (diameter of 10 [mm]) laser comparison at (0,0) shows that modelled data does not fit within the SD of the mean from the experimental data. Experimental data shows a T_{max}(delta T) ≈ 10 °C while the modelled data shows a T_{max}(delta T) ≈ 0.75 °C. At (5,0) and (10,0) the modelled data stays within the SD of the mean in the experimental data. At (10,0) the modelled data strongly correlates with the experimental data mean. The form of the curve in the modelled data and experimental data have a comparable shape. See data displayed in Figure 30.

Temporal profiles at following spots; (0,0),(5,0),(10,0), CO_2, 10 [mm], with stimulation intensities from experiment
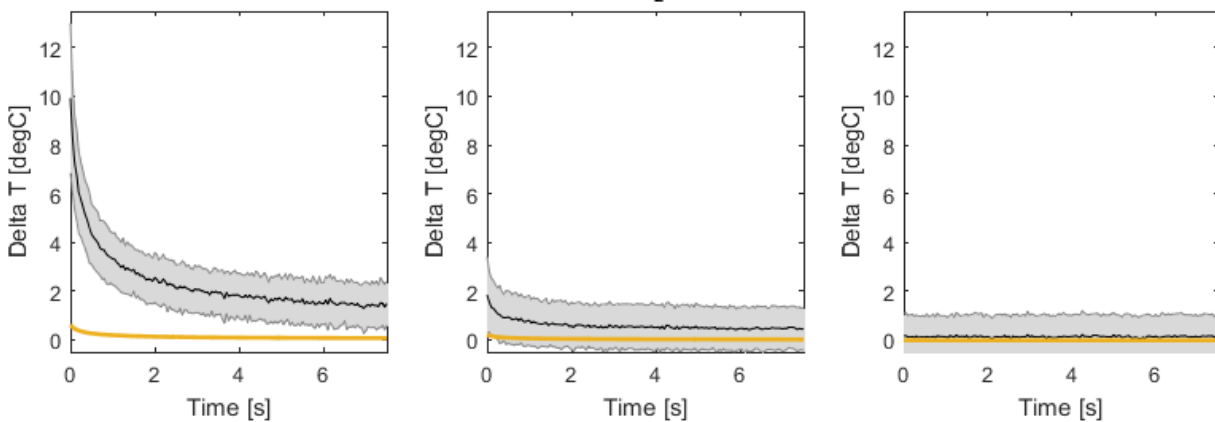
Figure 30 – The figures illustrates the absolute change in temperature of the cool down period on the surface of the skin at following spots; (0,0), (5,0), (10,0) [mm], after laser stimulation has been applied. The laser stimulation is applied with a CO_2 laser with a beam diameter of 10 [mm]. The black line represents the mean of the surface temperatures, the grey area represents the SD of the mean of the surface temperatures, and the orange line represents the output of the model at the same corresponding temporal coordinates as the experimental data.

Data from CO_2 (diameter of 16 [mm]) laser comparison at (0,0) and (5,0) shows that modelled data does not fit within the SD of the mean from the experimental data. Experimental data shows a T_{max}(delta T) ≈ 10 °C while the modelled data shows a T_{max}(delta T) ≈ 1 °C. At (10,0) the modelled data stays within the SD of the mean in the experimental data. At (10,0) the modelled data strongly correlates with the experimental data mean. The form of the curve in the modelled data and experimental data have a comparable shape. Data displayed in Figure 30.

Temporal profiles at following spots; (0,0),(5,0),(10,0), CO$_2$, 16 [mm], with stimulation intensities from experiment
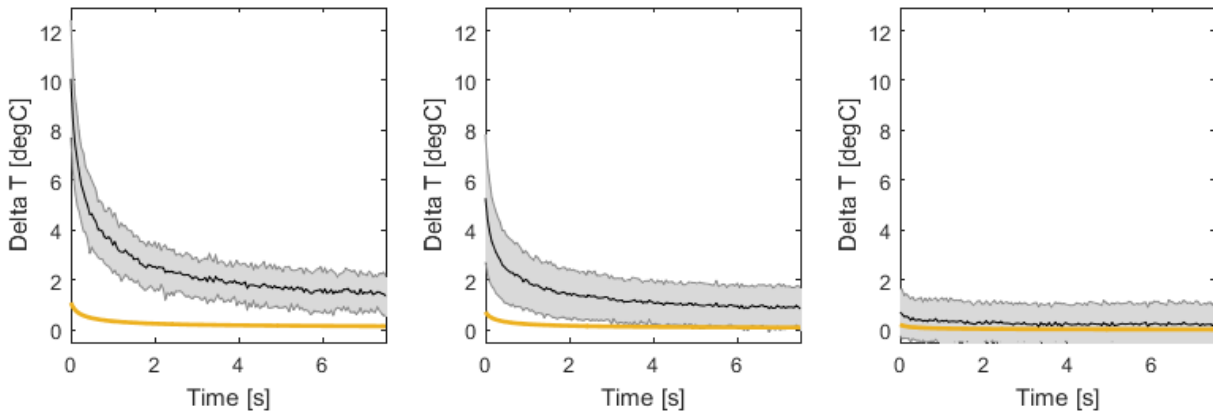
Figure 31 - The figures illustrates the absolute change in temperature for the cool down period on the surface of the skin at following spots; (0,0), (5,0), (10,0) [mm], after laser stimulation has been applied. The laser stimulation is applied with a CO$_2$ laser with a beam diameter of 16 [mm]. The black line represents the mean of the surface temperatures, the grey area represents the SD of the mean of the surface temperatures, and the orange line represents the output of the model at the same corresponding temporal coordinates as the experimental data.

Data from Nd: YAP (diameter of 6 [mm]) laser comparison at (0,0) and (5,0) shows that modelled data does not fit within the SD of the mean from the experimental data. Experimental data shows a T$_{max}$(delta T) ≈ 12.5 °C while the modelled data shows a T$_{max}$(delta T) ≈ 4 °C. At (10,0) the modelled data stays within the SD of the mean in the experimental data. At (10,0) the modelled data strongly correlates with the experimental data mean plus an offset. The form of the curve in the modelled data and experimental data does not have a comparable shape in (0,0) and (5,0), where T$_{max}$(delta T) are seen at different times. For the modelled data T$_{max}$(delta T) is seen at t > 7.5 [s] and in the experimental data it is seen in t = 0 [s]. See data displayed in Figure 32.

Temporal profiles at following spots; (0,0),(5,0),(10,0), ND:YAP, 6 [mm], with stimulation intensities from experiment
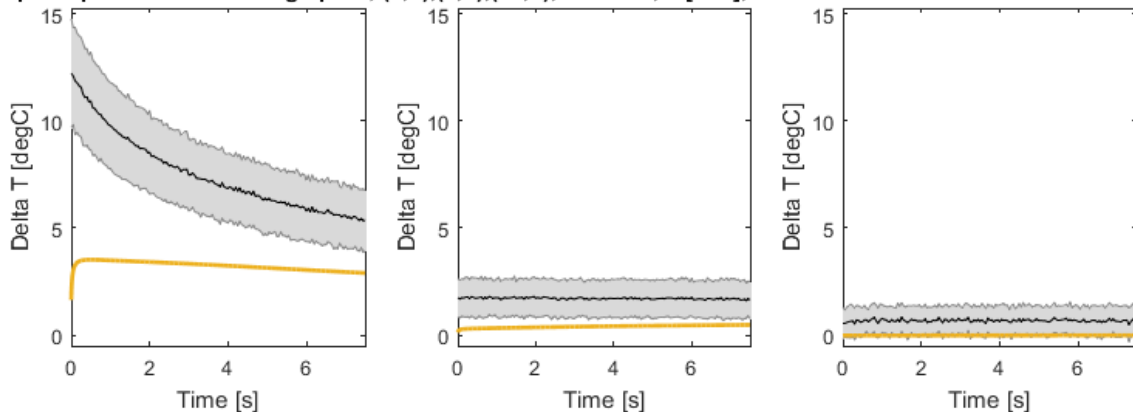
Figure 32 - The figures illustrates the absolute change in temperature for the cool down period on the surface of the skin at following spots; (0,0), (5,0), (10,0) [mm], after laser stimulation has been applied. The laser stimulation is applied with a Nd: YAP laser with a beam diameter of 6 [mm]. The black line represents the mean of the surface temperatures from the experiment, the grey area represents the SD of the mean of the surface temperatures from the experiment, and the orange line represents the output of the model at the same corresponding temporal coordinates as the experimental data.

Data from Nd: YAP (diameter of 12 [mm]) laser comparison at (0,0), (5,0), and (10,0) shows that modelled data does not fit within the SD of the mean from the experimental data. Experimental data shows a T_{max}(delta T) $\approx$ 12 °C while the modelled data shows a T_{max}(delta T) $\approx$ 2.5 °C. At (10,0) the modelled data strongly correlates with the experimental data mean plus an offset. The form of the curve in the modelled data and experimental data does not have a comparable shape in (0,0) and (5,0), where T_{max}(delta T) are seen at different times. For the modelled data T_{max}(delta T) is seen at t > 7.5 [s] and in the experimental data it is seen in t = 0 [s]. See data displayed in Figure 33.

Figure 33 - The figures illustrates the absolute change in temperature for the cool down period on the surface of the skin at following spots; (0,0), (5,0), (10,0) [mm], after laser stimulation has been applied. The laser stimulation is applied with a Nd: YAP laser with a beam diameter of 12 [mm]. The black line represents the mean of the surface temperatures from the experiment, the grey area represents the SD of the mean of the surface temperatures from the experiment, and the orange line represents the output of the model at the same corresponding temporal coordinates as the experimental data.

5   Results of model validation

This chapter contains the results from the validation of the model. Light absorption coefficients are kept the same when modelling the CO_2 laser, due to the shape of the cool down period of the model and experimental data looked alike, see Figure 30 and Figure 31. Only stimulation intensity for modelling the CO_2 laser stimulation is changed. There is conducted a sensitivity analysis for the heat transfer coefficients when modelling the Nd: YAP laser, to get an overview of how much each coefficient influence T_{max}(delta T). Furthermore, there is established a new μ_a of epidermis as validation of the model, by trial and error, where only the end final value will be displayed here in this chapter.

5.1   Sensitivity analysis of heat transfer coefficients

All heat transfer coefficient sensitivity analysis is conducted with the Nd: YAP laser with a beam width of 6 [mm]. All simulations are run with the same parameter setup. Changes within the heat transfer coefficients ranges from the literature, did not excel higher T_{max}(delta T) changes than <2 °C. See heat transfer coefficient ranges in Table 17 and the related changes in T_{max}(delta T) in Table 18.

Table 17 – Table gives an overview of the heat transfer coefficients ranges used in the sensitivity analysis. The coefficient ranges are derived from the literature, which may be found in Table 7, Table 8 and Table 9, for ρ, k and Cp, respectively. Analysis is conducted with the Nd: YAP laser.

Heat transfer coefficient ranges			
	SC	Epidermis	Dermis	Hypodermis
Cp	3590-3700	3590-3700	3200-3800	2300-2675
ρ	1330	1200-1600	1000-1200	850-1000
k	0.21-0.27	0.21-0.27	0.45-0.53	0.16-0.19

Table 18 – The table gives an overview of the related changes to T_{max}(delta T), related to shifting heat transfer coefficients within the ranges found in Table 17. The highest change of T_{max}(delta T) is related to shifting ρ of epidermis and may induce a temperature rise <2 °C. Analysis is conducted with the Nd: YAP laser.

Changes in T_{max}(Delta T)			
	SC	Epidermis	Dermis	Hypodermis
Cp	<1 °C	<1 °C	<1 °C	<1 °C
ρ	<1 °C	<1 °C	<2 °C	<1 °C
k	<1 °C	<1 °C	<1 °C	<1 °C

5.2   Adjustment of light absorption coefficients when modelling Nd: YAP laser stimulation

Following section contains the new value of μ_a of epidermis, modelled with the Nd: YAP laser. The goal of T_{max}(Delta T) for Nd: YAP with a beam width of 6 and 12 [mm] is around 12-12.2 °C in relation to experimental data, see Figure 32 and Figure 33. The new value μ_a of epidermis, is set to 10 [cm^{-1}], which is about 10x increase in relation to the previous modelled value of μ_a = 1.05 [cm^{-1}]. See energy distributions with previous and new value μ_a of epidermis in Figure 34. New value of μ_a, shows higher amounts of energy absorbed in epidermis compared to the previous energy distribution. This is estimated to produce higher temperatures in epidermis and in the proximal surrounding tissues, i.e. stratum Corneum and dermis.

Figure 34 – Adjusted energy distributions of Nd: YAP laser with a beam width of 6 [mm]. The distributions are the output from the MC implementation. Left figure is the non-adjusted distribution with a value of μ_a equal to 1.05 [cm^{-1}]. Right figure is the adjusted distribution with a value of μ_a for epidermis of 10.0 [cm^{-1}]. Distribution is mirrored at r = 0. Higher absorption in epidermis is present in the adjusted energy distribution, compared to the non-adjusted distribution.

The adjusted μ_a yields a T_{max}(Delta T) for (0,0) at 12.25 °C with a beam width of 6 [mm] and 7.95 °C with a beam width of 12 [mm]. See overview of values in Table 19.

Table 19 – Table gives an overview of the modelled Nd: YAP laser setups with adjusted values of μ_a for epidermal tissue.

Modelled Nd: YAP laser, 1340 [nm]		
Beam width	6 [mm]	12 [mm]
Multiplier of μ_a	10x	10x
New μ_a	10 [cm^{-1}]	[cm^{-1}]
New T_{max}(Delta T)	12.25 °C	7.95 °C

The temporal profiles with adjusted μ_a showed at (0,0) a similar T_{max}(Delta T) between experimental data and modelled data with a beam width of 6 [mm], see (0,0) in Figure 35. With a beam width of 12 [mm], the T_{max}(Delta T) between experimental data and modelled data were not similar lacking around 4 °C, see (0,0) in Figure 36. The cool down period of the modelled data has a higher gradient near t < 0.24 [s] and a lower gradient at t > 0.25 [s] compared to experimental data, see (0,0) in Figure 35 and [(0,0) (5,0)] in Figure 36. At (5,0) and (10,0) at a beam width of 6 [mm], the curves are comparable in terms of shape, but there is seen an offset of 1-2 °C in delta T, see Figure 35. A similar offset is seen at (10,0) at a beam width of 12 [mm], see Figure 38

Temporal profiles at following spots; (0,0),(5,0),(10,0), ND:YAP, 6 [mm], with stimulation intensities from experiment
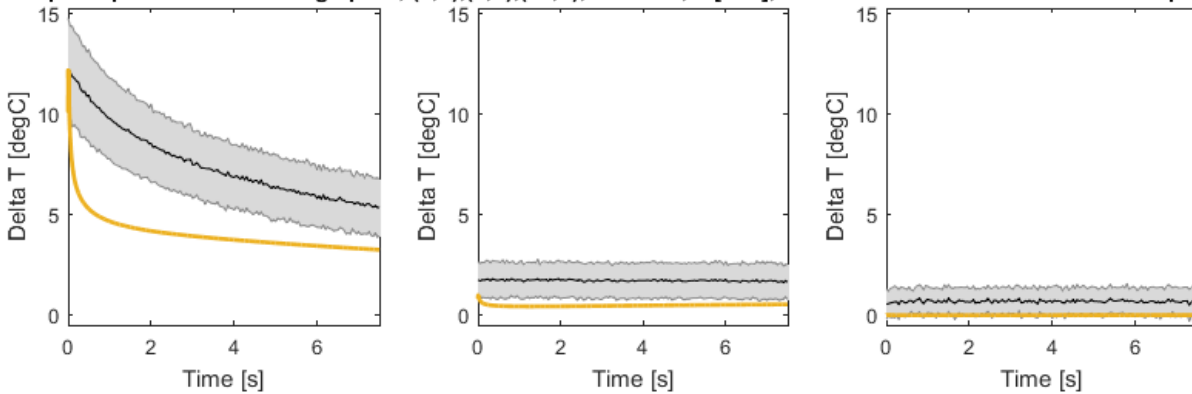
Figure 35 - The figures illustrates the absolute change in temperature for the cool down period on the surface of the skin at following spots; (0,0), (5,0), (10,0) [mm] (left, middle and right subfigure respectively), after laser stimulation has been applied and with the adjusted μ_a for epidermis. The laser stimulation is applied with a Nd: YAP laser with a beam diameter of 6 [mm]. The black line represents the mean of the surface temperatures from the experiment, the grey area represents the SD of the mean of the surface temperatures from the experiment, and the orange line represents the output of the model at the same corresponding temporal coordinates as the experimental data.

Temporal profiles at following spots; (0,0),(5,0),(10,0), ND:YAP, 12 [mm], with stimulation intensities from experiment
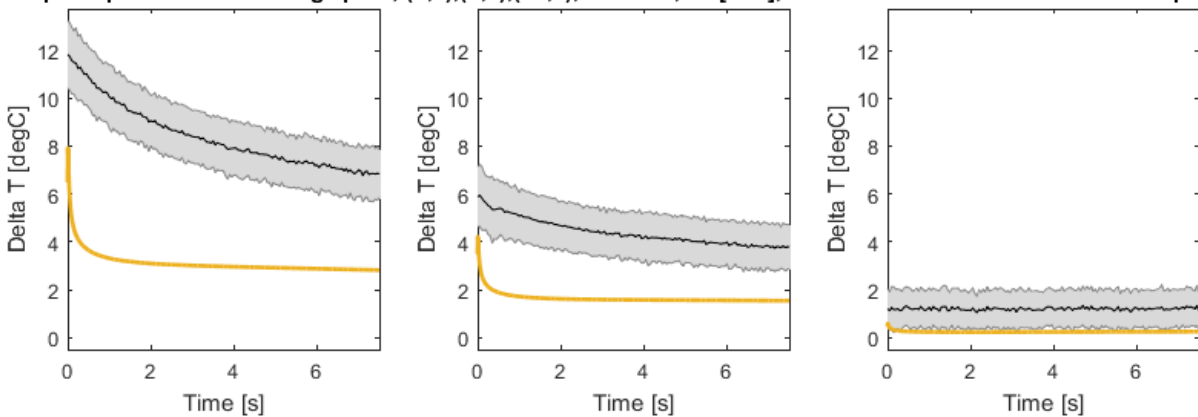
Figure 36 - The figures illustrates the absolute change in temperature for the cool down period on the surface of the skin at following spots; (0,0), (5,0), (10,0) [mm] (left, middle and right subfigure respectively), after laser stimulation has been applied and with the adjusted μ_a for epidermis. The laser stimulation is applied with a Nd: YAP laser with a beam diameter of 12 [mm]. The black line represents the mean of the surface temperatures from the experiment, the grey area represents the SD of the mean of the surface temperatures from the experiment, and the orange line represents the output of the model at the same corresponding temporal coordinates as the experimental data.

5.3   Adjustment of stimulation intensity when modelling CO_2 laser stimulation

The results from the comparison the model with the experiment yielded a 9-9.5 °C lower T_{max}(delta T) than expected. The cool down curve of the model data compared to the experimental data are comparable in all spots and lies within the SD of the mean of delta T, see Figure 30 and Figure 31. Based on these two information, only the stimulation intensity in the model is being adjusted to fit the experimental data. See new adjusted stimulation intensities in Table 20 and temporal spot profiles in Figure 37 and Figure 38.

Table 20 – Table gives an overview of the modelled CO_2 laser setups with adjusted stimulation intensities.

	Modelled CO_2 laser, 10,600 [nm]	
Beam width	10 [mm]	16 [mm]
Multiplier of stimuli intensity	12.5	7.5
Adjusted energy deposited	600 [mJ]	1500 [mJ]
Wattage	3 [W]	7.5 [W]
Energy per area	7639.4 [J/m^2]	7460.4 [J/m^2]
New Tmax(Delta T)	10 °C	10 °C
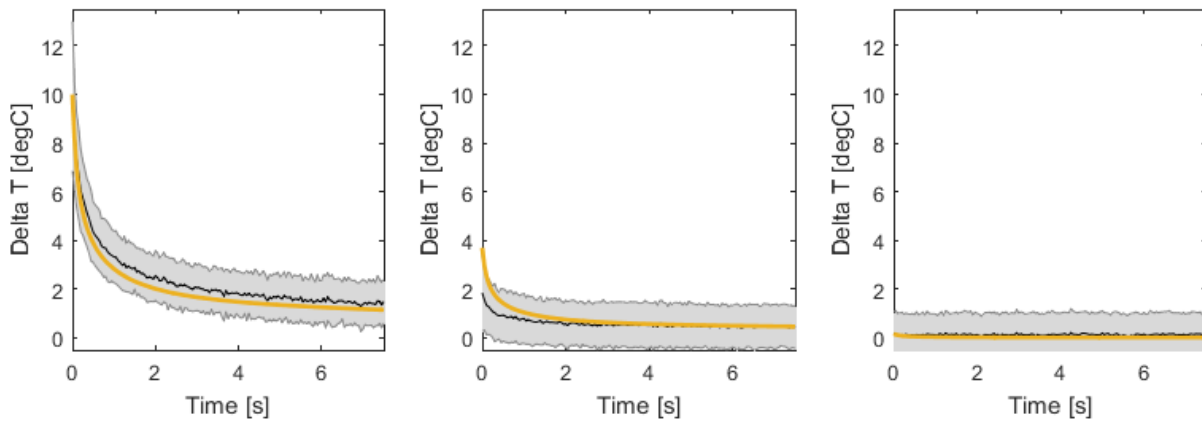
Figure 37 - The figures illustrates the absolute change in temperature of the cool down period on the surface of the skin at following spots; (0,0), (5,0), (10,0) [mm] (left, middle and right subfigure respectively), after the adjusted laser stimulation has been applied. The laser stimulation is applied with a CO_2 laser with a beam diameter of 10 [mm]. The black line represents the mean of the surface temperatures, the grey area represents the SD of the mean of the surface temperatures, and the orange line represents the output of the model, at the same corresponding temporal coordinates as the experimental data. The modelled data is for all temporal spot profiles within the SD of the mean of experimental data.

Figure 38 – The figures illustrates the absolute change in temperature of the cool down period on the surface of the skin at following spots; (0,0), (5,0), (10,0) [mm] (left, middle and right subfigure respectively), after the adjusted laser stimulation has been applied. The laser stimulation is applied with a CO_2 laser with a beam diameter of 16 [mm]. The black line represents the mean of the surface temperatures, the grey area represents the SD of the mean of the surface temperatures, and the orange line represents the output of the model, at the same corresponding temporal coordinates as the experimental data. The modelled data is for all temporal spot profiles within the SD of the mean of experimental data.

6 Discussion

The model describing noxious stimulation for Nd: YAP and CO_2 lasers was successfully optimized in relation to following: Stimulation area, boundary conditions, Grid resolution, Solver configuration, iteration count / simulation, MESH, Laser ON/OFF function and estimation of nociceptive activation. Results of temporal surface profiles of experimental data at (0,0), (5,0) and (10,0) were presented and compared to modelling data. The model was adjusted per the planned validation of the model. Validation of CO_2 laser showed modelled data to be within the SD of the mean of experimental data, and is therefore deemed to produce meaningful results. Validation of Nd: YAP laser showed modelled data was not within the SD of the mean of experimental data.

6.1 Methods of the model

The grid resolution was optimized in relation to *r*. Optimizing the grid in relation to *z* is also a possibility and would increase computational speeds in the MC implementation. Since the highest gradients of heat propagation happens closest to the surface of the model, it would be interesting to have a high grid resolution near laser spot centre and lower the further away from spot centre both in *r* and *z* directions. There were not conducted a convergence analysis on the grid resolution optimization, but it is estimated to converge based on visual inspection, see similarities of beam profile in Figure 14 compared to Figure 13.

Variations of skin pigmentation is not included in the model. The amount of skin pigmentation may be strongly influencing the amount of heat generated in the skin (Churyukanov et al. 2012). Measuring amount of pigmentation in the skin could contribute to personalization of coefficients in the model.

6.2 Experimental methods and observations

The beam profile of the Nd: YAP laser in the experiment had changing form in relation to what beam diameter is chosen. Choosing the lowest beam diameter resulted in a near flat top beam profile, where larger beam diameters would result in a beam profile which is more Gaussian (El.En. S.p.A. 2005). The beam widths of 6 [mm] and 12 [mm] would then yield a mixed beam profile of a flat top and Gaussian form. In the model, the Nd: YAP laser was modelled as having a Gaussian beam profile and it uncertain what effect it might have to the results in terms of maximum heat generated and heat propagated. The beam profile of the CO_2 laser was measured to be 10 [mm] when keeping the laser still when stimulating, and 16 [mm] while moving it around in small circles. It is estimated that the 10 [mm] beam spot diameter has a more Gaussian shape than the 16 [mm] beam spot diameter. Measuring the experimental laser beam profiles would contribute with data to increase the precision of modelled beam profiles.

Quantifying nociceptive activation of A-delta fibres from subject feedback is challenging the reliability of the data, while studying LEP from EEG instead would eliminate the need of subject feedback (R. Treede et al. 2003).

Due to the low 20 [FPS] recording speed of the thermal camera used in the experiment, it is uncertain whether the peak T_{max} of the heat generated from laser stimulation has been recorded. It is highly probable that peak T_{max} has not been established for all recordings, since there is assumed to be a large cooling gradient shortly after stimulation onset.

6.3   Validation methods

Based on the results without model adjustment, see Results in chapter 4, it was chosen to complete a simple validation of the model where, only stimulation intensity for modelling the CO_2 laser and μ_a of epidermis for modelling Nd: YAP laser was changed. These changes are assumed to be part of successful validation but not adequate for evaluation of the model in a real setting. Further validation of the model would need parameter sweeps of optical and thermal coefficients within the ranges found in the literature, to find the most suitable solution for modelling CO_2 and Nd: YAP lasers. Another approach would be to collect more experimental data on.

6.4   Results

Similar form of cool down periods after stimulation onset when comparing the model and the CO_2 laser stimulation parameters, but the model data differed in terms of amplitude. Comparing Nd: YAP laser stimulation with model data showed weak comparable cool down periods after stimulation onset in terms of form of the cool down period and amplitude from modelled data. Validation of model when comparing the CO_2 laser showed that modelled data lied within SD of the mean of experimental data with both 10 [mm] and 16 [mm] beam widths. Validation of model when comparing the Nd: YAP laser showed that modelled data gained equal T_{max}(delta T) of mean over the cool down period but differed in the form of the cool down period.

The stimulation intensities measured from experimental CO_2 laser stimulation were lower than what is seen in other CO_2 laser stimulation studies. There, stimulation intensities for evoking nociceptive activation with equal beam widths of 10 [mm] is around 785-825 [mJ] (Ragé et al. 2010; Svensson et al. 1997), compared to 48 [mJ] in the experiment. It is estimated that the measuring device used in the experiment had been setup wrongly or that it was defect during the measurements.

The identified A-δ pain threshold from the experiment yielded between 2.15-3.07 °C lower T_{max} compared to equal values from (Churyukanov et al. 2012). These differences could be caused by the low caption rate (20 FPS) of the thermal camera used in the experiment, and it is therefore uncertain if the peak temperature was captured in the data. Using a higher FPS of the thermal camera recordings would raise the probability of capturing the peak temperature of the heating in the skin cause by laser stimulation. In the model, the extracted data was only from the specific points of (0,0), (5,0) and (10,0). Measuring over an area instead would probably generate more comparable results to the experimental data since the thermal camera has a low resolution (8x10 [pixels] per 1 [cm^2]). The low-resolution measurements generate average temperatures over each pixel.

Another contributor to the lowered A-delta pain thresholds in the experimental data could be related to the transparency in of stratum Corneum in relation to heat radiation. The thermal camera may see thermal radiation between 2000-5000 [μm]. Within this interval, the absorption of light energy in stratum corneum varies between 0.8-550 [cm^{-1}], see Figure 6. Water in stratum corneum is seen as the main contributor to light absorption and is defined as 5 % (Meglinski & Matcher 2002). What the thermal camera captures while recording heating on the skin may therefore summation of heat radiation from epidermis through stratum corneum. Combing experimental measurements with spot measurements directly on stratum corneum in the model, could therefore have caused lower T_{max} in the model. Bypassing stratum Corneum by measuring directly on epidermis in the model may lead to a more successful validation. The theory could be tested by comparing experimental data at (0,0) with measurements directly on epidermis in the model at (0, [stratum corneum-epidermis boundary]).

The beam profiles in the experiment is not assessed and it is there uncertain whether the modelled gaussian beam profiles fit the actual beam profile of the lasers used in the experiment. Producing results comparing sigmoid spatial profiles in the experiment with the modelled data could provide insights into the gaussianity of the beam profiles in the experiment.

6.5   Future of the study

Next step in the validation is comparing the results with other studies using CO2 and/or Nd: YAP lasers. Since the only changed parameter of CO_2 laser stimulation was the stimulation intensity, it would be interesting to compare the stimulation intensity and setup with other relatable literature. If the results are comparable, next step would to perform further validation in an experiment with more data and finally evaluate the model in solving a real problem. Modelling the Nd: YAP laser was not successfully validated since the model data did not lie within the SD of the mean Tmax of the experimental data. Therefore, next step would be to conduct further validation in relation to the experimental data by performing trial and error parameter sweeps within coefficient ranges found in the literature, and by conducting experiments investigating the Nd: YAP related stimulating skin tissue coefficients. Experimental A-δ activation stimulation intensities of the Nd: YAP laser may also be compared with other relevant literature. Since Nd: YAP and CO_2 lasers are not the only types of lasers used in noxious laser stimulation it would be interesting to include more different lasers in the model and in the validation of the model.

7   Conclusion

Pain is one of the most important physiological mechanism to ensure survival from external stimuli. Pain serves as a protective system which functions by alerting us from injuries which require evasion or acute treatment. In pain research, the use of lasers has been a popular tool in causing pure heat stimulation and selectively activation of A-δ and C-fibres. Different lasers have different levels of penetration throughout the skin. The higher the level of penetration the harder it is to understand how the laser-light is distributed and the heat is propagating in the skin. Through mathematical modelling it is possible to predict and describe the phenomenon. Such a model may simplify the use of lasers in research related or clinical problems where laser stimulation is being used or may be used.

The present study was based on a previous made 4-layered (Stratum Corneum, Epidermis, Dermis and Hypodermis) 2D-axial (r,z) model describing light absorption for laser wavelengths between 250-10600 [nm] in skin tissue and how the consequential heat is propagating (Cid Royo et al. 2016). The model was constructed on a verified Monte Carlo model implemented in MATLAB R2015b (MathWorks Inc.) describing light absorption and a Finite Element model implemented in COMSOL Multiphysics 5.2 (COMSOL Inc.) describing the heat transfer. In the present study, the model was optimized to accommodate for an experimental validation on 5 healthy subjects of the model in relation to noxious stimulation of A-δ fibres on the volar forearm using both a Carbon Dioxide (CO_2) laser (Synrad Firestar, TI-100, USA) and a Neodymium: Yttrium-Aluminium-Perovskite (Nd: YAP) laser (STIMUL 1340, El.En. S.p.A., 50041 Firenze, Italy). Each laser type has relatively different penetration depths. Experimental data was based on thermographic recordings of the stimulation site and subject feedback related to the A-δ pain threshold.

The model was adjusted in relation to obtaining same maximum temperature in the model as in the experimental data at the centre of the laser beam spot after less than 50 [ms] from stimulation onset. The CO_2 laser was adjusted in relation to stimulation intensity and the Nd: YAP laser was adjusted in relation to the absorption coefficient in the epidermal layer. Results from the CO_2 laser validation showed that modelled data lied within the SD of the mean temperature at (0,0), (5,0) and (10,0) [mm] over a cool down period of 7.5 [s] after stimulation onset. Results from the Nd: YAP laser validation showed that the modelled maximum temperature was equal to the experimental maximum temperature but the modelled data was not within the SD of mean temperature over a cool down period of 7.5 [s] after stimulation onset.

Next step of the model would be to compare the modelled laser stimulation intensities with other related laser stimulation references in relation to estimation of nociceptive activation. The adjusted model may provide insights into the laser light absorption and heat propagation of different lasers types with relatively different penetration depths, and into further planning of validation. Further adjustment of coefficients is needed when modelling the Nd: YAP laser to achieve a successful validation. Through a successful validation, it would be possible to evaluate the model functionality to produce meaningful results in relation to pain research related problems.

8 References

Agema Infrared Systems, 1992. Thermovision ® 900 Series , Users Manual.

Arendt-Nielsen, L. & Chen, A.C.N., 2003. Lasers and other thermal stimulators for activation of skin nociceptors in humans. *Neurophysiologie Clinique/Clinical Neurophysiology*, 33(6), pp.259–268. Available at: http://linkinghub.elsevier.com/retrieve/pii/S0987705303000765.

Bashkatov, A.N. et al., 2005. Optical Properties of the Subcutaneous Adipose Tissue in the Spectral Range 400 – 2500 nm. *Optics and spectroscopy*, 99(5), pp.868–874.

Bashkatov, A.N., Genina, E.A. & Tuchin, V. V., 2011. OPTICAL PROPERTIES OF SKIN, SUBCUTANEOUS, AND MUSCLE TISSUES: A REVIEW. *Journal of Innovative Optical Health Sciences*, 4(1), pp.9–38. Available at: http://www.worldscientific.com/doi/abs/10.1142/S1793545811001319.

Blank, I.H. et al., 1984. The diffusion of water across the stratum corneum as a function of its water content. *The Journal of investigative dermatology*, 82(2), pp.188–94. Available at: http://www.ncbi.nlm.nih.gov/pubmed/6693781.

Blum, W. et al., 2007. *Modelling and Applications in Mathematics Education* W. Blum et al., eds., Boston, MA: Springer US. Available at: http://dx.doi.org/10.1007/978-0-387-29822-1.

Cencič, B., Možina, J. & Jezeršek, M., 2013. Laser tattoo removal with preceding ablative fractional treatment. In L. D. Lilge & R. Sroka, eds. p. 88030D. Available at: http://proceedings.spiedigitallibrary.org/proceeding.aspx?doi=10.1117/12.2032765.

Chang, C.-H., Wilson, C.R. & Fried, N.M., 2015. Comparison of four lasers (λ = 650, 808, 980, and 1075 nm) for noninvasive creation of deep subsurface lesions in tissue. In L. D. Lilge & R. Sroka, eds. p. 95420G. Available at: http://proceedings.spiedigitallibrary.org/proceeding.aspx?doi=10.1117/12.2183478.

Chaoying, T. & Wang, B., 2015. A Fast Optical Method to Estimate Melanin Distribution from Colour Images. , 525, pp.408–415. Available at: http://link.springer.com/10.1007/978-3-662-47791-5.

Churyukanov, M. et al., 2012. Thermal Detection Thresholds of Aδ- and C-Fibre Afferents Activated by Brief CO2 Laser Pulses Applied onto the Human Hairy Skin. *PLoS ONE*, 7(4), pp.1–10.

Cid Royo, A. et al., 2016. *Modeling Nociceptive Activation by Different Laser Wavelength*, Aalborg. Available at: https://www.dropbox.com/s/l32xqo0zfug7rcm/16gr8402.pdf?dl=0.

Comsol, 2012. Comsol Multiphysics User's Guide. *The Heat Transfer Branch*, 4.3, p.709–745, The Heat Transfer Branch.

Cook, R.D. et al., 2001. *Concepts and applications of finite element analysis* 4th ed.,

Cornsweet, T.N., 1962. The Staircase-Method in Psychophysics. *The American Journal of Psychology*, 75(3), p.485. Available at: http://www.jstor.org/stable/1419876?origin=crossref.

Cruccu, G. & Truini, A., 2009. Tools for assessing neuropathic pain. *PLoS medicine*, 6(4), p.e1000045. Available at: http://www.pubmedcentral.nih.gov/articlerender.fcgi?artid=2661248&tool=pmcentrez&rendertype=abstract [Accessed March 24, 2016].

de Dear, R.J. et al., 1997. Convective and radiative heat transfer coefficients for individual human body segments. *International journal of biometeorology*, 40(3), pp.141–156.

Ding, H. et al., 2006. Refractive indices of human skin tissues at eight wavelengths and estimated dispersion

relations between 300 and 1600 nm. *Phys. Med. Biol*, 51, pp.1479–1489.

El.En. S.p.A., 2005. STIMUL 1340 Nd : YAP LASER SYSTEM OPERATOR ' S MANUAL. , pp.1–93.

ElMasry, G. & Nakauchi, S., 2015. Prediction of meat spectral patterns based on optical properties and concentrations of the major constituents. *Food Science & Nutrition*, 4(2). Available at: http://doi.wiley.com/10.1002/fsn3.286.

Frahm, K.S. et al., 2010. Spatial temperature distribution in human hairy and glabrous skin after infrared CO2 laser radiation. *Biomedical engineering online*, 9(1), p.69. Available at: http://www.biomedical-engineering-online.com/content/9/1/69.

Van Gemert, M.J.C. et al., 1989. Skin Optics. *IEEE Transactions on Biomedical Engineering*, 36(12), pp.1146–1154.

González-Roldán, A.M. et al., 2016. Controllability and hippocampal activation during pain expectation in fibromyalgia syndrome. *Biological Psychology*, 121, pp.39–48. Available at: http://dx.doi.org/10.1016/j.biopsycho.2016.09.007.

Gowrishankar, T.R. et al., 2004. Transport lattice models of heat transport in skin with spatially heterogeneous, temperature-dependent perfusion. *Biomedical engineering online*, 3(1), p.42.

Gracely, R.H. et al., 1988. A multiple random staircase method of psychophysical pain assessment. , 32, pp.55–63.

Göppner, D. et al., 2011. Wide-field, high-resolution two-photon tissue mapping of human skin ex vivo. *Medical Laser Application*, 26(4), pp.158–165. Available at: http://linkinghub.elsevier.com/retrieve/pii/S1615161511000482.

Hale, G.M. & Querry, M.R., 1973. Optical Constants of Water in the 200-nm to 200-microm Wavelength Region. *Applied optics*, 12(3), pp.555–563.

Hartmann, S. et al., 2015. Phantom of Human Adipose Tissue and Studies of Light Propagation and Light Absorption for Parameterization and Evaluation of Noninvasive Optical Fat Measuring Devices. , (February), pp.33–67.

Hecht, J., 2005. *Beam : The Race to Make the Laser: The Race to Make the Laser*, Oxford: Oxford University Press, USA. Available at: https://books.google.com/books?id=2ggTSh0PRDoC&pgis=1 [Accessed February 16, 2016].

Holbrook, K.A. & Odland, G.F., 1974. Regional Differences in the Thickness (Cell Layers) of the Human Stratum Corneum: An Ultrastructural Analysis. *Journal of Investigative Dermatology*, 62(4), pp.415–422. Available at: http://dx.doi.org/10.1111/1523-1747.ep12701670.

Hüllemann, P. et al., 2017. Reduced laser-evoked potential habituation detects abnormal central pain processing in painful radiculopathy patients. *European Journal of Pain*, pp.1–9. Available at: http://doi.wiley.com/10.1002/ejp.994.

Iannetti, G.D. et al., 2001. Usefulness of dorsal laser evoked potentials in patients with spinal cord damage : report of two cases. , pp.792–794.

Isak, B. et al., 2016. Laser and somatosensory evoked potentials in amyotrophic lateral sclerosis. *Clinical Neurophysiology*, 127(10), pp.3322–3328. Available at: http://dx.doi.org/10.1016/j.clinph.2016.08.008.

Jacques, S.L., 2013. Optical properties of biological tissues: a review. *Physics in medicine and biology*, 58(11), pp.R37-61. Available at: http://iopscience.iop.org/article/10.1088/0031-9155/58/11/R37.

Jacques, S.L. & Prahl, S.A., 1998. ECE532 Biomedical Optics 3. Optical Properties. *Oregon Graduate Institute*. Available at: http://omlc.org/classroom/ece532/class3/index.html [Accessed June 1, 2016].

Jakovels, D. et al., 2013. Evaluation of skin melanoma in spectral range 450-950 nm using principal component analysis. *Proc. SPIE 8803, Medical Laser Applications and Laser-Tissue Interactions VI*, 8803, p.88030C. Available at: http://proceedings.spiedigitallibrary.org/proceeding.aspx?doi=10.1117/12.2032526.

Jiang, S.C. et al., 2002. Effects of thermal properties and geometrical dimensions on skin burn injuries. *Burns*, 28(8), pp.713–717.

Kakigi, R. et al., 1991. Estimation of conduction velocity of A delta fibers in humans. *Muscle & nerve*, 14(12), pp.1193–6. Available at: http://www.ncbi.nlm.nih.gov/pubmed/1766450.

Kamping, S. et al., 2013. Deficient modulation of pain by a positive emotional context in fibromyalgia patients. *Pain*, 154(9), pp.1846–1855. Available at: http://dx.doi.org/10.1016/j.pain.2013.06.003.

Kandel, E.R., 2013. *Principles of Neural Science*, New York: McGraw-Hill Professional. Available at: http://lib.myilibrary.com/Open.aspx?id=396874.

Karsten, A.E. & Smit, J.E., 2012. Modeling and verification of melanin concentration on human skin type. *Photochemistry and Photobiology*, 88(2), pp.469–474. Available at: http://doi.wiley.com/10.1111/j.1751-1097.2011.01044.x.

Karsten, a. E. & Singh, A., 2013. Quantifying the influence of the epidermal optical properties on laser treatment parameters. In L. D. Lilge & R. Sroka, eds. p. 88030J. Available at: http://proceedings.spiedigitallibrary.org/proceeding.aspx?doi=10.1117/12.2032511.

Kirillin, M. et al., 2015. Towards advanced OCT clinical applications. In L. D. Lilge & R. Sroka, eds. *Proceedings of SPIE-OSA*. p. 95420I. Available at: http://proceedings.spiedigitallibrary.org/proceeding.aspx?doi=10.1117/12.2183794.

Krahé, C. et al., 2015. Attachment style moderates partner presence effects on pain: a laser-evoked potentials study. *Social Cognitive and Affective Neuroscience*, 10(8), pp.1030–1037. Available at: https://academic.oup.com/scan/article-lookup/doi/10.1093/scan/nsu156.

Kroese, D.P. et al., 2014. Why the Monte Carlo method is so important today. *Wiley Interdisciplinary Reviews: Computational Statistics*, 6(6), pp.386–392.

Lanvin, T. et al., 2015. Ultrafast laser ablation for targeted atherosclerotic plaque removal. In L. D. Lilge & R. Sroka, eds. p. 95420Z. Available at: http://proceedings.spiedigitallibrary.org/proceeding.aspx?doi=10.1117/12.2197919.

Lu, P.-L. et al., 2012. Temporal and spatial temperature distribution in the glabrous skin of rats induced by short-pulse CO2 laser. *Journal of biomedical optics*, 17(11), p.117002. Available at: http://www.ncbi.nlm.nih.gov/pubmed/23117813.

Madden, V.J., Bellan, V., et al., 2016. Pain by Association? Experimental Modulation of Human Pain Thresholds Using Classical Conditioning. *The Journal of Pain*, 17(10), pp.1105–1115. Available at: http://dx.doi.org/10.1016/j.jpain.2016.06.012.

Madden, V.J., Catley, M.J., et al., 2016. The effect of repeated laser stimuli to ink-marked skin on skin temperature—recommendations for a safe experimental protocol in humans. *PeerJ*, 4(January),

p.e1577. Available at: https://peerj.com/articles/1577.

Marchandise, E. et al., 2014. Finite element analysis of thermal laser skin stimulation for a finer characterization of the nociceptive system. *Journal of Neuroscience Methods*, 223, pp.1–10. Available at: http://dx.doi.org/10.1016/j.jneumeth.2013.11.010.

Marchesini, R. et al., 1992. Optical properties of in vitro epidermis and their possible relationship with optical properties of in vivo skin. *Journal of Photochemistry and Photobiology B: Biology*, 16(2), pp.127–140.

Martini, F.H., Nath, J.L. & Bartholomew, E.F. eds., 2012. *Fundamentals of Anatomy & Physiology* 9th ed., Pearson.

Meglinski, I. V & Matcher, S.J., 2002. Quantitative assessment of skin layers absorption and skin reflectance spectra simulation in the visible and near-infrared spectral regions. *Physiological measurement*, 23(4), pp.741–753.

Melzack, R. & Wall, P.D., 1967. PAIN MECHANISMS: A NEW THEORY. *Science*, 11(2), pp.89–90.

Museux, N. et al., 2012. Skin burns after laser exposure: Histological analysis and predictive simulation. *Burns*, 38(5), pp.658–667. Available at: http://linkinghub.elsevier.com/retrieve/pii/S0305417911003548.

Nasouri, B., Murphy, T.E. & Berberoglu, H., 2014. Simulation of laser propagation through a three-layer human skin model in the spectral range from 1000 to 1900 nm. *Journal of Biomedical Optics*, 19(7), p.75003. Available at: http://biomedicaloptics.spiedigitallibrary.org/article.aspx?doi=10.1117/1.JBO.19.7.075003.

Paloyelis, Y. et al., 2016. The Analgesic Effect of Oxytocin in Humans: A Double-Blind, Placebo-Controlled Cross-Over Study Using Laser-Evoked Potentials. *Journal of Neuroendocrinology*, 28(4).

Patwardhan, S. V., Dhawan, A.P. & Relue, P.A., 2005. Monte Carlo simulation of light-tissue interaction: Three-dimensional simulation for trans-illumination-based imaging of skin lesions. *IEEE Transactions on Biomedical Engineering*, 52(7), pp.1227–1236.

Pennes, H.H., 1948. Analysis of Tissue and Arterial Blood Temperatures in the Resting Human Forearm. *Applied Physiology*, 1(2), pp.93–122.

Perchet, C. et al., 2008. Evoked potentials to nociceptive stimuli delivered by CO2 or Nd:YAP lasers. *Clinical Neurophysiology*, 119(11), pp.2615–2622. Available at: http://dx.doi.org/10.1016/j.clinph.2008.06.021.

Petrov, G.I. et al., 2012. Human tissue color as viewed in high dynamic range optical spectral transmission measurements. *Biomedical Optics Express*, 3(9), pp.2154–61.

Prahl, S., 1999. Optical Absorption of Hemoglobin. *omlc.org*. Available at: http://omlc.org/spectra/hemoglobin/index.html.

Prahl, S.A. et al., 1989. Monte-Carlo model of light propagation in tissue. *SPIE Institute series*, IS(5), pp.102–111. Available at: http://www.ncbi.nlm.nih.gov/pubmed/14562703.

Ragé, M. et al., 2010. The time course of CO2 laser-evoked responses and of skin nerve fibre markers after topical capsaicin in human volunteers. *Clinical Neurophysiology*, 121(8), pp.1256–1266. Available at: http://linkinghub.elsevier.com/retrieve/pii/S1388245710002634.

Rohde, I. et al., 2013. Cardiovascular damage after cw and Q-switched 2µm laser irradiation. In L. D. Lilge & R. Sroka, eds. p. 88030I. Available at: http://proceedings.spiedigitallibrary.org/proceeding.aspx?doi=10.1117/12.2033550.

Rolke, R. et al., 2006. Quantitative sensory testing: a comprehensive protocol for clinical trials. *European Journal of Pain*, 10(1), pp.77–77. Available at: http://doi.wiley.com/10.1016/j.ejpain.2005.02.003.

Salomatina, E. et al., 2006. Optical properties of normal and cancerous human skin in the visible and near-infrared spectral range. *Journal of Biomedical Optics*, 11(6), p.64026.

Sandwell, D.T., 1987. Biharmonic Spline Interpolation of GEOS-3 and SEASAT Altimeter Data. , 14(2), pp.139–142.

Seifert, E. et al., 2013. Automatic irradiation control by an optical feedback technique for selective retina treatment (SRT) in a rabbit model. In L. D. Lilge & R. Sroka, eds. *Proc. SPIE*. p. 880303. Available at: http://dx.doi.org/10.1117/12.2033560.

Seteikin, A.Y. & Krasnikov, I. V., 2006. An analysis of thermal effects resulting from laser radiation interaction with a multilayered biotissue. *Russian Physics Journal*, 49(10), pp.1139–1144. Available at: http://link.springer.com/10.1007/s11182-006-0234-2 [Accessed March 14, 2016].

Stancak, A. et al., 2016. Mapping multidimensional pain experience onto electrophysiological responses to noxious laser heat stimuli. *NeuroImage*, 125, pp.244–255. Available at: http://dx.doi.org/10.1016/j.neuroimage.2015.10.028.

Svensson, P. et al., 1997. Cerebral processing of acute skin and muscle pain in humans. *Journal of neurophysiology*, 78(1), pp.450–60. Available at: http://www.ncbi.nlm.nih.gov/pubmed/9242293.

Treede, R.-D., Lorenz, J. & Baumgärtner, U., 2003. Clinical usefulness of laser-evoked potentials. *Neurophysiologie Clinique/Clinical Neurophysiology*, 33(6), pp.303–314. Available at: http://www.sciencedirect.com/science/article/pii/S0987705303000807 [Accessed April 19, 2016].

Treede, R., Lorenz, J. & Baumgärtner, U., 2003. Clinical usefulness of laser-evoked potentials. , 33, pp.303–314.

Treede, R.D. et al., 1995. Evidence for two different heat transduction mechanisms in nociceptive primary afferents innervating monkey skin. *The Journal of physiology*, 483 (Pt 3, pp.747–58. Available at: http://www.ncbi.nlm.nih.gov/pubmed/7776255.

Truini, A. et al., 2003. Laser-evoked potentials in post-herpetic neuralgia. *Clinical Neurophysiology*, 114(4), pp.702–709.

Udart, M. et al., 2011. Inactivation of bacteria by high-power 940nm laser irradiation. *Medical Laser Application*, 26(4), pp.166–171. Available at: http://dx.doi.org/10.1016/j.mla.2011.08.004.

Veen, R. Van & Sterenborg, H.J., 2004. Determination of VIS-NIR absorption coefficients of mammalian fat, with time-and spatially resolved diffuse reflectance and transmission spectroscopy. *Biomedical Topical Meeting*, p.SF4. Available at: http://www.opticsinfobase.org/abstract.cfm?uri=BIO-2004-SF4.

Wang, L. & Jacques, S., 1992. Monte Carlo modeling of light transport in multi-layered tissues in standard C. *The University of Texas*, pp.1–167. Available at: http://www.researchgate.net/publication/15612297_MCML--Monte_Carlo_modeling_of_light_transport_in_multi-layered_tissues/file/32bfe50f033cc525b8.pdf.

Weber, M.J., 1999. *Handbook of Laser Wavelengths* 1st ed., CRC press.

Welch, A. j. & Gemert, M.J.C. van, 2011. *Optical-Thermal Response of Laser-Irradiated Tissue* 2nd ed. A. J. Welch & M. J. C. van Gemert, eds., Dordrecht: Springer Netherlands. Available at: http://ebooks.cambridge.org/ref/id/CBO9781107415324A009.

Wells, J.D. et al., 2011. *Optical-Thermal Response of Laser-Irradiated Tissue* A. J. Welch & M. J. C. van Gemert, eds., Dordrecht: Springer Netherlands. Available at: http://link.springer.com/10.1007/978-90-481-8831-4.

Welzel, J., 2016. *Optical Coherence Tomography* A. Girach & R. C. Sergott, eds., Cham: Springer International Publishing. Available at: http://link.springer.com/10.1007/s00105-009-1879-x.

Wilson, S.B. & Spence, V. a, 1988. A tissue heat transfer model for relating dynamic skin temperature changes to physiological parameters. *Physics in medicine and biology*, 33(8), pp.895–912.

Xu, F. et al., 2008. Modeling of nociceptor transduction in skin thermal pain sensation. *Journal of biomechanical engineering*, 130(4), p.41013. Available at: http://www.ncbi.nlm.nih.gov/pubmed/20417502.

Zamora-Rojas, E. et al., 2013. Double integrating sphere measurements for estimating optical properties of pig subcutaneous adipose tissue. *Innovative Food Science and Emerging Technologies*, 19, pp.218–226. Available at: http://dx.doi.org/10.1016/j.ifset.2013.04.015.

Zeng, H. et al., 1997. Reconstruction of in vivo skin autofluorescence spectrum from microscopic properties by Monte Carlo simulation. *Journal of photochemistry and photobiology. B, Biology*, 38(2–3), pp.234–40. Available at: http://www.ncbi.nlm.nih.gov/pubmed/9203387 [Accessed February 26, 2016].

9 Appendix A – Experimental protocol

9.1 Purpose of experiment

The purpose of the experiment is to validate the constructed laser-skin model, through assessing A-δ pain threshold, and collecting data about spatial and temporal profiles across the surface of stimulation site. Data will afterwards be compared with the output of the model using the same stimulation parameters as in the experiment.

9.2 Subjects

- Healthy
- Age between 20-40
- Male or female
- Only non-pregnant
- No previous history of neuropathic diseases
- No previous history of dermatological diseases
- Not under the influence of anaesthetics or euphoric drugs during experiment
- Volar side of subject' forearm, dominant side, must be unbruised and intact

9.3 Equipment list

- CO_2 laser (Synrad Firestar TI-series 100 W) setup
- Protective eyewear for 10,600 nm lasers
- ND: YAP laser (STIMUL 1340, Electronic Engineering, Italy)
- Protective eyewear for 1340 nm lasers
- Thermal responsive paper (measure diameter)
- Ambient thermometer
- 1x1x0.2 cm aluminium plate
- Calliper
- Thermal camera + Recording software
- USB stick

9.4 Preparation procedures

9.4.1 Safety checklist before lasing start

- Close door and make sure that the door is marked for experimentation for the time the experiment is running
- Close all windows
- Draw blinds and roll curtains in front of windows to decrease amount of laser light polluting external environment
- Both subject and experiment leader must wear respectable eye-protection before lasers are initialized/switched on

9.4.2 Experimental Setup CO$_2$ laser
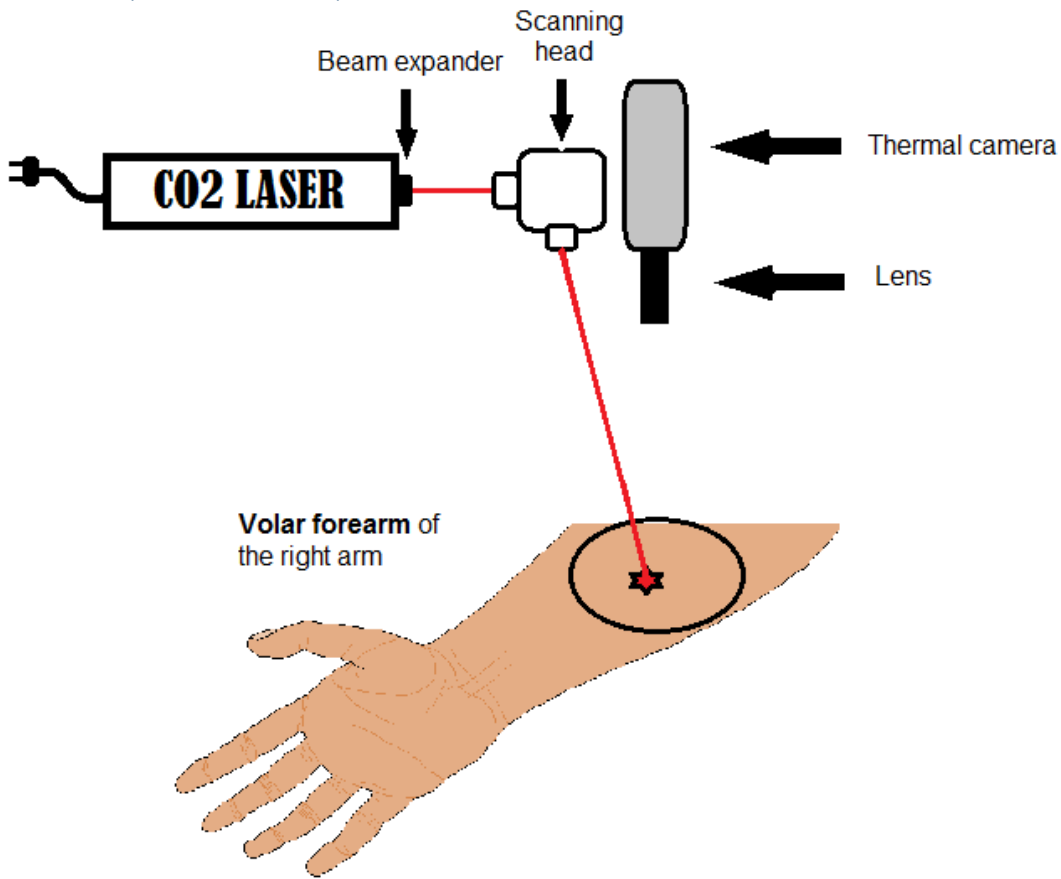
Figure 39 – Figure illustrates the CO$_2$ laser setup with scanning head and thermal camera.

9.4.3

9.4.4 Experimental Setup ND: YAP laser
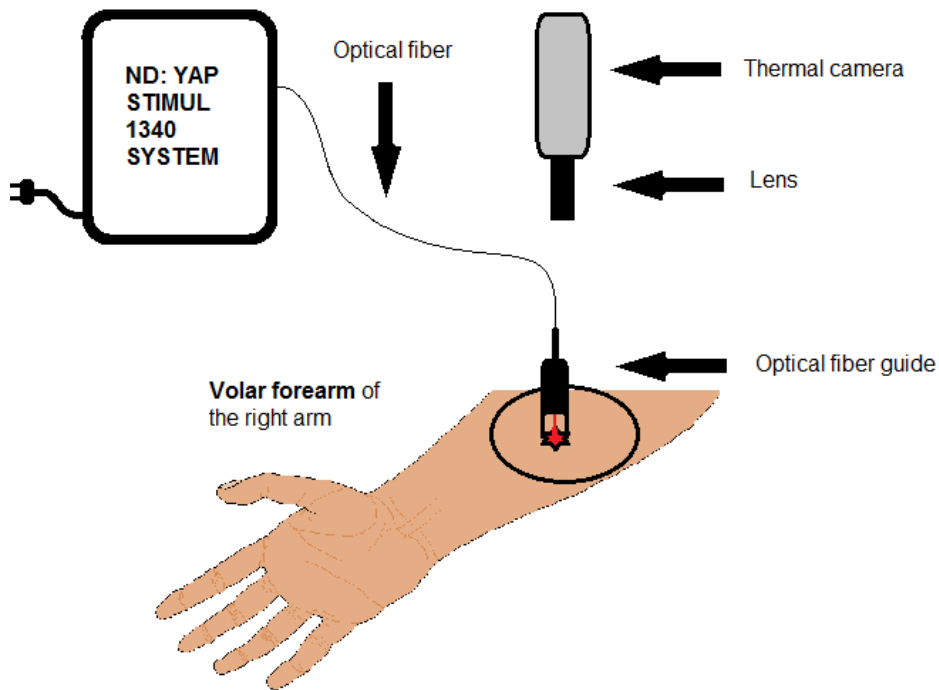
Figure 40 – Figure illustrates the ND: YAP laser setup with fibre guide and thermal camera.

9.4.5 Ambient conditions

Room temperature will be kept at a constant temperature at 22.5 °C, and lighting in the room will be turned on during the procedure.

9.4.6 Setting up CO_2 10600 nm software and calibration

INPUT TWO DIFFERENT GCX FILES

- Shoot_200ms.gcx
- circleNtimes.gcx + picture

Stimulation times assessed by using oscilloscope (measure up period of control signal).

CO2 laser is limited at 10 % of maximum power as a safety mechanism

9.4.7 Calibrating thermal imaging

I need to find the exact settings used, so I can make sure they are the same every time.

9.5   Experimental procedures

9.5.1   Preparing subject

1. Before starting the experiment, the subject must sign the participant information (see participant information). Information must be received both orally and in writing. Furthermore, the subject must sign an informed consent, to ensure they have received sufficient information about the procedures of the experiment (see informed consent).
2. Make sure they are aware of the limitations of the experimental procedures and that they can draw from it at any time
3. Place them in the experimental setting with their right forearm exposed under the scanner head.
4. Measure ambient temperature, and note it
5. Shave area if needed
6. Mark the four stimulation areas with a plus sign (see Figure 41 – Figure sketches the volar side of the arm, with the stimulation areas, A, B, C, and D. Stimulation starts at A, then B, then C, then D and then back to A.Figure 41). No stimulation will be given on the marking.

9.5.2   Stimulation with CO_2 and ND: YAP lasers

To avoid habituation and tissue damage to the skin, an inter stimulus interval is defined as minimum 120 [s] at same location. To decrease total experiment time, risk of habituation and increase safety, stimulation site will be altered around in a square, see Figure 41.
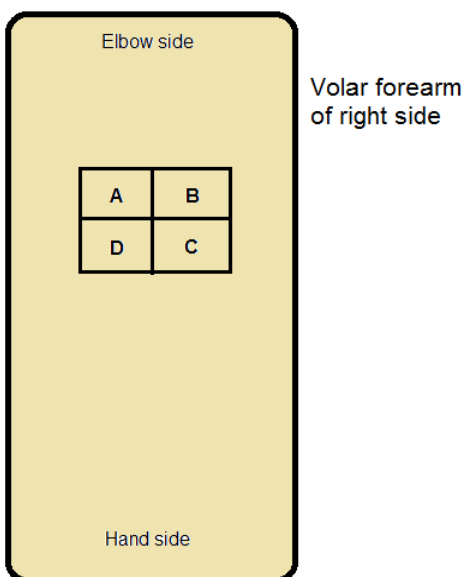
Figure 41 – Figure sketches the volar side of the arm, with the stimulation areas, A, B, C, and D. Stimulation starts at A, then B, then C, then D and then back to A.

Exact stimulation procedures are listed in following sequence:

Before starting, make sure subject and experimental leader wears protection googles for 10.600 nm.

1. First part: Identify heat perception threshold and A-delta pain threshold using two different beam diameters using the CO_2 laser
   a. Set beam diameter to 6 [mm] (**shoot_200ms.gcx**)
      i. Make sure **Q_switch_period = 500**
   b. Staircase method of (Cornsweet 1962) is used to identify the a-delta threshold, and is described in chapter *Identifying A-δ pain* threshold.
   c. Starting from a low intensity at 0.08 [J] over 200 [ms], incrementing with 0.08 [mJ] (equivalent to an increment of 1 Q_width with the specific stimulation parameters).
   d. When subject starts perceiving the stimuli, note the stimulation parameters and define as perception threshold
   e. Proceed the staircase to find A-delta pain threshold using the staircase method (Cornsweet 1962)
      i. Each turning point is noted in the experimental schemes
   f. When threshold is found for 6 [mm] beam diameter, note the stimulation parameters, and Record spatial and temporal data.
      i. Place 10x10 mm aluminium plate on skin, and make sure it can be seen on the thermal image. The plate should **NOT** be near the stimulation site.
      ii. Record minimum 10 s before stimulation and 60 s after stimulation (total recording minimum 70 s)
      iii. Save the recording as: sub**X**CO2diameter**XX**mm, where X indicates the specific number/letter related to the prefix
   g. Change the beam diameter to 10 [mm] (**circleNtimes.gcx**) and repeat from step **a.** and then proceed to second part**.**
      i. Make sure **Q_switch_period = 500, scaling = 200, step_period = 200**
2. Second part: Identify heat perception threshold and A-delta pain threshold using two different beam diameters using the ND: YAP laser
   a. Shift protection googles from 10.600 nm (plastic) to 1340 nm (aluminium metal).
   b. Set beam diameter to 6 [mm]
   c. Staircase method of (Cornsweet 1962) is used to identify the A-delta threshold, and is described in chapter *Identifying A-δ pain* threshold.
   d. Starting from a low intensity at 1 [J] over 10 [ms], incrementing with 0.25 [J].
   e. When subject starts perceiving the stimuli, note the stimulation parameters and define as perception threshold
   f. Proceed the staircase to find A-delta pain threshold using the staircase method (Cornsweet 1962)
      i. Each turning point is noted in the experimental schemes
   g. When threshold is found for 6 [mm] beam diameter, note the stimulation parameters, and Record spatial and temporal data.
      i. Place 10x10 mm aluminium plate on skin, and make sure it can be seen on the thermal image. The plate should **NOT** be near the stimulation site.
      ii. Record minimum 10 s before stimulation and 60 s after stimulation (total recording minimum 70 s)
      iii. Save the recording as: sub**X**CO2diameter**XX**mm, where X indicates the specific number/letter related to the prefix
   h. Change the beam diameter to 10 [mm] and repeat from step **a.**

10 Appendix A - Experimental note schemes

Listed schemes below are used to ensure data quality and safety of the stimulations in the experiment.

Subject ___

	data	unit
SUBJECT AND ENVIRONMENT DATA		
Sex		
Ambient temperature at start		[degC]
Ambient temperature at end		[degC]
time start		tt:mm
time end		tt:mm
PERCEPTION THRESHOLDS CO2		
6 [mm]	/ /	Q_width / W / J
10 [mm]	/ /	Q_width / W / J
A-DELTA PAIN THRESHOLD CO2		
6 [mm]	/ /	Q_width / W / J
10 [mm]	/ /	Q_width / W / J
PERCEPTION THRESHOLDS ND: YAP		
6 [mm]		[J]
10 [mm]		[J]
A-DELTA PAIN THRESHOLD ND: YAP		
6 [mm]		[J]
10 [mm]		[J]
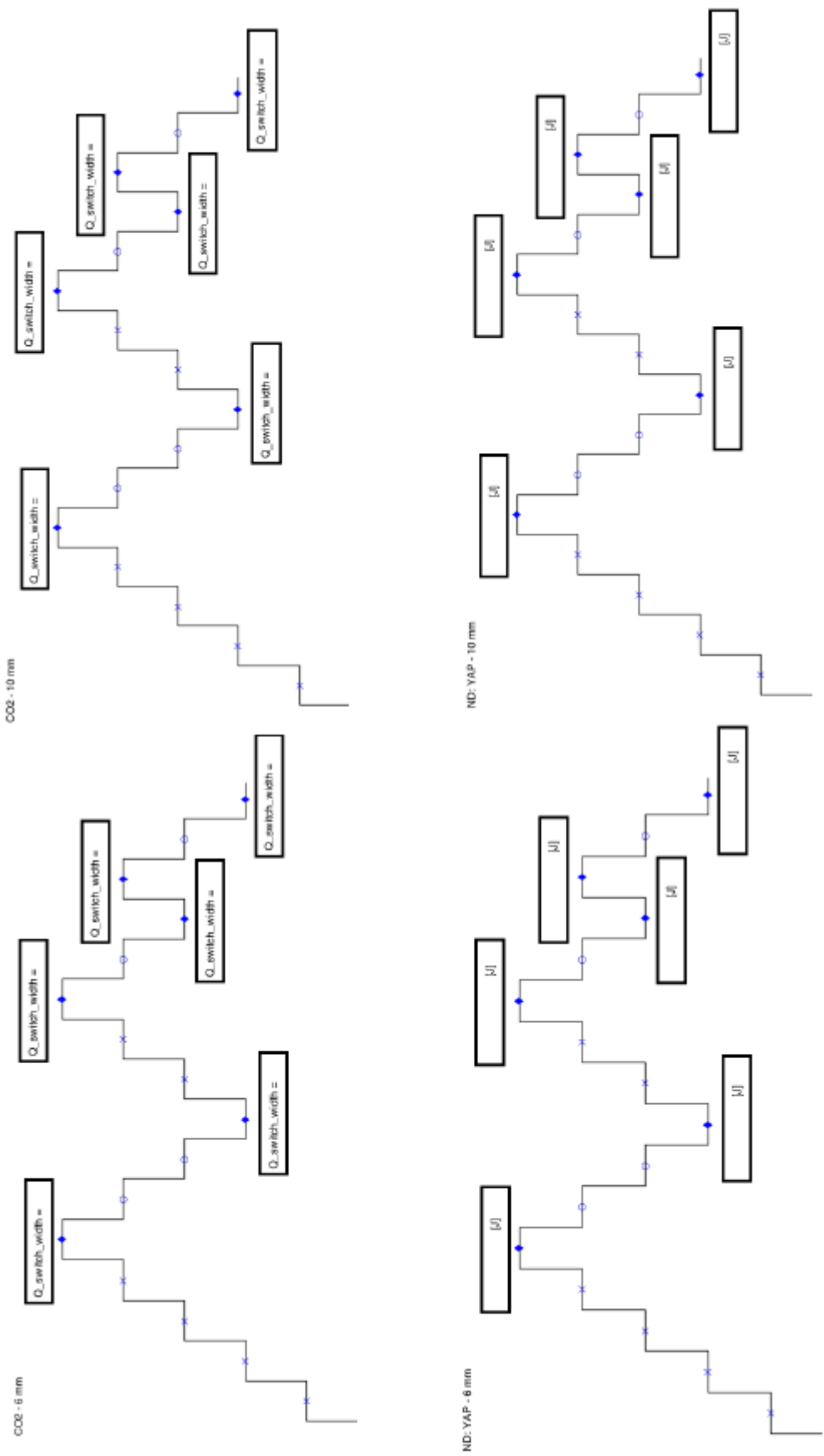
11 Appendix B – Participant information

Project title: Modelling noxious laser stimulation for ND: YAP and CO2 lasers

We would like to enquire if you are interested in participating in a research project which is to be performed at Centre for Sensory-Motor Interaction (SMI), Aalborg University.

Before you decide to participate in the research project, it is important that you fully understand the procedures of the experiment. Therefore, we ask you kindly to read this information carefully.

We will invite you to participate in an information meeting where we will elaborate the information about the project and where you have the opportunity of asking any questions you may have. You are welcome to bring a family member or a friend to the meeting.

If you decide to participate in the project, we will ask you to sign a declaration of consent. Please remember that you have the right to time for reflection before you sign the declaration of consent.

Participation in the project is voluntary. You can at any time and without stating a reason withdraw your consent.

11.1.1 Purpose of the Experiment

The purpose of the experiment is to validate the constructed laser-skin model, through assessing A-δ pain threshold, and collecting data about spatial and temporal profiles across the surface of stimulation site. Data will afterwards be compared with the output of the model using the same stimulation parameters as in the experiment.

11.1.2 Methods

There will be recruited a total amount of 6 test subjects. To participate you must:

- Be between 18-60 years old
- Be healthy
- Not be pregnant
- Not have used any painkilling drugs of any kind, 48 hours prior to the experiment.

Is one or more of the inclusion criteria not met, please inform the experimental leader.

During the experiment, you will receive thermal stimulation from two different lasers (CO2 10,600 nm and ND: YAP 1340 nm) on the volar side of your right forearm. Some of the stimulations will be above your A-delta pain threshold. When stimulation is given over pain threshold, you will feel the stimulation as prickly or prickling pain. Threshold is assessed via a staircase method, where multiple stimulation is giving just above and under pain threshold. Being stimulated above pain threshold, may induce the nociceptive withdrawal reflect, which may result in involuntary contractions of the right arm. This is normal and is not harmful.

If you have a hairy volar forearm, you can expect it to be shaved during subject preparation.

11.1.3 Plan for the Experiment

The experiment will run for approximately 60 minutes. And will divided into following four parts:

1. Find A-Delta pain threshold with CO2 10,600 nm laser at 6 mm spot diameter
   a. Record spatial and temporal changes at stimulation site
2. Find A-Delta pain threshold with CO2 10,600 nm laser at 10 mm spot diameter
   a. Record spatial and temporal changes at stimulation site
3. Find A-Delta pain threshold with ND: YAP 1340 nm laser at 6 mm spot diameter
   a. Record spatial and temporal changes at stimulation site
4. Find A-Delta pain threshold with ND: YAP 1340 nm laser at 10 mm spot diameter
   a. Record spatial and temporal changes at stimulation site

During painful stimulations, you might experience discomfort. This is perfectly normal.

When the sessions are over, you are free to ask questions about the experiment.

11.1.4 Risks, Side Effects and Disadvantages

There might be risks about the experiment that we do not know yet. Therefore, we ask you kindly to inform us if you experience any health problems during the experiment. If we discover side effects of which you have not been informed, we will of course inform you immediately, and in this case, we will ask you to re-consider your participation.

11.1.5 Benefits of the Experiment

The aim of the study is to explore how laser stimulation interacts with skin tissue. The results from the experiment will contribute to validation of a model which describes the exact same scenario. For future use, the model will be able show us what is going on in the layers of the skin before/during/after laser stimulation, which will give us great insights into laser stimulation, both in terms of pain and non-pain research.

11.1.6 Exclusion from and Suspension of Experiment

If you, according to the assessment of the investigator, react unexpectedly on the procedures of the project or in any other way are not suitable for continuing in the experiment, the experiment can be terminated at any time. You will then receive compensation corresponding to the part of the experiment in which you have participated. In general, the experiment will be terminated if it turns out that the subjects in general cannot tolerate the procedures of the project or find the experiment too exhausting.

11.1.7 Project Economy

The project is financed exclusively by University funds at Aalborg University, in collaboration with Ken Steffen Frahm.

11.1.8 Access to Results

The results will be published in the internal database of AUB-project library (http://projekter.aau.dk/projekter/), and is only accessible by student or **employees** at Aalborg University.

The experiment has been approved by Den Videnskabsetiske Komité for Region Nordjylland, project number N-20140093.

We hope that this information has given you sufficient knowledge of the experiment to make a decision about participation. Please also refer to the attached leaflet The Rights of a Trial Subject in a Health Scientific Research Project.

If you require further information about the project, please do not hesitate to contact the undersigned.

Yours faithfully

Alan Tahhan

Email: atahha12@student.aau.dk

Tlf.nr.: +45 60 62 71 11

12 Appendix C – The Rights of a Trail Subject in a Health Scientific Research Project

As a participant in a health scientific research project you should know that:

- Your participation in the research project is completely voluntary and can only take place after you have received both written and oral information about the research project and signed the consent form.

- You may at any time orally, in writing or by any other clear notification withdraw your consent to participation and withdraw from the research project. If you withdraw your consent, this will not affect your right to any current or future treatment or any other right you may have.

- You are entitled to bring a member of your family, a friend or an acquaintance with you to the informative interview.

- You are entitled to time to think it through before you sign the consent form.

- Strict confidentiality is observed with regard to information about your health, other purely private matters and other confidential information about you disclosed in connection with the research project.

- Information about you, including information about tissue and blood samples from you, will be stored according to the provisions specified in the Danish Act on Processing of Personal Data and the Health Act.

- You will be able to get access to research protocols according to the provisions of the Danish Open Administration Act. This means that you can gain access to all documents concerning your participation in the project apart from the parts containing business secrets or confidential information about others.

- You have the right to complain and compensation can be paid pursuant to the Act on the Right to Complain and Receive Compensation within the Health Service.

(The above Appendix is published by the research ethics committee system and can be attached to the written information about the health scientific research project. Questions about a specific project should be directed to the regional committee who has approved the project).

13 Appendix D – COMSOL Mesh's

U3

U2

U1
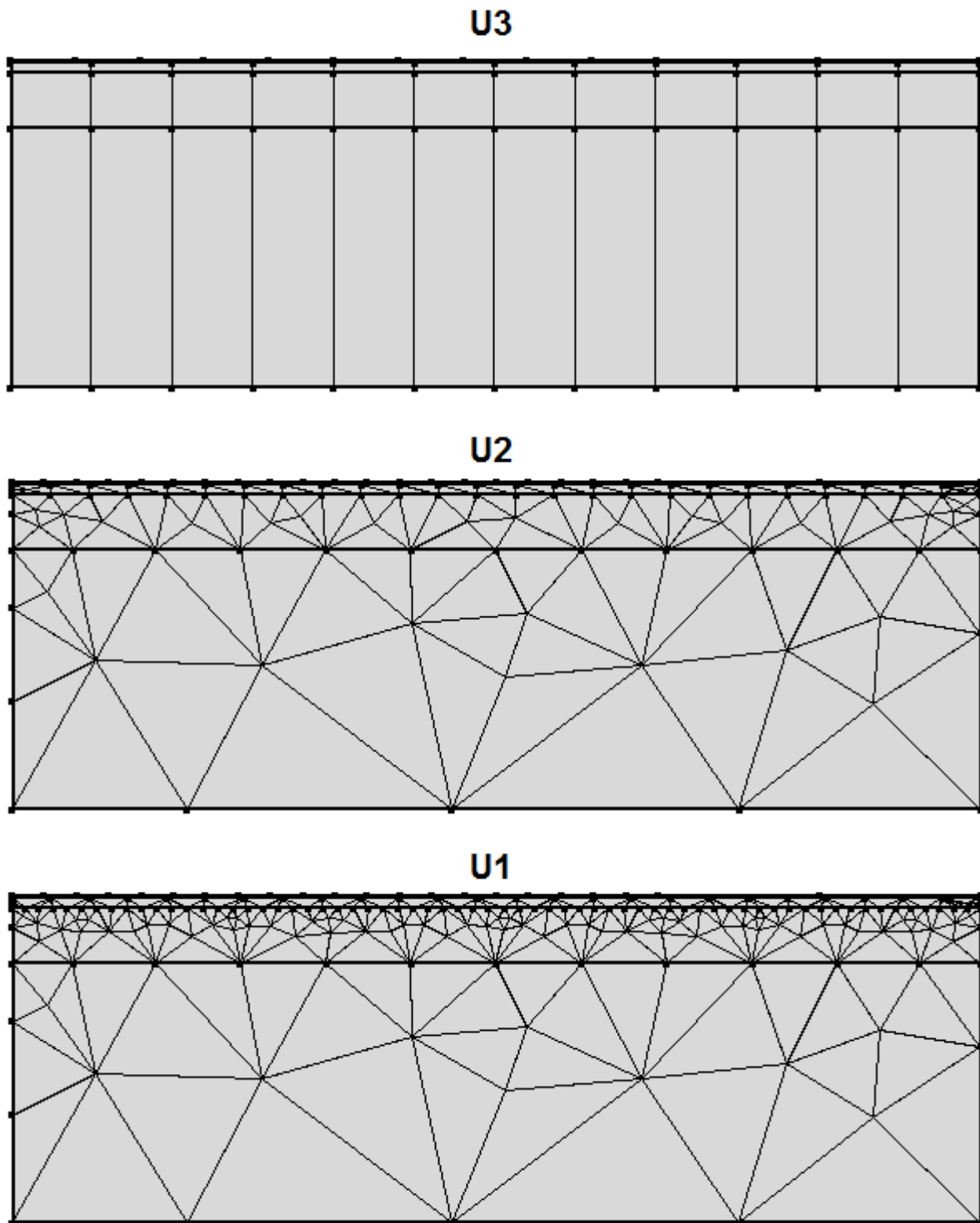
Figure 42 – The figure illustrates three user-generated mesh's: U3, U2, and U1. U3 contains 60 domain elements and 82 edge elements. U2 contains 317 domain elements and 130 edge elements. U1 contains 481 domain elements and 170 edge elements.
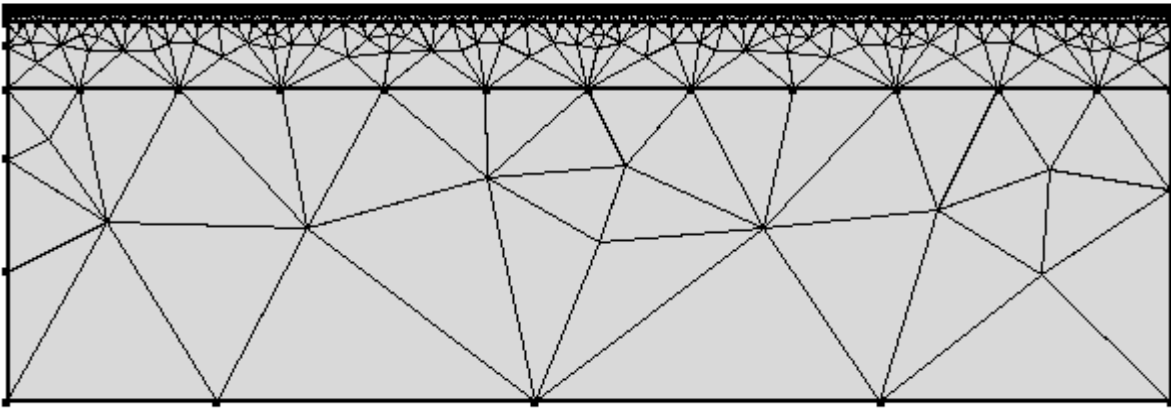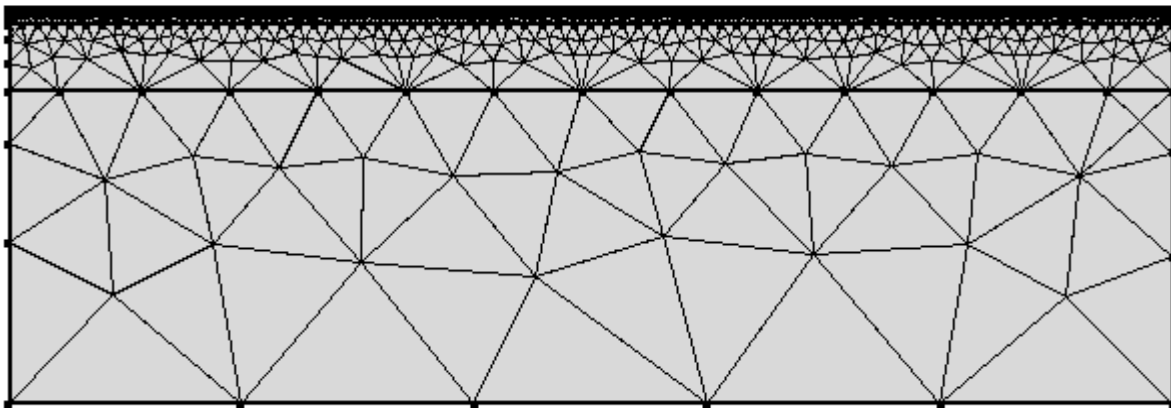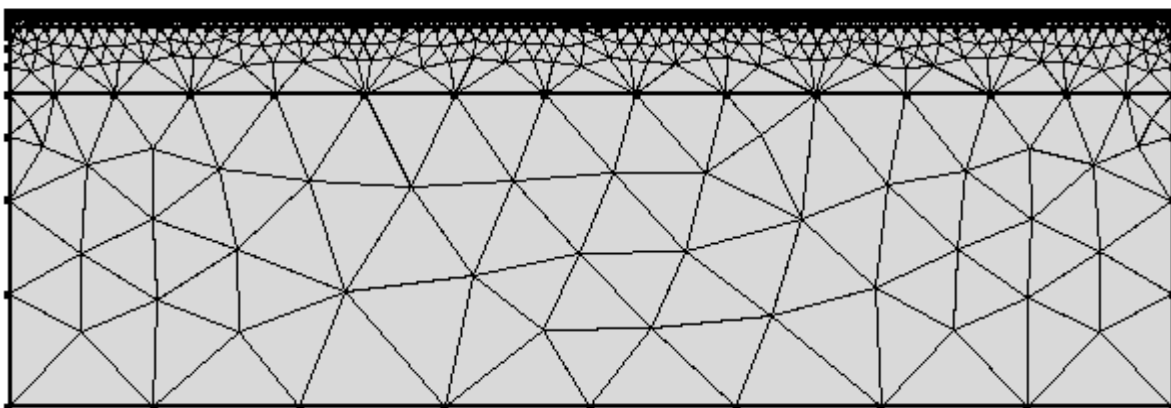
Figure 43 - The figure illustrates three default-generated mesh's: D1, D2, and D1. D1 contains 4680 domain elements and 1789 edge elements. D2 contains 6371 domain elements and 2069 edge elements. D3 contains 7390 domain elements and 2084 edge elements.

D4
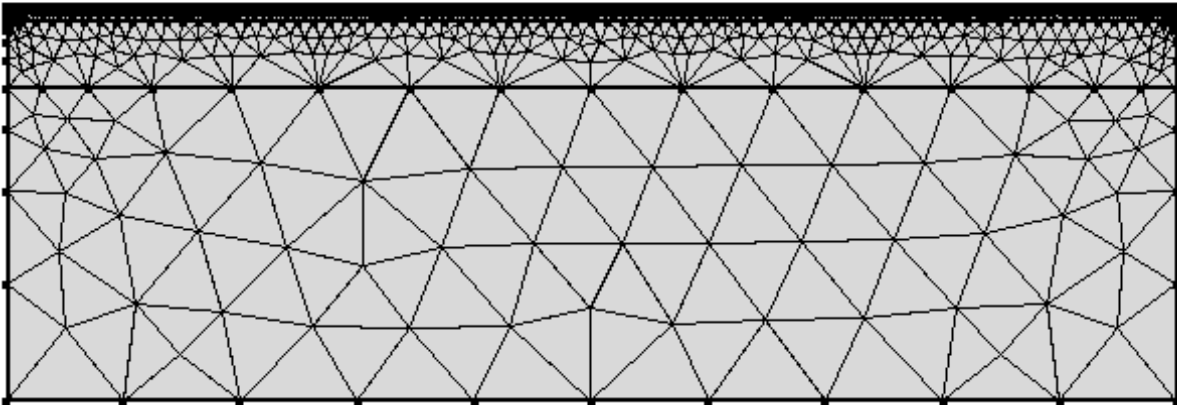
D5
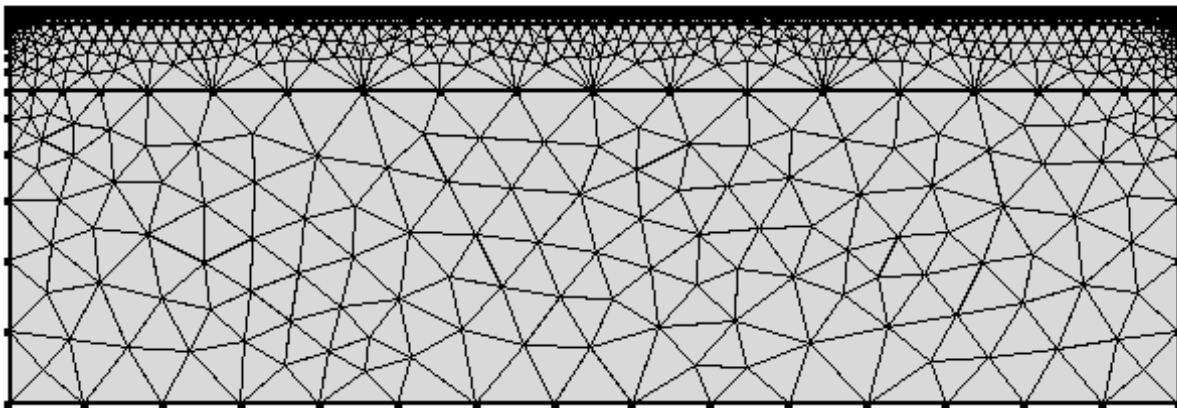
D6
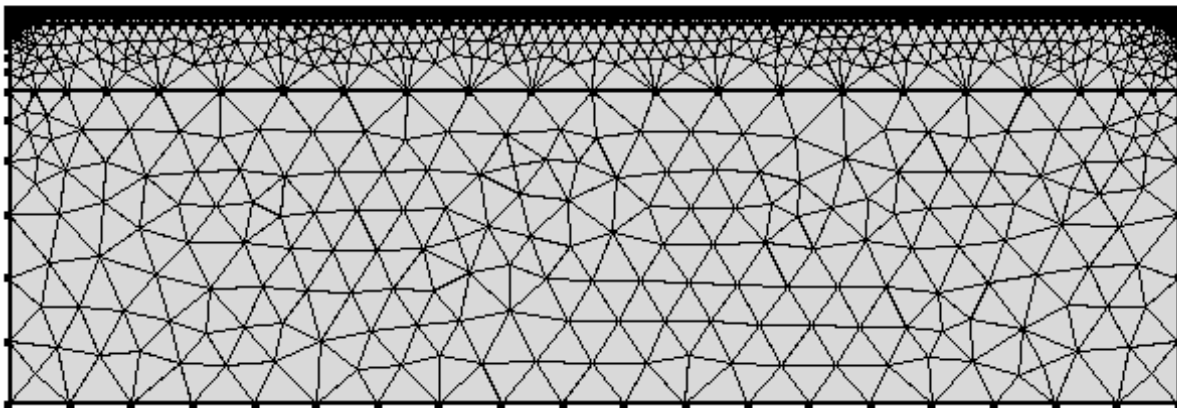
Figure 44 - The figure illustrates three default-generated mesh's: D4, D5, and D6. D4 contains 7714 domain elements and 2088 edge elements. D5 contains 8360 domain elements and 2112 edge elements. D6 contains 8492 domain elements and 2118 edge elements.
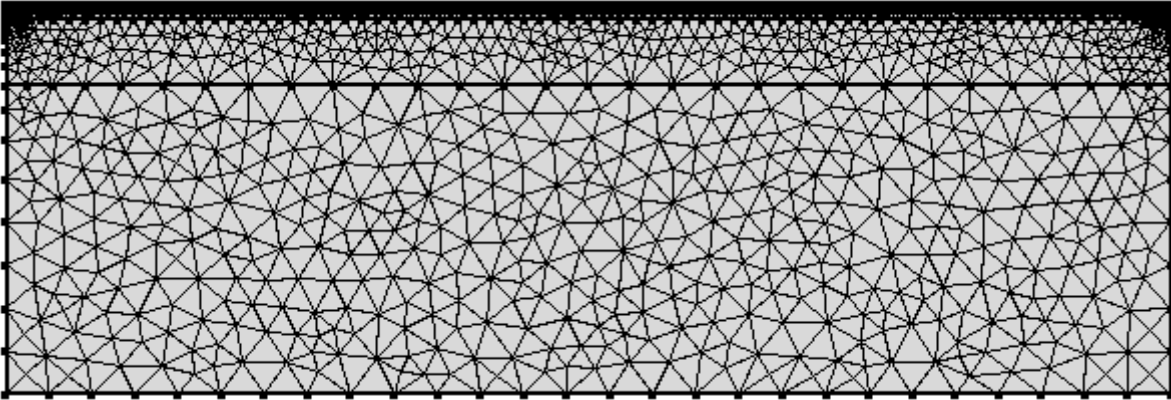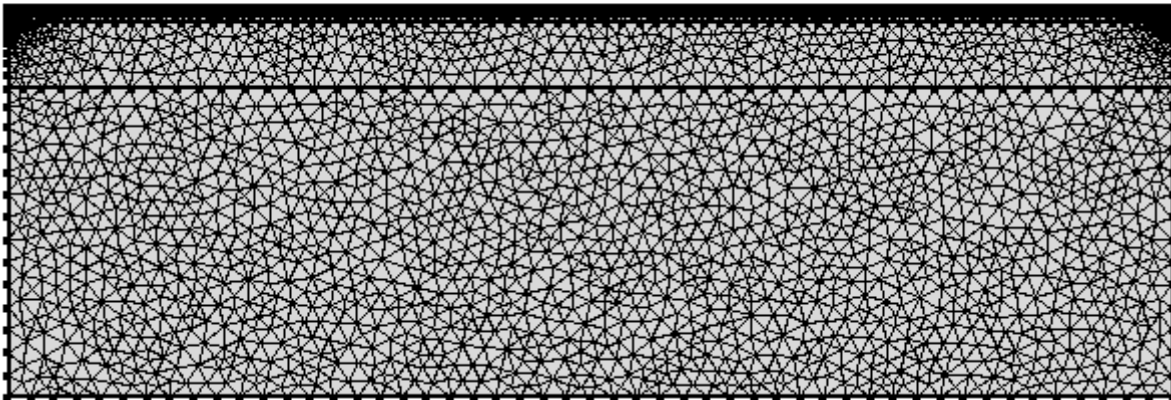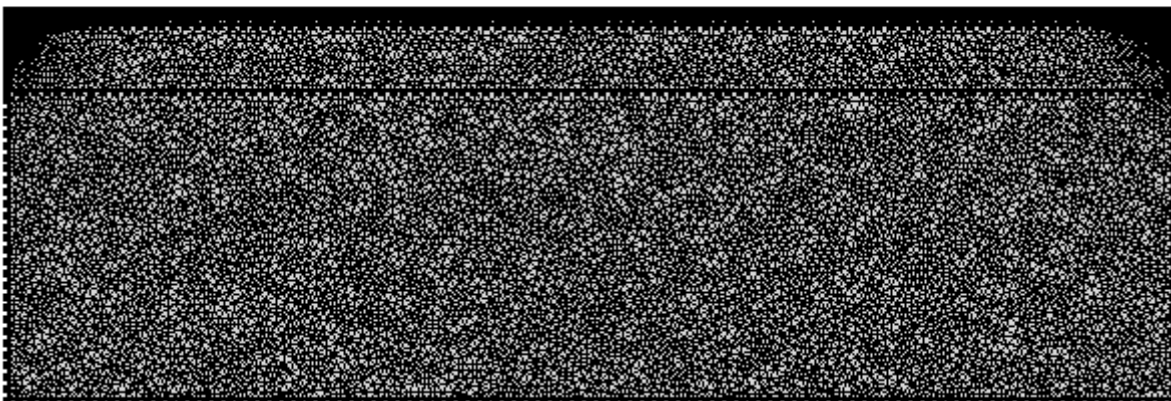
Figure 45 - The figure illustrates three default-generated mesh's: D7, D8, and D9. D7 contains 9498 domain elements and 2140 edge elements. D8 contains 11740 domain elements and 2215 edge elements. D9 contains 23202 domain elements and 2404 edge elements.

14 Appendix E – Laser evoked potentials and practical application

Evoked potentials are brain activity related to an external stimulation. An evoked potential is a summarization of activity from thousands of cells, and may be recorded via surface electroencephalography (EEG). (Kandel 2013)

An evoked potential may be acquired in many ways. In functional pain research, it may be acquired via thermal-, electrical-, or tactile-stimulation, or somatosensory evoke potentials (SEP). SEP are often assessed by electrical stimulation which always contains more than one modality. One way to perform singular modality stimulation is with laser stimulation, where the recorded response in the brain is referred to as LEP. Because of the singular modality nature of LEP, they have grown to have a clinical usefulness in functional testing of the peripheral nervous system and tracts of the central nervous system. LEP can help to differentiate between psychogenic or neurogenic hypoalgesia. Examples of psychogenic hypoalgesia diseases are: Conversion disorder and Borderline personality disorder. Examples of neurogenic hypoalgesia diseases are: Diabetic neuropathy, Multiple sclerosis, and Postherpetic neuralgia. (R. Treede et al. 2003)